LEAF HYDRAULIC GEOMETRY

A Dissertation

Presented to the Faculty of the Graduate School

of Cornell University

in Partial Fulfillment of the Requirements for the Degree of

Doctor of Philosophy

by

Mónica Juliana Ramírez Carvalho

August 2017

LEAF HYDRAULIC GEOMETRY

Mónica Juliana Ramírez Carvalho, Ph.D.

Cornell University 2017

The phloem and the xylem form the plant hydraulic system that mediates long-distance water, nutrient, and signaling transport necessary for survival and growth. In leaves, these microfluidic tissues are formed as files of tracheary and sieve elements that ensure the effective distribution of water and the collection of sugars throughout the lamina. The xylem provides the water required to compensate for water losses during CO_2 uptake, and the phloem collects sugar and provides the osmotically-mediated pressure differential between sources and sinks required for long-distance transport.

Whereas form-function relations of xylem hydraulics have been extensively studied in numerous species and organs, comparatively little is known about many of the basic structural properties of phloem that have direct effects on sap translocation. Using a combination of light, fluorescent, multiphoton, and transmission electron microscopy, I quantify and compare the phloem and xylem hydraulic structure in two topologically distinct leaf types, *Ginkgo* and *Populus x canescens*, which have leaves with an open dichotomous venation pattern and a hierarchical reticulate pattern, respectively.

In both leaf types, phloem and xylem hydraulic transport areas scale isometrically across all leaf vein levels. The conductive areas of individual veins, as well as the cross-sectional areas and lengths of sieve and tracheary elements

increase from minor veins to the petiole in poplar, and from the leaf margin to the leaf base in *Ginkgo*. This pattern effectively increases sap flow as sugars exit the leaf. At the whole leaf level, however, the hydraulic structure of both leaf types differs significantly. The scaling of *Ginkgo* hydraulics complies with that observed in single-veined leaves of other gymnosperms, and is consistent with theoretical models based on phloem transport that minimize flow energy dissipation. The leaf hydraulic structure of both leaf types is consistent with the predictions of Münch's Pressure Flow Hypothesis.

Finally, previously used models for describing vascular branching render themselves too simplistic and fail to describe the hydraulic geometry of *Ginkgo* or poplar leaves. However, the scaling of conductive diameters across vein branching levels are consistent with da Vinci's area-preservation model, and not with Murray's law of volumetric conservation.

BIOGRAPHICAL SKETCH

Coffee-addict and obsessive baker, Mónica R. Carvalho (b. 1986, Medellín, Colombia) is a plant morphologist working on leaf form-function and plant evolution. She obtained a BSc degree in Biology (emphasis in Botany), from the Universidad de Antioquia (Medellín, Colombia) in 2009. During her time as an undergraduate, she volunteered in the Molecular Genetics Laboratory (Genmol) and worked on the genetic structure of Native American populations and molecular phylogenetics of Andean plants. She joined the Smithsonian Tropical Research Institute in 2007 as an intern, and spent 4 months in northern Colombia digging for fossil plants and vertebrates at the fossil sites now considered to contain the remains of the earliest known Neotropical rainforest. Between 2007 and 2009 she worked on various projects including leaf architecture of Malvaceae and plant-insect interactions.

In 2009, Mónica moved to State College, PA where she worked under the supervision of Dr. Peter Wilf on various fossil sites from the Paleocene and early Eocene of Patagonia. She contributed with the description of the fossil ferns from the Laguna del Hunco fossil site and obtained a MSc in Geosciences from the Pennsylvania State University in 2011. She then pursued a PhD in Plant Biology at Cornell University, where she worked on form-functions relations in leaf vasculature under the advisory of Dr. Karl Niklas.

Mónica will continue to work on leaf morphology as a postdoctoral fellow at the Smithsonian Tropical Research Institute.

ACKNOWLEDGEMENTS

The work here presented is based upon research conducted at the Cornell High Energy Synchrotron Source (CHESS), supported by the National Science Foundation (NSF) and the National Institutes of Health/National Institute of General Medical Sciences under NSF award DMR-1332208; the Macromolecular Diffraction at CHESS (MacCHESS) facility, supported by award GM-103485 from the National Institute of General Medical Sciences/National Institutes of Health; and made use of the Cornell Center for Materials Research (CCMR) Shared Facilities, supported through the NSF MRSEC program (DMR-1120296). Imaging data was acquired through the Cornell University Biotechnology Resource Center, with NYSTEM (CO29155) and NIH (S10OD018516) funding for the shared Zeiss LSM880 confocal/multiphoton microscope. This PhD was partly funded by the Schlumberger Faculty for the Future Foundation.

None of the work here presented would have been possible without the unconditional support provided by my *Doktorvater* Professor Karl J. Niklas, whose utmost encouragement and unconditional support were essential for developing this work. His vision on plant structure and evolution has been and will always be an inspiration. I thank my committee members, Robert Turgeon and Tom Owens, for the very vivid and insightful discussions they enabled. I could not have asked for a finer committee.

I especially thank William Crepet for all his support during these years, and for all his helping when I needed it most.

Numerous people contributed to this project in technical or logistical support. I would like to thank Arthur Woll (CHESS), Edward Cobb, Maria Gandolfo, Nicholas Glynos, Adrienne Roeder, Lilan Hong, Leon Kochian, John L. Grazul (CCMR), Rebecca Williams and Joanna de la Cruz (Imaging Facilities, Cornell Biotechnology Center) for their help at various instances in the development of this work.

I thank Karin Jantz, Tara Nihill, and Tara Reed, who endured all of my last minute administrative, financial, and scheduling requirements during these years.

Finally, I thank my friends and family. In the midst of graduate school-life, those closest to us become our family. Samir Kiuhan, Francisco Leal, José Vargas, Diego Muriel, Camila Martinez, Juana Muñoz, Gwynne Lim, Simon Gunner, Thereis Choo, CT Chua, Amin Saied, Clare Saied, Max Fishman, Ian Small, Andy Read, *et alia* …

Credo quia absurdum est.

TABLE OF CONTENTS

LIST OF FIGURES

LIST OF TABLES

LIST OF ABBREVIATIONS

A_{phl}	Phloem conductive area
A_x	Xylem conductive area
c_{leaf}	Sugar concentration in the leaf phloem (sources)
c_{root}	Sugar concentration in the roots (sinks)
d_o	Conductive diameter at branching level *0*
d_n	Conductive diameter at branching level *n*
K_T	Phloem conductance
LPI, lp	Leaf plastochron index
P_{leaf}	Phloem pressure at the leaf (sources)
P_{root}	Phloem pressure in the roots (sinks)
Q	Volumetric flow rate
r	Phloem conduit radius
STM	Sieve tube member
VM	Vessel member
R	Ideal gas constant
T	Temperature
η	Viscosity

CHAPTER I

INTRODUCTION

The phloem and xylem constitute the long-distance hydraulic transport system in vascular plants that mediates water and nutrient allocation as well as the signaling necessary for survival and growth. The evolution of these two tissue systems overcame the diffusional limitations of internal water and nutrient transport in terrestrial plants, and favored the concomitant evolution of larger body plans on which leaves later developed.

This work

The thesis presented herein contributes to filling the conceptual gap between phloem and xylem hydraulic research. Historically, plant hydraulics has been dominated by research on the xylem and water transport processes under the premise that these are the backbone of whole plant physiological performance (Tyree & Zimmermann, 2002; Brodribb, 2009; Sack *et al.*, 2015). However, increasing evidence indicates that phloem dynamics equally determine plant hydraulic performance (see Knoblauch & Peters, 2016; Savage *et al.*, 2016). This thesis examines the functional and structural coupling of the phloem and xylem hydraulic systems leaves of *Ginkgo biloba* L. and *Populus x canescens* (Aiton) Sm. (also known as *Populus tremula x alba*). The leaves of these two taxa have an open dichotomous and a hierarchical reticulate venation pattern, respectively. They therefore represent two distinct topological types within the wide spectrum of leaf architectural patterns observed across extant

and extinct plants. Chapter 2 examines the structural and functional coupling between phloem and xylem in minor veins required for leaf photosynthetic maturation during the sink-to-source transition. Using a state-of-the-art elemental analysis technique, the coordination between phloem and xylem maturation was examined across a leaf developmental gradient. Chapters 3 and 4 describe the leaf hydraulic architecture of *Ginkgo* and poplar, and examine the scaling relationships across levels of vein branching and between the phloem and xylem hydraulic architectures. Two structural branching models were used to test for scaling relationships across vein branching levels: da Vinci's rule and Murray's Law, which predict for area- and volumetric-preserving scaling relationships across vein branching levels, respectively. These two chapters also emphasize the hydraulic linkages with the xylem that are required for adequate phloem transport. Finally, Chapter 5 compares the leaf hydraulic geometry of *Gingko* and poplar in relation to topology, phloem transport, and future efforts to provide biologically sensible models for phloem transport.

Background: Structure and function of vascular tissues

Together, phloem and xylem form parallel microfluidic systems with different conductive properties and driving forces. Xylem conduits are nearly hollow tubes formed by files of lignified tracheary elements (tracheids or vessel elements) connected end-to-end. Because tracheary elements are dead, water conduction occurs through the apoplast and is driven by the hydrostatic pressure gradient between the roots and leaf evaporative surfaces. Inside the xylem conduits, cohesion forces between water molecules maintain the integrity of the water column and allow for the ascent of water against the gravitational force.

Even though controversy remains around the adhesion-cohesion theory (Pickard and Melcher, 2006), the biophysics of xylem flow has been described extensively generally from the perspective of simplified pipe systems with laminar flow that follow the fluid mechanics described by Hägen-Poiseuille formulations (e.g., Tyree and Zimmermann, 2002).

In contrast, phloem conduits are formed by files of living sieve elements that therefore mediate flow though their symplast. Sieve elements are devoid of most organelles at maturity and are connected end-to-end via clusters of pores or plasmodesmata-like channels, forming a low-resistance pathway between photosynthetic (source) and metabolically active or storage (sink) tissues. Currently, Münch's Pressure Flow Hypothesis remains the most widely accepted model for phloem flow. This hypothesis states that transport through the phloem follows an osmotically-generated hydrostatic pressure gradient between sources and sinks (Münch, 1930). Experimental evidence indicating mass flow though the phloem is consistent with predictions from Münch's Pressure Flow Hypothesis (Kockenberger *et al.*, 1997; Knoblauch & van Bel, 1998; Imlau, 1999; Windt *et al.*, 2006). However, whether the physical mechanisms that control phloem transport are related to changes in the turgor pressure gradient or biologically-induced changes in flow resistance remain poorly understood (Knoblauch & Oparka, 2012). This gap in our knowledge is particularly true in the case of trees, in which the observed turgor pressure gradients are much lower than those of herbaceous plants, despite the longer distance (and thus higher total resistance) between sources and sinks (Turgeon, 2010). Most of the basic phloem structural information required for understanding phloem transport from sources to sinks is either unknown or has shown unexpected results. For example, pipe flow

dynamics predict that flow resistance and flow velocities are inversely related, and that flow resistance decreases with increasing sieve element and sieve pore areas. Reports by Müllendore *et al.* (2011) and Froelich *et al*. (2011) compared observed phloem flow velocities with resistance estimates based on sieve pore and sieve element areas, and found that the observed relationship between flow velocity and resistance did not meet expectations. Instead, an inverse relation between the areas of sieve elements and flow velocity was observed, indicating that some of the basic assumptions involved in estimating phloem transport need to be revised (Knoblauch & Oparka, 2012).

Relationships between phloem transport and hydraulic structure

Direct and concurrent measurements of the parameters required to describe phloem transport, such as turgor pressure, flow velocity, symplast viscosity, and conduit geometry, are difficult to obtain, in large part owing to intrinsic features of phloem conducting cell types. For example, sieve elements are thin walled, operate under positive pressure, and are deeply buried under layers of tissue. Collectively, these features make sieve elements highly susceptible to mechanical damage that, in turn, makes measurements of phloem translocation inherently difficult to visualize and quantify in living plants. Nevertheless, Knoblauch *et al*. (2016) recently examined the relationship between plant height, phloem conduit conductance, and turgor pressure gradient using newly developed methods for direct pressure measurements in intact sieve elements. They found that the turgor pressure gradient and sieve tube conductivity increase notably as the distance between source and sink tissues increases with plant height. Their observations were consistent with predictions

based on Münch's Pressure Hypothesis and highlight the basic form–function coupling in phloem structure.

Given the difficulties in quantifying phloem flow, hydrodynamic models based on Münch's hypothesis and Hägen-Poisuille formulations have provided insight into the relation between phloem geometry and transport dynamics. For example, the geometry of sieve elements has been found to maximize translocation rates in relation to transport distances (Jensen *et al.*, 2011), and the resistance of sieve plates has been found to scale with the sieve element lumen resistance (Jensen *et al.*, 2012b). Similarly, the geometry of phloem conduits imposes upper boundaries to sugar loading such that the concentration of sugars in the phloem is sufficiently high to maintain the osmotic-mediated hydrostatic pressure required for phloem translocation, but also sufficiently low to keep sap viscosity from obstructing phloem flow (Hölttä *et al.*, 2006; Jensen *et al.*, 2013). Finally, the differences between the geometry of the sieve tube members of most angiosperms and sieve cells of gymnosperms may explain the slower phloem flux rates observed in gymnosperms compared to those of angiosperms (Liesche *et al.*, 2015). Some of these formulations have successfully predicted flow dynamics in microfluidic systems that mimic long-distance phloem transport (Comte *et al.*, 2017).

Most of these studies rely on simplifying phloem structures as single tubes formed by files of cells of constant size (Thompson and Holbrook, 2003). Many structural factors such as variable sieve tube size and interconnections between sieve tubes however are known to contribute to transport dynamics. More realistic structural parameters remain to be incorporated into modeling attempts. Even though mathematical approaches provide insight into flow dynamics in

relation to phloem structure, detailed descriptions of phloem conduit dimensions and connectivity are still required for a better understanding of phloem transport. The results presented in chapters 3 and 4 attempt to contribute to our understanding of the basic structural measurements required for describing the phloem transport pathways in source leaves of *Ginkgo* and poplar.

Hydraulic coupling of phloem and xylem

Increasing evidence indicates that the phloem and xylem are functionally coupled in ways that ensure the transport of water and photosynthates (Savage *et al.*, 2016). Daily variations in phloem cell diameters within trees reflect changes in the radial hydraulic conductance between the xylem and phloem (Sevanto *et al.*, 2011), and indicate the effective movement of water between both tissues along the transport pathway. This exchange allows for xylem to provide phloem with the water required for maintaining sugar translocation rates (Hölttä *et al.*, 2006; Windt *et al.*, 2006), and for phloem water to move back into the xylem following a water potential gradient. The latter scenario is intensified under drought conditions and represents an instance in which phloem acts as a water reservoir for water movement through the plant (Zweifel *et al.*, 2000; Sevanto *et al.*, 2005). It has also been suggested that phloem is functionally involved in mechanisms for xylem embolism repair (Salleo *et al.*, 2009; Nardini *et al.*, 2011; Brodersen & McElrone, 2013).

The structural linkages between phloem and xylem are also seen in the scaling relationships between the functional conductive transverse areas of both transport tissues in stems and leaves (Mencuccini et al., 2011; Jyske and Hölttä, 2015; this thesis). However, the hydraulic, mechanical, and physiological

implications of these scaling relationships remain unknown or at best poorly understood. This gap in our knowledge is largely due to a paucity of data quantifying the dimensional architecture of the phloem. Although the structure-function relationships of tracheary cell-types have been widely studied (e.g., Roth et al., 1995; Zwieniecki et al., 2002, 2007; Sack et al., 2004), the structure-function relationships of sieve cells and sieve tube members are still rarely reported (see however Petit and Crivellaro, 2014; Woodruff, 2014; Jyske and Hölttä, 2015).

The findings presented in chapter 2 provide evidence of the hydraulic coupling between phloem and xylem during leaf development, and the results shown in chapters 3 and 4 provide evidence of the structural link between both tissues in source leaves of *Ginkgo* and poplar.

Leaf hydraulic structure

Leaf vasculature provides mechanical support (Niklas, 1999) and ensures an effective distribution and collection system for water and sugars throughout the leaf lamina. The hydraulic structure of the leaf comprises the collection of transporting phloem and xylem conduits in the vasculature, and is determined by vascular topology (the spatial configuration of veins in a leaf) and conduit geometry, e.g., cell diameter and length.

Sugar loading in leaf phloem is essential for plant survival because it provides the osmotically-mediated pressure differential between sources and sinks required for long-distance transport (Münch, 1930; Turgeon & Ayre, 2005; Comtet *et al.*, 2017). Despite the structural and physiological linkages between the phloem and the xylem, most of the literature dealing with leaf hydraulics

focuses on the xylem, partly because the physics of water flow through hollow conduits is well established. For example, xylem geometry (the radii and numbers of vessels) is closely related to water transport efficiency (Roth-Nebelsick *et al.*, 2001; Sack & Scoffoni, 2013). Wide vessel member lumens such as those in major veins enable greater hydraulic conductivity in accordance with the Hagen-Poiseuille equation (Sperry *et al.*, 2005; Sommerville *et al.*, 2012), although they also increase the susceptibility to embolism (Brodribb *et al.*, 2016) due to the number of inter-conducting pit membranes present in larger vessels (Hargrave *et al.*, 1994; Wheeler *et al.*, 2005; Lens *et al.*, 2011). Similarly, the length of veins per leaf area (VLA) is linked to enhanced hydraulic conductance and broadly correlates with gas exchange rates (Sack & Frole, 2006; Brodribb *et al.*, 2007; Boyce *et al.*, 2009; McKown *et al.*, 2010).

The architecture of leaf venation is related to a number of other functionalities (Roth-Nebelsick *et al.*, 2001). However, the relationship between leaf topology and hydraulics has not been thoroughly studied. Most studies only evaluate broad aspects of reticulate venation and are mainly focused on their relation to water transport (e.g., Roth et al., 1995). For example, the topology of looped vascular networks as opposed to less interconnected systems confers redundancy in transport pathways, resilience to damage (Wylie, 1951), an advantage against herbivory (Haberlandt, 1914; Wagner, 1979), and higher hydraulic conductance due to increased vascular connectivity (Roth-Nebelsick *et al.*, 2001). Recent theoretical approaches indicate that vein interconnectivity also provides flexibility in coping with fluctuating loads (Katifori *et al.*, 2010; Corson *et al.*, 2010). Even though the ideas of redundancy and response to fluctuating loads are in principle applicable to phloem transport, the effects of vein damage

in reticulate veined leaves are likely to differ for water and for phloem transport (Wylie, 1938; Roth-Nebelsick et al., 2001). The effective redundancy of leaf vasculature depends on the adequate movement of water and solutes between adjacent tracheary or sieve conduits within vascular strands. Whereas adjacent vessels and tracheids are connected by pores that enable water flow, the lateral connectivity between sieve cells and sieve tube members is more restricted. The number of lateral sieve areas connecting adjacent sieve tubes and sieve cells determines the potential interconnectivity between adjacent conduits within a vascular strand.

The following chapters contribute to our understanding of leaf vasculature by describing the leaf hydraulic structure of *Ginkgo* and poplar in relation to their vascular topology. Finally, the section on Concluding remarks examines the implications of these topologies on the physiological processes involved in the phloem loading and on the pathways for phloem export.

CHAPTER II

SPATIOTEMPORAL DISTRIBUTION OF ESSENTIAL ELEMENTS THROUGH *Populus* LEAF ONTOGENY

Mónica R. Carvalho[1], Arthur Woll[2], Karl J. Niklas[1,]

[1]School of Integrative Plant Sciences, Plant Biology Section, Cornell University, Ithaca, NY 14853, USA

[2]Cornell High Energy Synchrotron Source, Cornell University, Ithaca, NY 14853, USA

Published: *Journal of Experimental Botany* 67 (9): 2777-2786, 2016

Short running title: Element distribution in developing leaves

Research highlight

We document the preferential spatiotemporal distribution of Zn, Ca and K throughout a developmental sequence at the organ level, and match the compartmentalization of Ca in poplar leaves with the enhancement of the evapotranspiration stream and phloem maturation.

Abstract

Optimal concentrations and distribution patterns of essential elements in plants can vary spatially and temporally. Here, we examine the spatiotemporal distribution and accumulation of zinc, calcium, and potassium throughout leaf growth and maturation. Eight developing leaves of grey poplar (*Populus x canescens*) covering leaf plastochrons 1 through 10 were selected to ensure observation of the sugar sink-to-source transition. This transition requires coordinated changes of multiple core metabolic processes, and is expected to involve alterations in essential and non-essential element distributions as tissues mature and effect a reversal in phloem flow direction. Whole-leaf elemental maps were obtained from dried specimens using micro x-ray fluorescence spectroscopy. Additional cross-sections of fresh leaves were scanned to check for tissue-specificity in element accumulation. Whereas the anatomical distribution of Zn and K remains relatively consistent throughout leaf development, Ca accumulation varied across leaf developmental stage. Allocation of Ca into the leaf mesophyll occurs basipetally, matching spatially and temporally the sequence of phloem maturation, positive carbon balance, and sugar export from leaves. The accumulation of Ca likely reflects the maturation of xylem in minor veins and the enhancement of the transpiration stream. Our results independently confirm that xylem and phloem maturation is spatially and temporally coordinated with the onset of sugar export in leaves.

Keywords: calcium, essential elements, leaf development, leaf maturation, phloem loading, *Populus*, x-ray fluorescence spectroscopy

Introduction

Essential elements (e.g., Zn, Ca, and K) are required for adequate plant growth and reproduction (Hawkesford *et al.*, 2011). Along with other non-essential elements, these are taken up by roots from the soil and are subsequently moved into the shoot by long distance transport (White, 2011). Once within the shoot, their distribution and compartmentalization varies both spatially and temporally across organs and tissues, following metabolic requirements and uptake availability (Conn & Gilliham, 2010).

Element requirements and tolerance widely vary at the tissue, cellular and subcellular levels. Whereas some elements exist within a broad concentration range, others become toxic if they accumulate beyond a critical level, indicating that metabolic controls must sense and regulate the targeted translocation of elements in order to maintain plant function. Transport proteins found in xylem and phloem tissues have been shown to mediate the movement of some essential elements into and out of the vascular system of several species (Yamaji & Ma, 2014; Zhai *et al.*, 2014). However, the specific mechanisms and timing behind the preferential distribution and accumulation of most essential elements between cell types in plants remain poorly known (Yamaji & Ma, 2014). The documentation of spatiotemporal patterns of essential element accumulation at the organ and tissue levels is necessary for gaining deeper insights into mineral distribution, sequestration, and compartmentalization of essential elements in plants.

Our knowledge on the distribution of elements at a macroscopic level has greatly increased in the past two decades with the application of

numerous techniques that allow fast *in situ* detection and quantification (Wu & Becker, 2012; Zhao *et al.*, 2014). Interest in the accumulation of heavy metals has driven the application of less traditional methods such as energy dispersive x-ray microanalysis (EDX) and proton-induced x-ray emission (PIXE) for detecting distribution of macronutrients or heavy metals in hyper-accumulating plants at the cellular level. However, mapping the distribution of non-metalloid and/or lighter elements at low concentrations remains challenging and requires analytical methods that provide both high sensitivity and high spatial resolution. Synchrotron-based techniques using high-energy photon beams that allow for the detection of a wide array of elements have proved useful for visualizing element distribution at the tissue, cellular, and subcellular levels. Recently developed detector systems for synchrotron-based micro x-ray fluorescence (μ-XRF) spectroscopy have enhanced detection speed as well as the ability to spatially resolve elements in low concentrations (Kirkham et al., 2010). This method has been successfully used to document *in situ* distributions of elements in commercially important crop plants including wheat (Regvar *et al.*, 2011), rice (Moore *et al.*, 2014) and grapefruit (Tian *et al.*, 2014), and in the hyper-accumulator *Noccaea (Thlaspi) praecox* (Koren *et al.*, 2013).

Here, we make use of synchrotron-based μ-XRF to explore the temporal and spatial accumulation of essential elements in developing leaves of grey poplar (*Populus x canescens*.). As in many other species, the leaf primordia of this species act as sinks that rely on carbohydrates and other nutrients that unload from long distance phloem transport. As leaves grow and photosynthetic rates increase, sink strength decreases and leaves

become net sources of photosynthates to newer developing leaves. This sink-to-source transition denotes the irreversible loss of import capacity and the initiation of net carbon export from leaves as they reach full maturity. This process requires a shift in transport direction and involves major changes in central metabolism, enzymatic machinery, symplastic connectivity, and anatomical modifications that are expected to correlate with element provenance, requirements, and allocation (Turgeon, 2006).

The distribution of essential elements in leaves is expected to match metabolic requirements throughout leaf ontogeny. The sink-to-source transition in developing leaves provides a system in which to follow preferential element distribution in relation to the mechanical and metabolic changes associated with leaf growth. Because most developing tissues have low transpiration rates, young leaves are mostly unlinked from the transpiration stream and must rely on phloem transport for delivery of nutrients and mineral elements. As sink strength decreases, an increasing proportion of the inorganic nutrients entering the leaves come directly from the roots and through the xylem (Milthorpe & Moorby, 1969). Net concentrations of essential elements in leaves vary through development as cell division ceases and differentiation initiates. For example, phosphorous distribution and accumulation in developing leaves of *Cucumis sativus* has been well documented to reach a maximum concentration before the sink-to-source transition occurs and subsequently declines due to net export initiation (Hopkinson, 1964). Contrastingly, the targeted translocation of xylem-transported elements such as Ca from fully mature leaves is unlikely given that specific transport proteins mediating their export have not yet

been found in phloem and that Ca specifically is known to have low phloem mobility. The accumulation patterns differ between mineral elements (Meiri *et al.*, 1992; Karley *et al.*, 2000; Karley & White, 2009) and are likely to reflect nutrient function, tissue specificity, and differences in transport pathways. However, the preferential distribution and temporal behavior of most mineral elements in leaf tissues remains unknown.

Our goal in this study was to examine the spatiotemporal distribution and the relative abundance of mineral elements throughout leaf growth and maturation. We here describe the distribution of potassium, calcium, and zinc in leaves of grey poplar, making reference to leaf growth, anatomical development and photosynthetic sink to source transition. The distribution of these three elements were emphasized because K is the most abundant cation in plants, Ca has low mobility in the phloem, and Zn is a well studied trace-element model.

Materials and Methods

Plant material and growing conditions

Grey poplar (*Populus x canescens*) was selected as a model species because it belongs to a species complex whose leaf development has been extensively studied and in which the use of leaf plastochrons has provided a precise ontogenetic control for understanding leaf development (Dickmann, 1971; Larson & Isebrands, 1971; Larson *et al.*, 1972; Isebrands & Larson, 1973; Dickmann & Gordon, 1975; Dickson & Larson, 1981). It was also selected because it employs passive rather than active phloem loading, which makes

inferences about essential element transport more transparent (Zhang *et al.*, 2014).

Clones of grey poplar were propagated *in vitro* from stem cuttings rooted in Cornell mix growing medium (Boodley & Sheldrake, Jr., 1982) and grown in a growth chamber on 12 h/12 h day/night cycles under 300 μmol photons/m^2 and day/night temperatures of 28˚C/23˚C. Once the plants reached ~ 25 cm in height (~3 weeks), they were transferred to a cold frame and grown under natural ambient conditions at Cornell University facilities in Ithaca, NY, between June and July 2014. Plants were watered daily and were supplemented weekly with a 15-15-15 complete nutrient solution.

Leaves were harvested from saplings > 60 cm in height and having reached a leaf plastrochron index (LPI; Larson and Isebrands, 1971) of at least 20. Leaves spanning LPI 1 to 10 were selected to compare element distribution between early developing and fully mature leaves, and to capture the leaf phloem sink to source transition. Leaves were placed in a plant press for 3 days until fully dried. A set of these leaves, spanning LPI 1 to 7 and a fully mature leaf at LPI 10 collected from a single plant was selected for μ-XRF analysis. A duplicate collection of leaves was freeze-dried for comparing sample preparation techniques. In this case, the harvested fresh leaves were snap frozen in dry ice and lyophilized for 5 days.

Anatomical details and transverse imaging of leaves were obtained from free hand sections through fully mature, fresh leaves at LPI 10. Transverse sections were observed under an Olympus BX60 microscope and photographed using a Sony Progressive 3CCD. Leaf area was calculated from high-resolution photographs taken using a Canon T2i camera and 60

mm macro lens (Canon, Japan), and images were processed with ImageJ software (Rasband, 2014).

Even though one of the advantages of μ-XRF is its ability to detect trace elements *in situ* using fresh samples, using dehydrated samples nevertheless increases the sensitivity for trace elements by increasing the signal to background ratio. We tried two leaf dehydration methods as a means to minimize water content in the sample and avoid possible noise caused by dehydration in long scans (>8 hours) of large leaves. Lyophilization of early developing leaves yielded poor results possibly related to the collapse of undifferentiated cells. Elements in freeze-dried leaves appeared to form irregular streaks throughout the leaf lamina, contrasting with oven-dried samples in which element distribution followed well-defined leaf veins. Because freeze-dried leaf tissues may have suffered damage, all of the following results are based on observations made from the oven-dried samples.

Elemental X-ray fluorescence

Dried leaves and transverse sections from fresh leaves were mounted between two layers of Kapton® polyimide film for elemental micro x-ray fluorescence (μ-XRF) spectroscopy at the Cornell High Energy Synchrotron Source (CHESS) facilities. Two beamlines were used upon availability. Whole leaves were scanned at the F3 bending-magnet beamline, equipped with a double crystal Si(111) monochromator ($\Delta E/E \sim 10^{-4}$) and a single-bounce monocapillary lens (capillary PeB605; Huang *et al*., 2014) that focused the beam to a spot size of 20 μm diameter. Leaf transverse sections

were scanned at the G3 undulator beamline, which employs synthetic W/B_4C multilayer monochromaters ($\Delta E/E \sim 10^{-2}$) for increased flux. A different single-bounce monocapillary was used in this setup (s/n) which focused the beam to a spot size of 10 μm diameter. Fluorescence spectra were obtained at 11.2 keV using a 384 element Maia detector (Kirkham *et al*., 2010) placed perpendicular to the incident beam and situated at 2mm from the sample. Samples were scanned horizontally at 20 μm step intervals and fluorescence was captured for 1, 5 or 10 ms per step on whole leaf and transversal section samples, as needed. The captured XRF spectra were analyzed using the dynamic analysis (DA) method to obtain elemental maps using the software GeoPIXE v7.1 (Ryan, 2000). The incident flux was calibrated using reference films of known mass. This flux, in turn, was used to calculate elemental mass from XRF peak areas using a fundamental-parameters approach (Ryan *et al*., 2014).

Elemental abundance, a dimensionless number that provides a metric for quantifying the spatial distribution of each element in leaves differing in size and age, was calculated in the following way. The elemental masses for Zn, Ca, and K for each leaf were retrieved as ppm per scanned spot area. Estimated mass per scanned spot area was retrieved assuming that cellulose was the major organic component within each scanned area. This assumption is consistent with prior stoichiometric measurements of intact eudicot leaves, which show that organic carbon is the most abundant element in leaves. The elemental abundance per surface area scanned was calculated by dividing ppm of each element per surface area by estimated dry mass per surface area. This procedure normalized the abundance of each

element with respect to the abundance of total dry mass. Changes in actual leaf dry mass as a function of leaf development were additionally determined by weighing dried leaves.

It is important to note that, as in most eudicots leaves, poplar leaves manifest significant anatomical heterogeneity (resulting from differences in the volume fractions of air, cell walls, and cytoplasm). This heterogeneity in tandem with the fact that leaves were dehydrated precluded attempts to measure elemental concentrations in conventional units such as μM.

Results

Leaf elemental maps showed a distribution that varied both spatially across the leaf blade and temporally as gauged by elemental distributions from LPI 1 to LPI 10 (Figure 2.1). We focus here on Zn, Ca, and K distributions because these elements manifested the most noticeable changes throughout leaf development (see Appendix for the elemental distributions of additional elements detected). The images shown in Figure 2.1 reveal the distributions and abundances of all three of these elements and the ontogenetic changes in these variables of interest. The spatial distribution of each of the three elements during different stages of leaf development are discussed in detail below (and are shown in Figures 2–3 and Figure 2.5). The co-accumulation of two or more elements obscures the distribution of single elements. For example, the co-accumulation of K and Zn obscures the accumulation of each of these elements particularly in the apices of lamina teeth and the basal regions of juvenile leaves (Figure 2.1A–B).

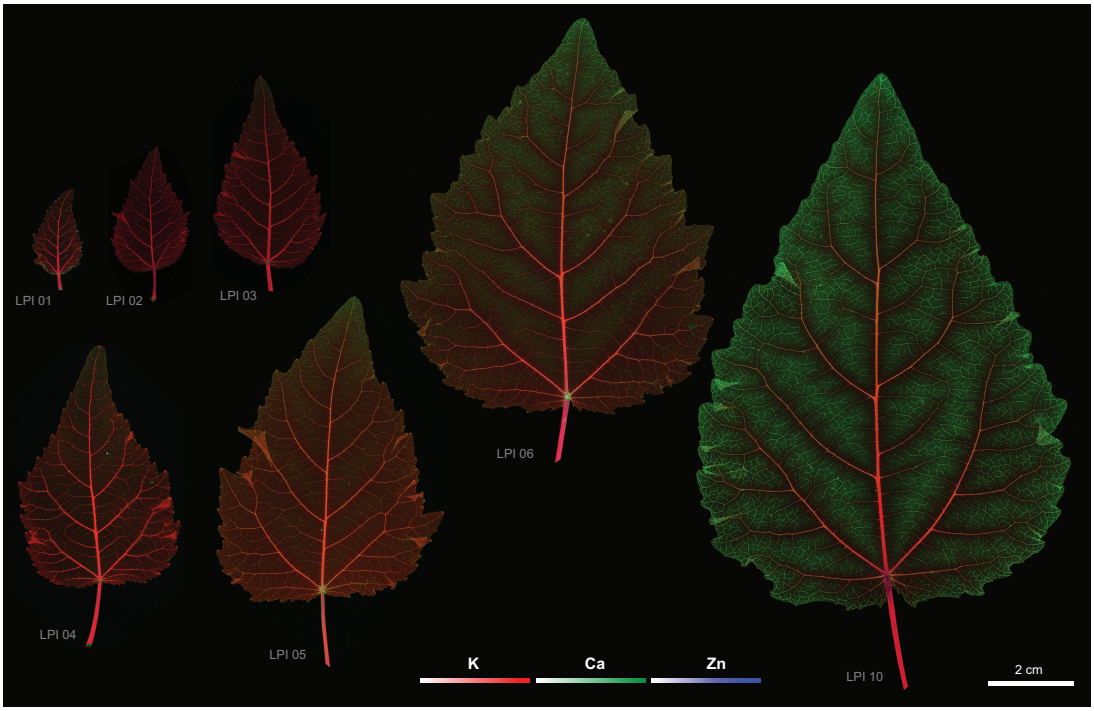

Figure 2.1. Composite μ-XRF maps of the abundance of K (red), Ca (green) and Zn (blue) (see color gradients at the bottom of the figure) in developing leaves of grey poplar at leaf plastochrons (LPI) 1 (CHESS scan cycle/run 2014–2/102), LPI 2 (CHESS 2014–2/107), LPI 3 (CHESS 2014–2/120), LPI 4 (CHESS 2014–2/110), LPI 5 (CHESS 2014–3/1530), LPI–6 (CHESS 2014–3/1534), and LPI 10 (CHESS 2014–2/494). Fluorescence intensities of elements were normalized using reference standards, and provide a direct comparison of element abundance across representative leaves for each of the plastochrons shown (see centered scale at bottom for each of the three elements). Maximum pixel brightness corresponds to maximum abundance for each element. Note basipetal accumulation of Ca as leaves mature as shown by green coloration in leaves LPI 05, LPI 06, and LPI 10. Insert A highlights areas characterized by high abundance of Ca and Zn in teeth apices in LPI 1. Insert B highlights areas characterized by high abundance of Ca and Zn at the base of LPI 2 (see arrows). Insert C highlights the absence of co-localized Ca and Zn in teeth apices LPI 10 (see arrows).

Zinc distributions in leaf development

Elemental maps indicated the preferential distribution of Zn adjoining the leaf vasculature (Figure 2.2A–E). In early developing leaves, the highest Zn abundance was observed at the apices of leaf teeth (Figure 2.2B), in the bundle sheath surrounding the midvein and secondary veins (Figure 2.2A-B), and in the upper and lower epidermis. Similar distribution patterns were observed for leaves between LPI 1 and 4, but the accumulation of Zn decreased in teeth apices with increasing LPI (compare Figure 2.1A–B with Figure 2.1C). Fully mature leaves (at LPI 10) no longer exhibited high Zn abundance in teeth apices (Figure 2.2C), but showed a more pronounced Zn accumulation surrounding veins of higher order and, once again, in the upper and lower epidermis (Figure 2.2D–E). As leaves matured, Zn continued to accumulate in these regions leaving a ghost-like image pattern in the midvein and higher order vascular strands owing to the greater abundance of Zn in these cells (Figure 2.2C–E). Because transverse sections made from fresh leaves and immediately mounted for analysis yielded the same patterns (albeit with lower spatial resolution), it was unlikely that Zn accumulation around the vasculature was due to element displacement toward the veins during whole leaf dehydration.

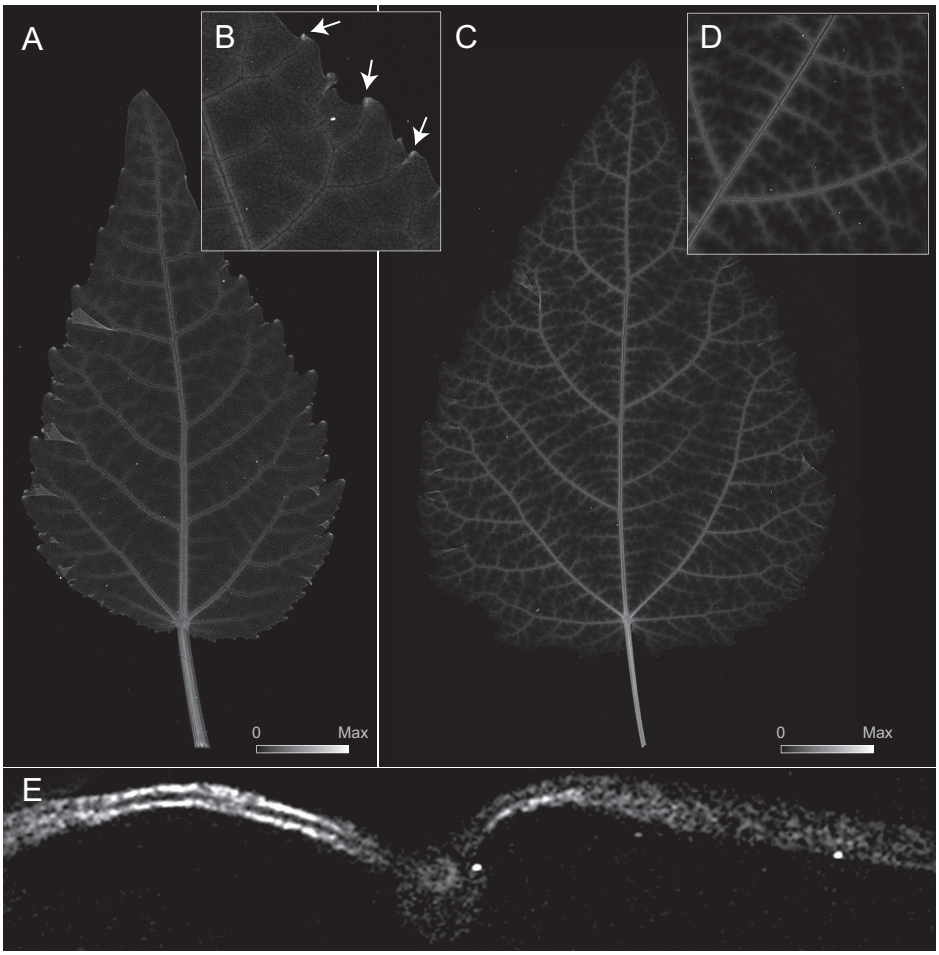

Figure 2.2. Elemental μ-XRF map for Zn abundance for developing leaves of gray poplar. Image intensity matches element abundance (see scales in A and C). **A**. Early developing leaf at LPI 3. Maximum Zn = 1615 μg Zn/g dry mass. **B.** Selected area from Figure 2.2A highlighting the localization of Zn at leaf teeth apices (see arrows). **C**. Fully mature leaf at LPI 10. Maximum Zn = 1305 μg Zn/g dry mass. **D.** Detail of Zn localization around major veins at LPI 7. **E**. Transversal section of a fully mature leaf at LPI 10 showing the accumulation of Zn in the upper and lower epidermis and in the peripheral vasculature of the midvein.

Calcium distributions in leaf development

Elemental maps indicated that Ca was highly concentrated in major veins as well as in teeth apices of early developing leaves (see arrows Figure

2.3A). Whereas the average abundance of Ca in major veins of the LPI 1 leaf was one-half that in teeth apices, the abundance of Ca within the leaf lamina was approximately one-half that of the midvein. The enhanced accumulation of Ca in major veins is observed as peaks in Ca abundance along the leaf longitudinal transects shown in Figure 2.4.

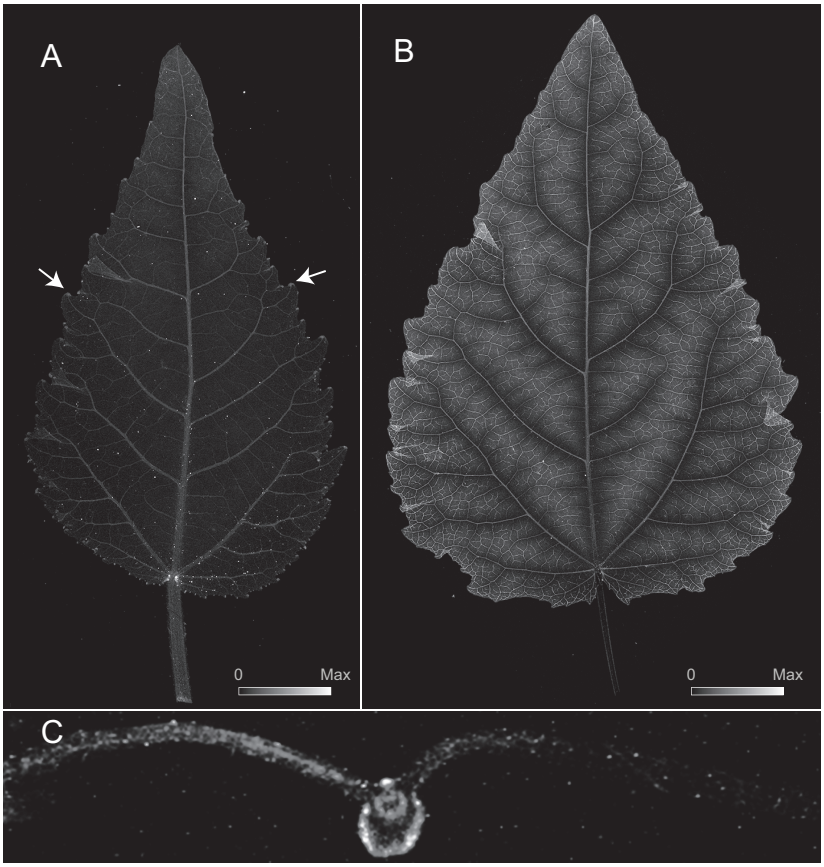

Figure 2.3. Elemental μ-XRF map for Ca for developing leaves of gray poplar. Image intensity matches element abundance (see scales in A and B). **A.** Early developing leaf at LPI 3, showing Ca localization teeth apices (see arrows) and major veins. Maximum Ca = 10625 μg Ca/g leaf dry mass. **B.** Fully mature leaf at LPI 10 showing the localization of Ca in higher order veins and in the mesophyll as seen from above (see C for a transverse section). Maximum Ca = 10670 μg Ca/g leaf dry mass **C.** Transversal section of fully mature leaf at LPI 10 showing Ca in mesophyll, the peripheral tissues in the midvein, and peripheral tissues of the midvein vascular strand.

With increasing LPI, the marked difference in Ca abundance between teeth apices and leaf veins decreased, and the accumulation of Ca in the lamina became more noticeable (see Figure 2.3B; see also Figure 2.1). At LPI 3, the accumulation of Ca in the laminar tissues as well as in minor veins increased towards the apex (Figure 2.3A) as illustrated by the deflection in the longitudinal Ca abundance transect in Figure 2.4. Contrastingly, the abundance of Ca in leaf teeth apices decreased at LPI 3 (see Figure 2.1). By LPI 6, more than half of the leaf lamina shows increased amounts of Ca (Figure 2.4). The increasing frequency of peaks observed in the Ca abundance transect shown for LPI 6 in Figure 2.4 indicates an enhanced accumulation of Ca in corresponding minor veins towards the leaf apex. At this developmental stage, the abundance of Ca in leaf teeth no longer differed from that of surrounding tissues (see leaf at LPI 6 in Figure 2.1).

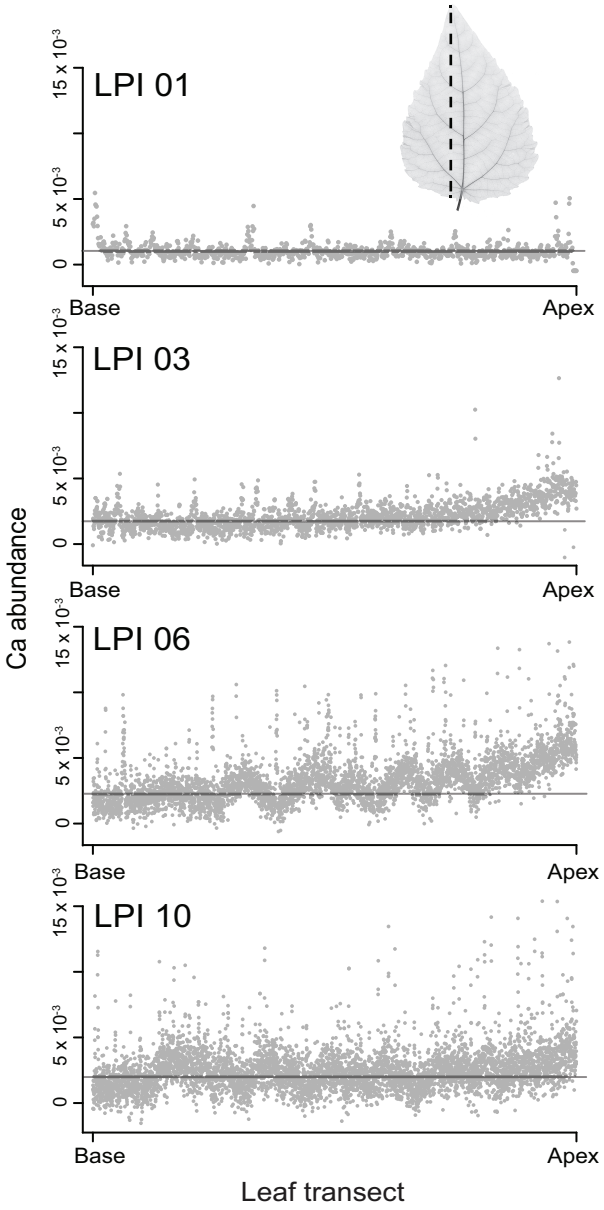

Figure 2.4. Variation in Ca abundance (i.e., ppm Ca/ppm dry mass) along longitudinal transects across gray poplar leaves in different stages of development (LPI 1, LPI 3, LPI 6, and LPI 10) (see dashed line in upper insert for transect orientation across each leaf). Solid lines in each graph indicate average leaf Ca abundance for each leaf. Ca abundance peaks in each graph correspond to the locations of major veins; peak maxima increase as leaves mature from LPI 1 to LPI 10. Ca accumulation occurs basipetally (from the apex to the leaf base) (see also Figure 2.1).

Fully mature leaves showed a different distribution pattern compared to that of early developing leaves (Figure 2.3B). Whereas Ca accumulation was noticeable only in major veins of early developing leaves, the Ca abundance in veins of third, fourth, and even fifth order in fully mature leaves averaged twice that in primary and secondary veins (Figure 2.3B).

The difference in Ca abundance between the major veins and the lamina was not as marked. Specifically, Ca abundance in the lamina was ~20% lower than that in major veins, compared to a 50% difference observed in early developing leaves (see Figures 3A–B). The maximum Ca abundance for all non-vascular leaf tissues was highest between secondary veins and lowest in proximity to primary and secondary veins. A leaf cross-section that included the primary veins indicated that Ca is localized in the bundle sheath and the external-most regions of the midvein (Figure 2.3C). Outside these regions, Ca was distributed within the mesophyll.

Potassium distributions in leaf development

The distribution of K in leaves was far more homogeneous than that observed in the elemental maps of Zn or Ca, and was largely invariant across leaf development (Figures 5A–C). K was more abundant in all vein orders than in the lamina, but its abundance decreased with increasing vein order (Figure 2.5A–B). This pattern was observed in both early developing and fully mature leaves (see Figure 2.5A–B). The difference in K abundance between the lamina and veins was most pronounced in fully mature leaves, and was 10 times lower in the lamina than in the larger veins. We compared vein thickness to K abundance in veins and found that it did not fully match estimates of leaf thickness (compare Figures 5D-E). The internal distribution of K indicated that this element was much more prevalent in the epidermis, mesophyll, and tissues surrounding veins than in either the xylem or phloem (Figure 2.5C).

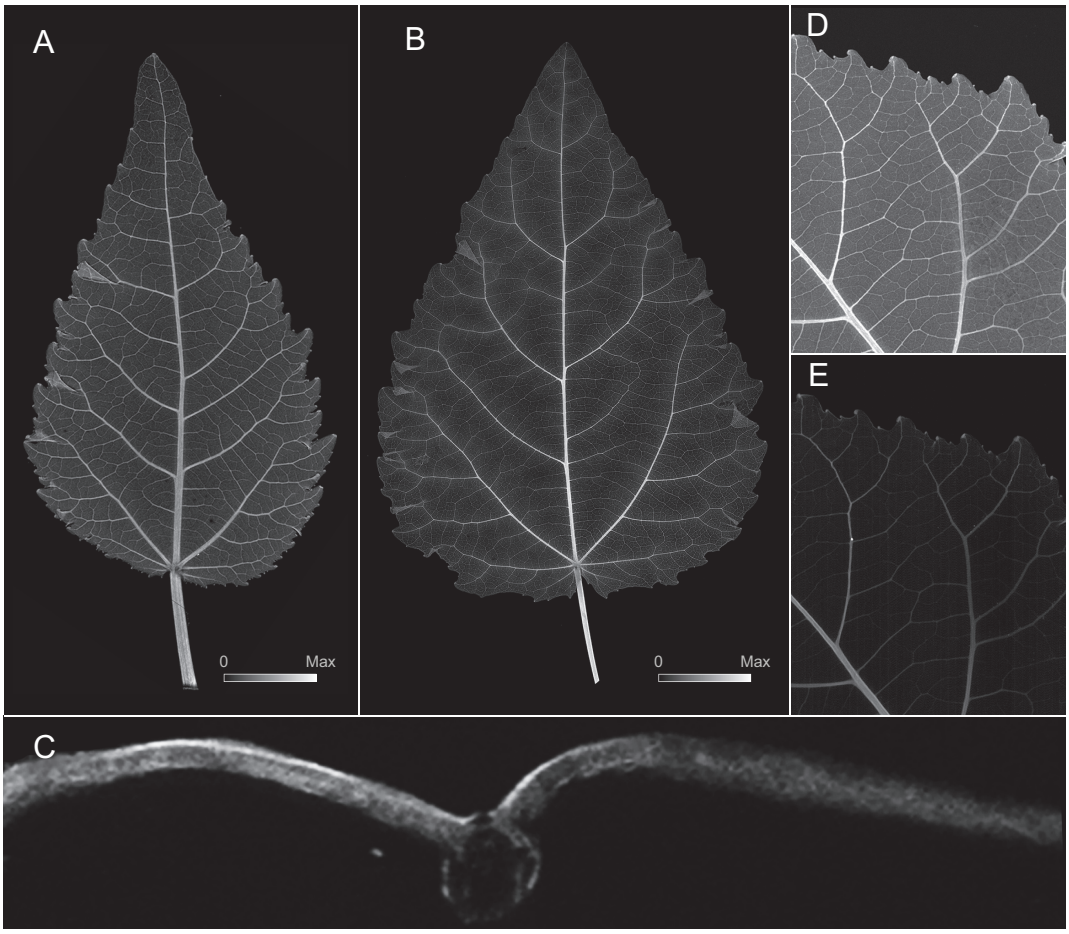

Figure 2.5. Elemental μ-XRF map for K for developing leaves of gray poplar. Image intensity corresponds to element abundance (see scales in A and B). A. Early developing leaf at LPI 3. Maximum K = 57290 μg K/g leaf dry mass. B. Fully mature leaf at LPI 10. Maximum K = 55900 μg K/g leaf dry mass. C. Transverse section of fully mature leaf LPI 10 showing accumulation of K in the upper epidermis and mesophyll. D. Detail of K accumulation in a developing leaf at LPI 4. E. Cellulose distribution as shown in D based on predicted leaf thickness (using μ-XRF data and assuming cellulose as the primary source of dry mass absorption). D.–E. The abundance of K in veins appears high because the veins are denser than lamina tissues.

Developmental changes

Poplar leaf growth conforms to a sigmoidal curve with an early exponential increase in leaf mass and area that plateaus once leaves reach plastochron 10. Leaf mass per area decreased in early development and reached a relatively constant value by plastochron 3 (Figures 6A–C).

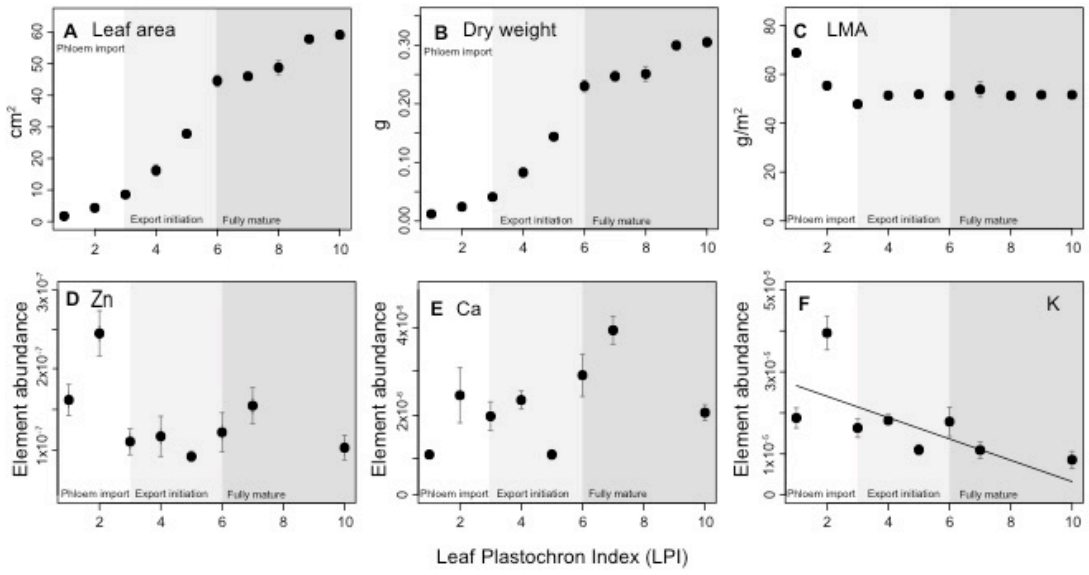

Figure 2.6. Leaf growth parameters and changes in element abundance (i.e., ppm element/ppm dry mass) in relation to leaf development and the transition from phloem importing (a) to phloem exporting (c) (b denoted the LPI during the transition from phloem importing to exporting) (see notation at the bottom of each graph). **A.** Leaf area **B.** Leaf dry weight. **C.** Leaf mass per area (LMA). **D.** Zn abundance. **E.** Calcium abundance. **F.** Potassium abundance (diagonal line denotes ordinary regression line for abundance vs. LPI).

The abundance of elements followed different patterns throughout leaf development. Whereas the total abundance of Zn, Ca and K increased as leaves expanded to full maturity, the relative abundance of these elements varied (Figure 2.6D–F). Zinc abundance decreased throughout leaf

development, but not statistically significantly (Figure 2.6D). Ca abundance remained fairly constant throughout the leaf plastochrons examined in this study (Figures 6E). In contrast, the average abundance of K in leaves decreased significantly with leaf growth ($r^2 = 0.40$, $P = 0.05$) (see Figure 2.6F).

Discussion

Developing leaves undergo a number of structural and biochemical changes as they reach full maturity. Here, we document the preferential spatiotemporal distribution of Zn, Ca, and K throughout a developmental sequence at the whole organ level, and correlate the compartmentalization of Ca in leaves with phloem maturation. The conversion from sink to source marks a fundamental transition in leaf physiology that involves the coordinated decline of respiration and leaf growth rates, and an increase of carbon fixation rates needed to create a positive carbon balance and reverse the direction of phloem flow (Dickmann, 1971; Turgeon, 2006). These metabolic changes require the formation of functional stomata, substomatal chambers, and intercellular spaces that enable gas exchange, as well as the maturation of minor veins that mediate sugar export from the leaf (Turgeon, 1989, 2006), which also provides the driving force for transpiration delivering water and solutes via the xylem.

Changes in leaf anatomy have been well characterized in species of poplar and have been linked to photosynthetic import and export capacities using the leaf plastochron index system (Dickmann, 1971; Larson *et al.*, 1972; Isebrands & Larson, 1973; Dickson & Larson, 1981). Our study contributes to this database by reporting that the spatial and temporal distributions of Zn,

Ca, and K in grey poplar changes in a manner that is consistent with major metabolic and developmental transitions in leaf ontogeny.

Calcium in the leaf lamina

Poplar leaf development resembles that of many other eudicots in that growth is both structural and expansive (Pantin *et al.*, 2012). Before LPI 0, the basic anatomical organization of the leaf lamina is established and leaf growth is determined by cell division and structural growth. Cell expansion begins once the leaf reaches LPI 0, and cell separation is noticeable only in the spongy mesophyll by LPI 1. At LPI 3, intercellular spaces in connection to functional stomata are found only at the leaf tip and spatially coincide with enhanced photosynthetic rates and the onset of sugar export (Dickmann, 1971; Isebrands and Larson, 1973). The development of intercellular spaces and sugar export are coordinated spatially and proceed basipetally until leaf maturation is attained at LPI 6 (refer to Figure 2.6).

Calcium accumulation in minor veins at the leaf tip (see Figure 2.1) is spatially and temporally consistent with the onset and progression of sugar export from the leaf. The accumulation of Ca in minor veins corresponds to minor vein maturation and the enhancement of the transpiration stream required for the onset of photosynthate export. It has long been thought that Ca is exclusively transported through the transpiration stream as transpiration rates are closely associated to leaf Ca content (Fricke *et al.*, 1995; Storey & Leigh, 2004; Kerton *et al.*, 2009; Gilliham *et al.*, 2011). However, Ca is required for juvenile organ development and phloem is the primary transport tissue in juvenile organs, such as leaf primordia. As

intercellular spaces develop and become connected to functional stomata during leaf expansion, transpiration and carbon fixation rates increase locally and enhance Ca availability in areas of the leaf transitioning from sink to source. This process also reflects the functional maturation of xylem and phloem in minor veins, even though the formation of minor veins precedes the initiation of cell separation. The vascular strands that form and free-ending veins are continuously connected at the leaf apex by LPI 0 (Isebrands and Larson, 1973). However, the structural and functional development of sieve elements in minor veins is synchronized with sugar export, or briefly predates the initiation of sugar export (Fellows & Geiger, 1974).

Calcium is an essential plant macronutrient, a crucial regulator of plant growth, and is involved in key structural and signaling processes (Hirschi, 2004). In leaves, Ca moves apoplastically and accumulates with leaf age. Free Ca content however is tightly controlled intracellularly because it is involved in numerous signaling processes triggered by changes in its concentration at the nM scale (McAinsh & Pittman, 2008). Because Ca is not redistributed through the phloem (Karley & White, 2009) assimilation into the cell wall and sequestration into trichomes, idioblasts and cell vacoules for long-term storage is essential for leaf function (Karley *et al.*, 2000; Karley & White, 2009). The distribution of Ca in mature poplar leaves reported here is consistent with other studies reporting the preferential accumulated of Ca in the mesophyll of eudicots leaves (Figure 2.3; (Storey & Leigh, 2004; Vogel-Mikuš *et al.*, 2008; Kerton *et al.*, 2009; Conn *et al.*, 2011; Gilliham *et al.*, 2011). The Ca content in minor veins reported here is consistent with the

accumulation of abundant calcium oxalate crystals, which are typically found in bundle sheath cells of poplar leaves.

Leaf teeth apices, and Ca and Zn in early development

Noticeable amounts of Ca and Zn are associated with the hydathodes in major vein terminations of early developing leaves (see Figures 1–3). As leaves grow, the high abundance of these elements decreases within hydathodes and match those seen in major veins after LPI 4. This pattern is consistent with the increases in gas exchange and carbon fixation rates towards the margin of toothed leaves during early development (Baker-Brosh & Peet, 1997; Royer & Wilf, 2006). Specifically, highly transpiring leaf-margins will experience increased water flux through major veins during early development, which will result in the accumulation of elements. However, this expectation does not fully explain the abundance of elements specifically in hydathodes or the decrease in elemental abundances attending leaf growth. An alternative scenario is that the accumulation of Ca and Zn is a byproduct of guttation and the exudation of water out of the leaf, which results in the accumulation of elements near the leaf margin. A third possibility may involve an active accumulation of elements in hydathodes that enhances the osmotic potential at secondary vein terminations. Active transport of solutes from the transpiration stream and into phloem parenchyma and epithem cells of leaf teeth has been shown to occur in other species of poplar (Vogelmann *et al.*, 1985; Wilson *et al.*, 1988), and is thought to contribute to maintaining water flow velocities in xylem vessels (Wilson *et al.*, 1991). However, mechanisms describing the targeted movement of ions

into hydathodes have yet to be described. Further work is required to resolve which among these possibilities, if any, is correct.

Potassium abundance and leaf age

Potassium is the second most abundant cation in the cytosol and is functionally related to a broad range of core cellular processes including pH maintenance, enzyme activation, cation/anion balance, and osmoregulation (Hawkesford *et al*., 2011). Our data show that K is preferentially located in the mesophyll of fully mature leaves, and that the average abundance of K decreases with leaf age (see Figure 2.6). Potassium is typically prevalent in high concentrations in dividing tissues, where it is closely involved in the synthesis of structural proteins and in regulating turgor-driven expansion processes (Szczerba *et al*., 2009). Long distance movement of K occurs through xylem and phloem. Since early developing tissues have overall low transpiration rates, it is likely that most of the K present in young leaves passes through the phloem and is distributed throughout the leaf symplastically. As leaves grow and their sink capacity declines, import rates decrease, which can in part explain decreasing K abundances with leaf growth.

Most elements become more readily available in leaves as they mature and transpiration rates increase. Yet, most are typically remobilized in order to avoid hyper accumulation, in response to metabolic demands in sink tissues, and during organ senescence. Plants growing under K-deprived conditions typically exhibit relocation of K from old to developing tissues. Potassium is closely linked to sugar export; it contributes to the osmotic

potential in phloem sap and is directly involved in sugar loading processes (Komor, 2000; Lalonde *et al.*, 2003). The expression of K^+ channels in minor vein phloem is controlled by photosynthate supply (Deeken *et al.*, 2000) and may be involved in increasing net export rates for K as leaves grow and contribute to the net decline in abundance observed in grey poplar.

Acknowledgements

This work is based upon research conducted at the Cornell High Energy Synchrotron Source (CHESS), which is supported by the National Science Foundation and the National Institutes of Health/National Institute of General Medical Sciences under NSF award DMR-1332208, using the Macromolecular Diffraction at CHESS (MacCHESS) facility, which is supported by award GM-103485 from the National Institute of General Medical Sciences, National Institutes of Health. We thank Dr. Leon Kochian (Cornell University) and two anonymous reviewers for valuable comments, and the Schlumberger Faculty for the Future Foundation for financial support (to MRC).

CHAPTER III

THE SCALING OF THE HYDRAULIC ARCHITECTURE IN POPLAR LEAVES

Mónica R. Carvalho, Robert Turgeon, Tom Owens, Karl J. Niklas
Plant Biology Section,School of Integrative Plant Science, Cornell University, Ithaca, NY 14853 (USA).
Published: *New Phytologist* 214 (1): 145–157, 2017

Summary

We report the hydraulic interconnectivity of the phloem and the xylem in the mature leaves of the model tree species, *Populus x canescens*, by describing the scaling relationships across all seven of the hierarchical orders of vasculature. Using a combination of electron and light microscopy, we found that (1) the conductive areas of phloem and xylem increase from minor veins toward the petiole; (2) the sum of all phloem (and xylem) conductive areas for each vein order exponentially increases from the petiole towards minor veins; (3) sieve tube (and vessel) member lengths match vein size, such that the volume of individual sieve tube (and vessel) members increases from minor veins toward the petiole; (4) phloem scaling is indicative of a system in which minor veins (5–7) serve as photosynthate collectors whereas vein orders 1–3 serve as a rapid export system; (5) an isometric (one-to-one) scaling relationship exists between phloem and xylem conductive areas across all vein orders, and (6) the scaling of

phloem and xylem conductive areas is consistent with branching systems modeled according to da Vinci's rule (i.e., the conservation of cross sectional areas). These data provide all the information required to mathematically model eudicot leaf hydraulics.

Key words: allometry; anatomy; form-function; leaf; morphology; Münch's Pressure Flow hypothesis; phloem; scaling; xylem

Introduction

Plant vascular tissues provide for the resource allocation and the signaling processes required for survival and growth. In leaves, these tissues must ensure an effective distribution of water throughout the leaf lamina and an adequate collection-export system for sugar to avoid water deficits and an excessive accumulation of photosynthates. Xylem provides the water required to compensate for water losses during CO_2 uptake. Concurrently, this tissue must supply the phloem with the water needed for maintaining the osmotic-regulated hydrostatic pressure gradient between source leaves and sinks, which is essential for sugar export (Münch, 1930; Turgeon & Ayre, 2005).

Despite the structural and physiological linkages between the phloem and the xylem, most of the literature dealing with leaf hydraulics focuses on the xylem; because, in addition to providing the lamina with mechanical support (Niklas, 1999), the physics of water flow through hollow conduits is well established. For example, xylem geometry (the radii and numbers of vessels) is closely related to water transport efficiency (Roth-Nebelsick *et al.*, 2001; Sack & Scoffoni, 2013). Wide vessel member lumens such as those in major veins enable

greater hydraulic conductivity in accordance with Hagen-Poiseuille flow (Sperry *et al.*, 2005; Sommerville *et al.*, 2012), although they also increase the susceptibility to embolism (Brodribb *et al.*, 2016) due to the number of inter-conducting pit membranes present in larger vessels (Hargrave *et al.*, 1994; Wheeler *et al.*, 2005; Lens *et al.*, 2011). Similarly, the length of veins per leaf area (VLA) is linked to enhanced hydraulic conductance and broadly correlates with gas exchange rates (Sack & Frole, 2006; Brodribb *et al.*, 2007; Boyce *et al.*, 2009; McKown *et al.*, 2010). It is also clear that the architecture of leaf venation networks is related to a large number of other functionalities (Roth-Nebelsick *et al.*, 2001). For example, the topology of looped vascular networks as opposed to less interconnected systems confers redundancy in transport pathways and hence resilience to damage (Wylie, 1951) as well as flexibility in coping with fluctuating loads (Katifori *et al.*, 2010; Corson *et al.*, 2010). Such interconnectedness in turn provides an advantage against herbivory (Haberlandt, 1914; Wagner, 1979) as well as higher hydraulic conductance due to increased vascular connectivity (Roth-Nebelsick *et al.*, 2001).

Although phloem and xylem are physically and developmentally linked in vascular bundles and many structural features that relate xylem to hydraulic performance should also apply to phloem, i.e., conduit dimensions (Russin & Evert, 1984), the form-function relationships affecting phloem flow are far less known compared to those of the xylem in part because phloem is a living tissue that operates under positive pressure. This feature makes direct flow measurements inherently difficult (see however Knoblauch *et al.*, 2016). Observations must be made *in vivo* using non-destructive techniques and taking care not to severe the phloem continuum, since this would lead to a pressure loss, sieve plate occlusion, and translocation disruption (Oparka & Turgeon,

1999; Knoblauch *et al.*, 2016). Current methods used to quantify phloem translocation rates include the injection of fluorescent dyes (Savage *et al.*, 2013), magnetic resonance imaging (Windt *et al.*, 2006), and radioisotopes (Babst *et al.*, 2005). Among these techniques, only the first has been used to record flux rates in individual leaf vascular bundles.

As a consequence, much of what is currently known about phloem hydraulics is based on biophysical inferences. For example, assuming that Hagen-Poiseuille flow parameters hold true, phloem conductance should scale with the diameter and length of sieve tube members or sieve elements (Thompson, 2006; Knoblauch & Oparka, 2012), although flow velocity measurements do not necessarily match conductance estimates (Mullendore *et al.*, 2010). Adding to difficulties, recent evidence indicates that phloem anatomy can change during plant growth to reduce axial resistance by increasing sieve pore size (Knoblauch *et al.*, 2016), yet highlighting a basic form-function coupling in phloem structure. Moreover, sieve tube members also impose an upper boundary for sugar transport rates at loading sites. Because sugar loading and increased sugar concentration rapidly elevates phloem sap viscosity, high sugar content in sieve tubes can reduce phloem translocation (Hölttä *et al.*, 2009), thereby down-regulating photosynthesis (Nikinmaa *et al.*, 2013). Conversely, at low sugar concentration, the osmotic potential in sieve tubes would be insufficient to generate the hydrostatic pressure differential between sources and sinks required for the bulk flow of phloem sap (Jensen *et al.*, 2013). Therefore, it is likely that the geometry of conduits follows the interplay between sugar concentration, viscosity, and hydrostatic pressure.

Phloem cross-sectional conductive areas have been reported to scale with those of xylem in the stems and petioles of various species (Jyske & Teemu, 2014; Smith *et al*., 2016), indicating a structural or developmental link between both tissues. In this context, phloem can act as a capacitor and radially transfer water into the transpiration stream during the day (Zweifel *et al*., 2000; Sevanto *et al*., 2011; Pfautsch *et al*., 2015b). Conversely, the movement of water from the xylem into the phloem is required for fueling phloem sap transport down a hydrostatic pressure gradient. In source leaves, the phloem effectively competes with the transpiration stream for the water required to drive the bulk flow of sap down sieve tubes. By the same token, gas exchange rates (and thus carbon fixation) are also dependent on transpiration. The close physiological coupling between photosynthesis and water transport undoubtedly requires a functional coordination between xylem and phloem across all plant organs.

In order to close the gap between our understanding of phloem functionality and its relationship to water flow in the xylem, we report the length and functional cross-sectional area of individual sieve tube members and vessel members across all seven orders of veins in the mature leaves of the symplastic loading tree species *Populus x canescens* (Zhang *et al*., 2014). We also report how these metrics scale with respect to one another to quantify the hydraulic architecture of xylem and phloem in mature leaves and to test whether the this architecture complies with Murray's law (Murray, 1926) or da Vinci's rule (Richter, 1980), which have been used to determine whether a branching system optimizes hydraulic flow (Canny, 1993; McCulloh *et al*., 2003; Price *et al*., 2013). The data to be presented indicate that the scaling of the phloem is tightly coupled

to that of the xylem in a manner that provides for an efficient influx-efflux system.

Materials and Methods

Leaf material

Ten clones of *Populus x canescens* were grown under controlled conditions to reduce intraspecific and developmental variability. Stem cuttings were rooted in 1-gallon pots with Cornell mix (Boodley & Sheldrake, Jr., 1982) and were grown under 800 μmol photons/m^2 of PAR, with 18 h/6 h day/night cycles, and day/night temperatures of 24˚C/18˚C. Plants were watered daily and fertilized 5 times a week using a 15/15/15 complete nutrient solution. Saplings were grown for 3-4 weeks or until the oldest leaves reached leaf plastochron (lp) 25 (Larson & Isebrands, 1971).

Vein cross-sectional area measurements were obtained from seven fully mature leaves at lp 10. Leaves were collected and photographed using a Canon T2i camera equipped with a 60mm macro lens. As in most angiosperms, poplar leaves exhibit a hierarchical-anastomosing vascular system, in which two distinct vein categories (major and minor veins) can be recognized (Sack *et al.*, 2012; Sack & Scoffoni, 2013). Based on previous anatomical descriptions of congeneric species (Russin & Evert, 1984, 1985), seven hierarchical orders of leaf veins were designated, following their vascular anatomy and standards established in the Manual of Leaf Architecture (Ellis *et al.*, 2009). Major veins include orders 1^{st} – 3^{rd}, while minor veins were divided into orders 4^{th} – 7^{th}. For each leaf, 10 representative portions were selected to characterize all seven vein orders and to visualize their anatomical details. These portions included 5 mm-long segments

of the petiole and primary vein sectioned at the leaf base; 5 mm-long fragments of the basal-most and apical-most secondary veins sectioned at their junction with the midrib, and six randomly selected leaf fragments that included all other remaining vein orders (3rd–7th). For the latter six, contiguous 2-cm^2 leaf fragments were cut and their adjoining edges marked for vein order identification and length measurements (see below). Leaf fragments were embedded in TissueTek® OCT fixative (Electron Microscopy Sciences) and 7-10 μm thick transverse sections were made using a cryomicrotome (Leica Microsystems). Sections were stained with 1% toluidine blue in aqueous solution and were observed under an Olympus BX60 microscope coupled to a Sony Progressive 3CCD camera. Images were taken at 800-1200X; for the largest veins, multiple overlapping images were taken and were subsequently merged into whole-vein images.

Additional sets of leaf fragments from two leaves were prepared for transmission electron microscopy. Fragments were fixed in 2% gluteraldehyde-cacodylate solution for 12 hours at 4˚C, stained with 1% osmium tetroxide for 1 hour, and dehydrated in a 10-30-50-75-100% ethanol series before embedding in Spur's resin (Spur, 1969; Electron Microscopy Sciences). Transverse 100 nm thin sections were made using a Leica UTC Ultramicrotome (Leica Microsystems) and were analyzed under a FEI T12 Spirit transmission electron microscope equipped with a LaB6 120 kV filament. Images were acquired using a coupled SIS Megaview CCD camera.

Sieve tube member (STM) length was measured from paradermal images of leaf vasculature obtained using multiphoton microscopy. Five leaf segments comprising the petiole, the base of the primary vein, and three 1 cm^2 leaf sections that included all other vein orders were collected from two leaves and were

stained following the protocols of Truernit et al. (2008). Additional staining with 0.05% aniline blue in 100 mM potassium phosphate buffer for 15 minutes was used for sieve plate identification. Samples were visualized under a Zeiss LSM880 confocal/multiphoton inverted microscope (Zeiss i880) using an excitation wavelength of 760 nm.

Vessel member (VM) length was quantified from single-vein macerations. Representative fragments of the petiole and vein orders 1–4 were dissected from two leaves. Because vein orders 5th–7th could not be individually isolated, small leaf fragments that excluded all other vein orders were also collected. All fragments were digested in a 1% HCl–50% ethanol solution for 24 h, rinsed, and incubated in 5% ammonium peroxide for 24 h. Samples were macerated directly on microscope slides, stained with 1% toluidine blue in aqueous solution and visualized under an Olympus BX60 microscope coupled to a Sony Progressive 3CCD camera. Figure 1 shows representative anatomical preparations. STM and VM diameters were statistically numerically comparable within each vein order when samples were prepared using different techniques and protocols. This was taken as evidence that tissue shrinkage and distortion (and the potential for corresponding measurement errors) were uniform across the multiple preparations.

Area measurements

Leaf area and vascular conductive area measurements were made using ImageJ (Rasband, 2016). Xylem and phloem transverse areas were measured from two 2nd order, five 3rd order, and fifteen 4th – 7th order veins per leaf using light microscopy images. Xylem lumen conductive area (A_x) was quantified as the

cross-sectional area covered by tracheary elements in a vein (cell wall transverse areas were excluded). Mean A_x values were computed for each vein order for each of the seven sample leaves.

Total phloem conductive area (A_{phl}) was measured as the sum of the areas of all functional STMs in each vein (the apoplastic components of STMs were excluded). STMs were identified and differentiated from companion cells or phloem parenchyma based on their low cytoplasmic density, occurrence of P-proteins and P-organelles, and the parietal placement of the endoplasmic reticulum (Figure 3.1L; Russin & Evert, 1984, 1985). For each vein order, the fraction of phloem area covered by STMs (f_{phl}) was determined using TEM images of representative veins. Conductive areas for individual STMs (A_{STM}) of each vein order were computed using the minimum cell diameter of at least 25 functional STMs, and mean A_{STM} values were then multiplied by the number of STMs to obtain A_{phl} of each vein. Minimum cell diameters were used because maximum or average diameters in even slightly oblique transverse sections would over-estimate A_{STM}. Whereas the numbers of STMs per vein were directly counted on the 3rd-7th vein orders, those of the petiole, 1st, and 2nd order veins were obtained from representative regions of each vein. Finally, A_{phl} was divided by phloem cross-sectional area to obtain the fraction of conductive area (f_{phl}) in each vein. These fractions were averaged to determine vein order-specific f_{phl} and to compute A_{phl} from phloem cross-sectional areas obtained from light microscopy images for the remaining sample leaves. This protocol was used because f_{phl} and A_{STM} could not be measured simultaneously owing to differences in size scale.

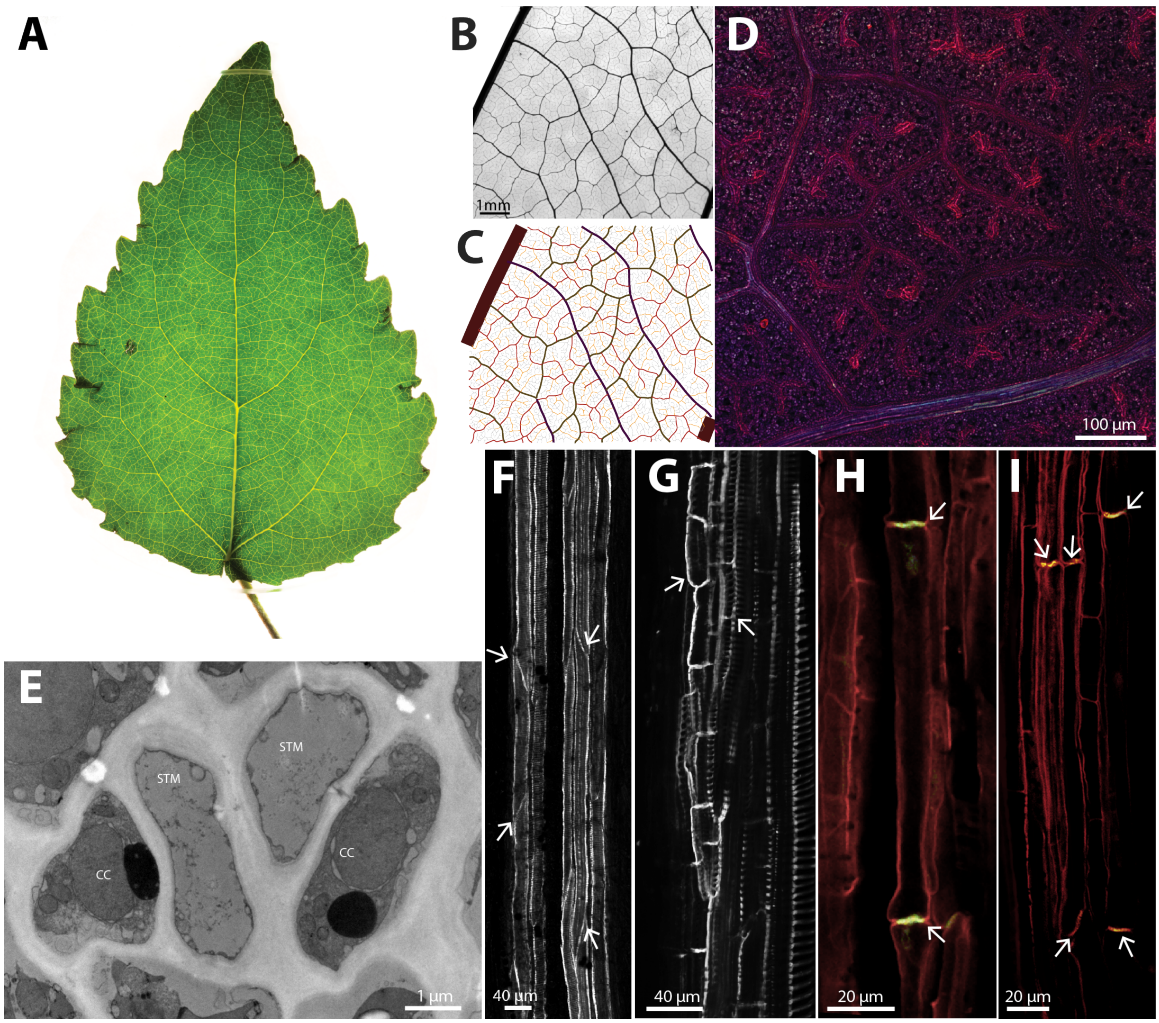

Figure 3.1. *Populus x canescens* leaf morphology and anatomy. A. Representative leaf at lpi 10, grown under controlled conditions. B. Cleared leaf fragment bounded by 3rd order veins. C. Vein orders 3rd-7th traced from (B). D. Paradermal optical section of leaf veins obtained using multiphoton microscopy and showing vessels of minor veins. E. Early metaxylem vessels of 1st order vein. Arrows indicate vessel terminations. F. Representative late metaxylem vessels (arrows) observed along 1st order vein. G. Longitudinal view of sieve tube members in primary vein. Arrows indicate sieve plates in green. H. Sieve tube members I. Transversal section of sieve tube members (STM) and companion cells (CC) in 4th order veins.

Length measurements

Whole-leaf photographs where used to quantify the numbers and lengths of 1st, 2nd, and 3rd order veins in each leaf. Veins of orders 4–7 were identified and mapped using six 2 cm^2 leaf fragments adjacent to samples used for measuring transverse areas (see above). The mean length and number of veins per leaf area were determined and used to compute total vein number (N_v) and total vein length (L_v) in each leaf. N_v values were used to compute total conductive areas for each vein order.

The lengths of STMs and VMs for each vein order were measured from optical sections obtained using multiphoton microscopy and vein macerations, respectively. Twenty-five length measurements of each cell type were taken from all vein orders and petiole. VM lengths taken from macerations were cross-validated with representative measurements taken from multiphoton microscopy preparations for consistency.

Geometric scaling

We compared the scaling relationships for STM and VM diameters across vein orders with two theoretical models (i.e., da Vinci's rule and the Murray's rule), both of which are purported to predict the optimal form of a branching hydraulic network and each of which has been reported to adequately describe different biological systems (LaBarbera, 1990; Canny, 1993; McCulloh *et al.*, 2003; Price *et al.*, 2013). Referring to Figure 3.2a, da Vinci's rule assumes that the cross sectional area of branching order *n* equals the sum of the total cross sectional areas of next higher order of branching such that

$$dn{=}do2n \qquad d_n = \frac{d_o}{2^{n/2}} \qquad \text{Equation 3.1}$$

where d_0 is the diameter of the branch order subtending the n–order of higher branching. Murray's rule assumes a conservation of hydraulic volume across all orders of branching such that

$$dn{=}do2n \qquad d_n = \frac{d_o}{2^{n/3}} \qquad \text{Equation 3.2}$$

Note that Equations 3.1 and 3.2 take the same general form but differ with respect to the exponent $n/2$ versus $n/3$ in the denominator. As a consequence, the manner in which d_n scales with respect to d_0 differs. We used Equations 3.1 and 3.2 to determine which of the two models adequately predicted the scaling of the diameters of higher vein orders across different levels of branching, successively using conduit diameters of the petiole and 1st – 4th vein orders as the 'parent branch' diameter (d_o). Regression protocols were used to determine if the observed diameters of veins were equivalent to those predicted by da Vinci's rule and by Murray's rule. Either model was rejected if the slopes of regression curves for predicted vs. observed cell diameter statistically significantly differed from 1.0. This criterion was applied to data collected from individual leaves and for the data pooled from all leaves sampled in the course of this study.

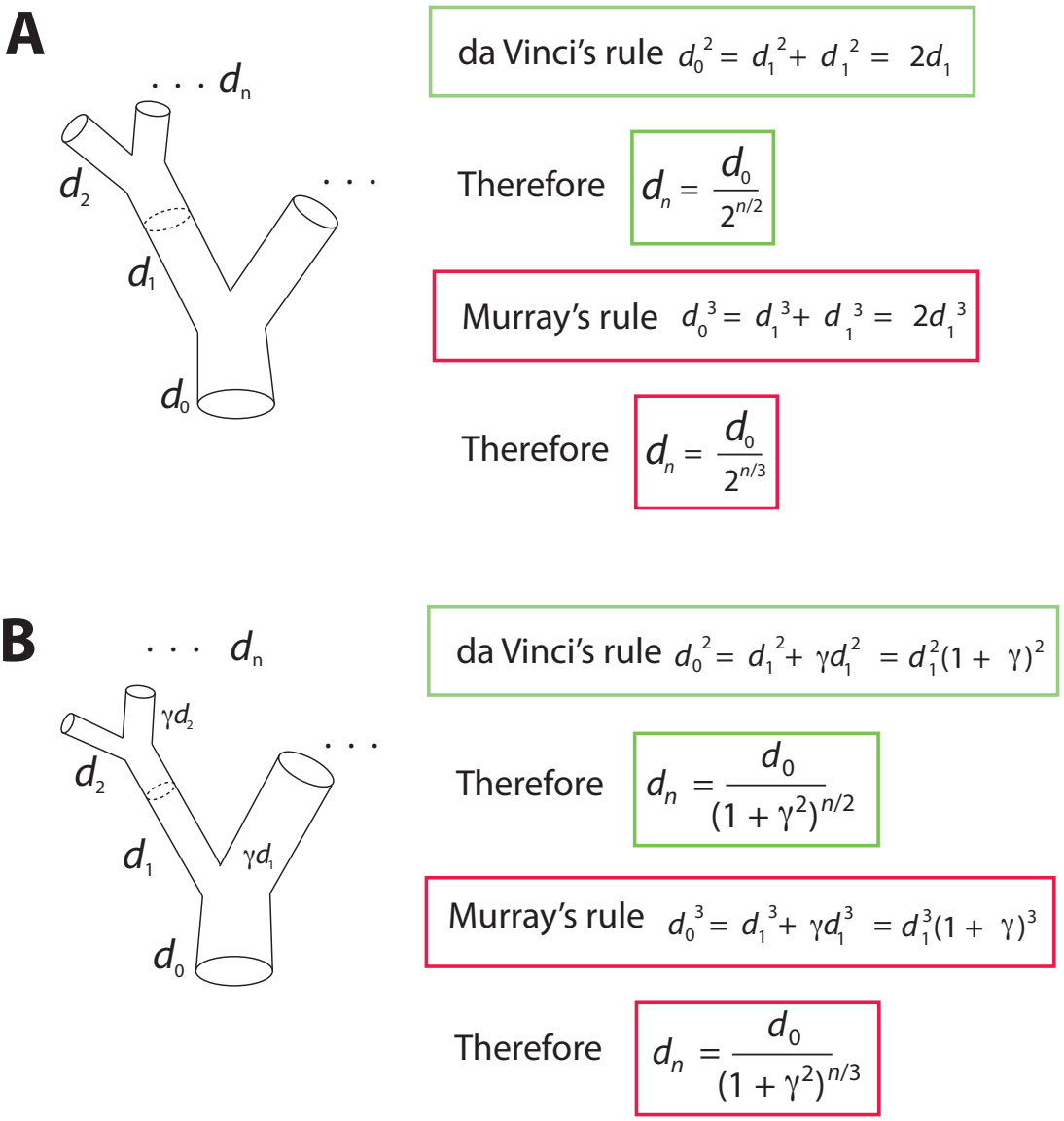

Figure 3.2. Schematics for open dichotomous hydraulic networks with equal and unequal branching orders (A and B, respectively), derivation of scaling relationships between parent branch order diameters (d_0) and higher branch orders (d_n) predicted by da Vinci's model (outlined in green) and Murray's model (outlined in red) (see Equations 3.1 and 3.2).

Both Murray's and da Vinci's rules assume that corresponding derivative branches have comparable diameters. However, this need not be the case.

Referring to Figure 3.2b, each of the two hydraulic models takes on a slightly different form from those in Equations 1 and 2, i.e.,

$$d_n = \frac{d_0}{(1+\gamma^2)^{n/2}} \qquad \text{Equation 3.3}$$

$$d_n = \frac{d_0}{(1+\gamma^2)^{n/3}} \qquad \text{Equation 3.4}$$

where g is a dimensionless number relating the different diameters of two corresponding branches of the same branch order, e.g., $d_{0^2} = d_{1^2} + g\, d_{1^2} = d_{1^2}(1 + g)$. Note that, if Equations 3.3 or .34 hold true for a data set, the slopes of bivariate plots of observed vs. predicted vein diameters will not equal 1.0 and will numerically increase as a function of increasing g values (Figure 3.3).

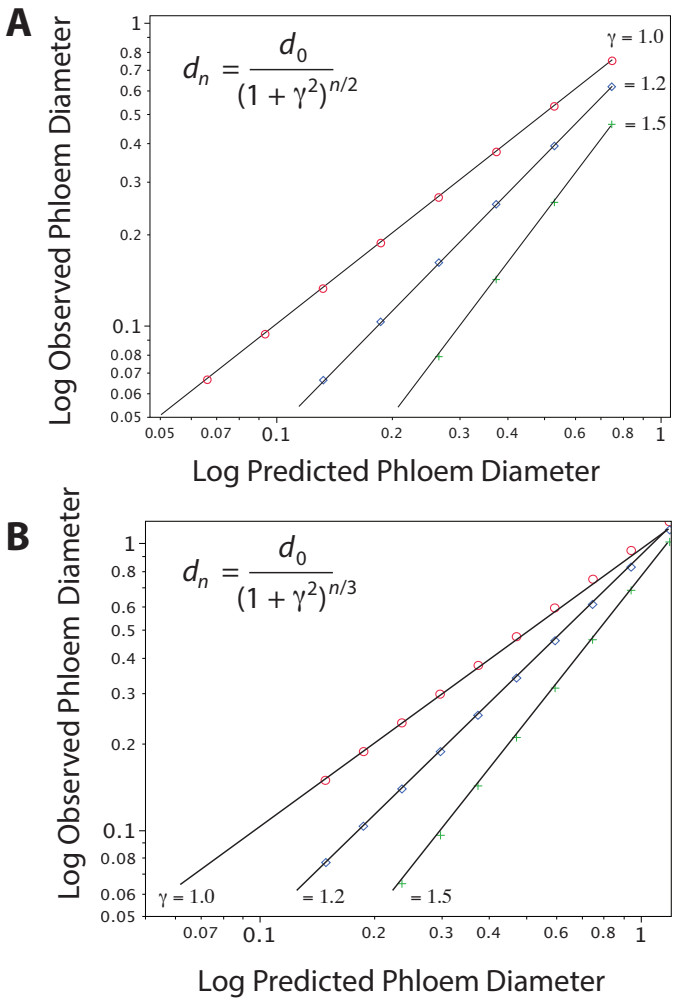

Figure 3.3. Bivariate plots of observed vs. predicted phloem diameters using da Vinc's model (**A**) and Murray's model (**B**) showing the effects of unequal diameters of corresponding branches (see Figure 3.2B). The parameter g is a measure of the inequality of diameters (as g increases, the diameters of corresponding branches increasingly differ). Compare with Figure 3.9.

Results

The hydraulic architecture of the phloem and xylem was examined from two perspectives: (1) the manner in which sieve tube member (STM) and vessel member (VM) conductive areas changed across the seven vein orders, and (2) how the sum of STM and VM conductive areas increased from the highest vein order (7th vein order) toward the petiole (0th order vein). These two perspectives

were considered essential because the first gives insights into the flow of sugars and water through individual STMs and VMs (from loading veins to the petiole and from the petiole to evaporation sites, respectively), whereas the second gives insights into the flow of sugars and water throughout the whole leaf.

Xylem and Phloem Conductive Areas

For each of the seven leaves, the hydraulically functional transverse areas of phloem and xylem (i.e., conductive area, A_{phl} and A_x) increased from 7th order veins to the petiole, whereas the sum of the transverse areas for each vein order in each leaf (i.e., total conductive area) decreased from the 7th order veins toward the petiole (Figsures 3.4–3.5). Specifically, the mean phloem conductive area (A_{phl}) across the seven leaves ranged from 2.77 μm^2 (SD ± 3.15; $n = 7$) in 7th order veins to ~31,000 μm^2 (SD ± 40,000; $n = 6$) in petioles (Figure 3.4A). Similarly, the mean xylem conductive area (A_x) ranged from 58.73 μm^2 (SD ± 26.03; $n = 7$) in 7th order veins to ~3.3 x 10^5 μm^2 (SD ± 180,000; $n = 6$) in the petiole (Figure 3.5A).

In contrast to the conductive areas of individual veins within each vein order, the total conductive area (i.e., the sum of the conductive areas of each vein order within a leaf) of 7th order veins significantly exceeded that of the petiole for both the phloem and the xylem (Figures 3.4B, 3.5B). The total conductive areas in the smallest loading veins were approximately 50-fold larger than the conductive areas of the petiole. Specifically, the mean total A_{phl} of 7th order veins was 5.7 x 10^5 μm^2(SD ± 0.4 x 10^6; $n = 7$) compared to a mean of 2.4 x 10^4 μm^2 (SD ± 0.7 x 10^4; $n = 6$) in the petiole. The total A_x of 7th order veins was 1.3 x 10^7 μm^2 (SD ± 0.5 x 10^7; $n = 7$), whereas the mean A_x in the petiole was 3.6 x 10^5 μm^2 (SD ± 0.2 x 10^5; $n = 6$).

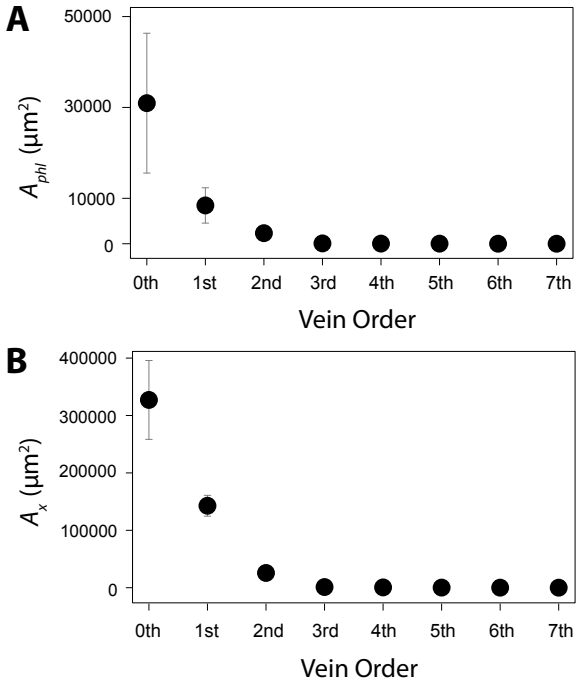

Figure 3.4. Mean phloem and xylem conductive areas of single veins, across seven vein orders and petiole (0th vein order), in leaves of *Populus x canescens*. Conductive areas in single veins decrease with increasing vein order. A. Phloem conductive area (A_{phl}) in each of seven vein orders and petiole (0th vein order). B. Mean xylem conductive area (A_x) in each of seven vein orders and petiole (0th vein order). Error bars depict standard errors.

Figure 3.5. Total phloem and xylem conductive areas in leaves of *Populus x canescens*. **A.** Total phloem conductive area (A_{phl}) in each vein order, averaged across whole leaves. **B.** Total mean xylem conductive area (A_x) in each vein order, averaged across whole leaves.

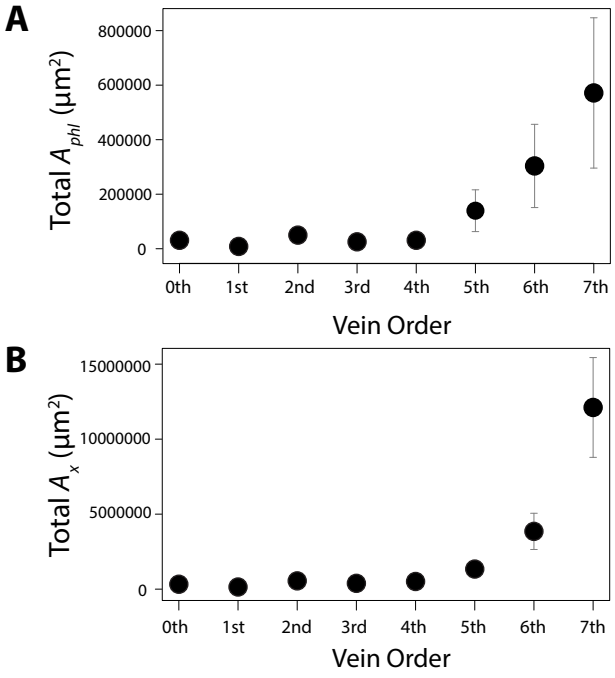

Sieve Tube Member and Vessel Member Areas and Lengths

The number and size of STMs and VMs per transverse section increased with decreasing vein order. For example, free-ending veinlets (FEVs) contained a single strand of 1-2 VMs that extended beyond the phloem and were surrounded by the bundle sheath (Figure 3.1), whereas up to 450 VMs were observed in cross-sections of the petioles. Even though STMs did not extend into FEVs, one or two STMs were present along the base of 7th order veins. The numbers of sieve tubes in each vein order increased exponentially from the 7th order veins to the petiole, wherein up to 2,600 sieve tubes were observed (not shown).

The mean lengths and diameters of STMs and VMs progressively increased from 7th order veins toward petioles, although the diameters and lengths of both conducting cell types were significantly greater in the petiole and the 1st and 2nd order veins (Figures 3.6 – 3.7). The lengths of STMs ranged from 85.2 μm in 7th order veins to 218 μm in petioles. STM diameters scaled isometrically with respect to STM lengths across all vein orders (i.e., scaling exponent $\alpha = 0.91$, $P < 0.001$; Figure 3.6), and ranged from ~1 μm in the minor veins to ~5 μm in petioles. Consequently, the volume (see insert in Figure 3.6) of individual STM increased from 7th order veins to the petiole. The increment in STM volume across major veins (1st – 3rd order veins) significantly exceeded that across minor veins (4th – 7th order veins).

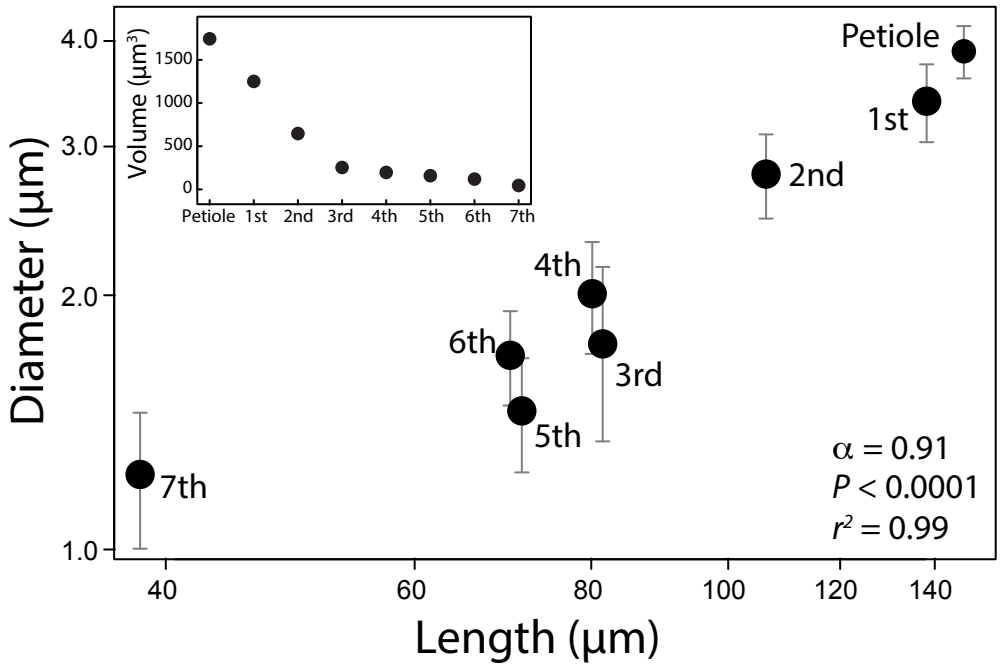

Figure 3.6. Allometric relationship of sieve tube member diameter and length across seven veins orders of leaf vasculature and petiole of *Populus x canescens*. Error bars depict standard error.

Two distinct classes of VMs were observed in petioles and in vein orders 1st –5th, but not in 6th and 7th order veins (Figure 3.7). These were interpreted to correspond to early and late metaxylem. Whereas the length of late metaxylem VMs did not differ across vein orders, the lengths of early metaxylem VMs increased from the minor veins toward the petiole. The smallest VMs were found in FEV terminations and measured 21.8 μm in length (Figure 3.1), whereas petiole VMs reached up to 728 μm in length. Early metaxylem VM diameters correlated with length (with a scaling exponent $\alpha = 0.53$, $P < 0.001$; Figure 3.7B).

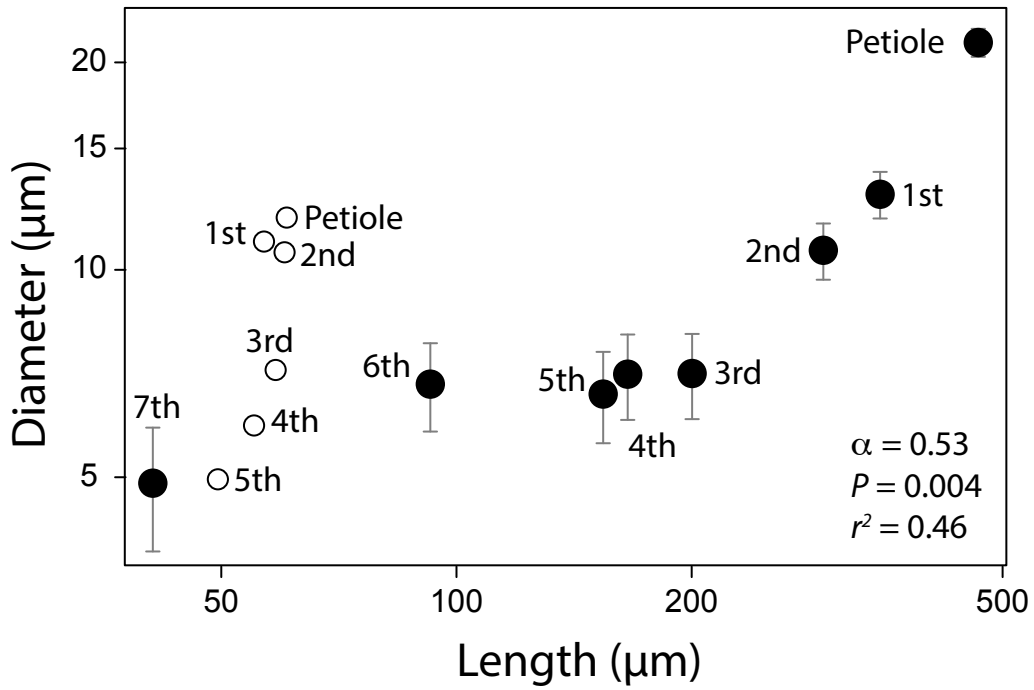

Figure 3.7. Allometric relationship of metaxylem vessel member diameter and length in leaves of *Populus x canescens*. Early metaxylem vessels are represented by filled circles. Late metaxylem vessels shown with hollow circles. Error bars depict standard error.

Scaling and Peripheral Contact of Phloem and Xylem

An isometric scaling relationship between the conductive areas of phloem and xylem (A_{phl} and A_x, respectively) was observed across all vein orders (Figure 3.8). This relationship was significant for A_{phl} and A_x within single veins, across all vein orders, and when comparing total A_{phl} with respect to total A_x. The mean values of A_{phl} and A_x in 7th order veins are 2.77 μm^2 (SD ± 3.15; $n = 7$) and 58.73 μm^2 (SD ± 26.03; $n = 7$), respectively, whereas such values on the petiole measured ~31,000 μm^2 (SD ± 40,000; $n = 6$) and ~330,000 μm^2 (SD ± 180,000; $n = 6$). On average, vein order mean values of A_{phl} and A_x within leaves differed by a factor of 10, indicating a constant difference of one order of magnitude between A_{phl} and A_x across all vein orders.

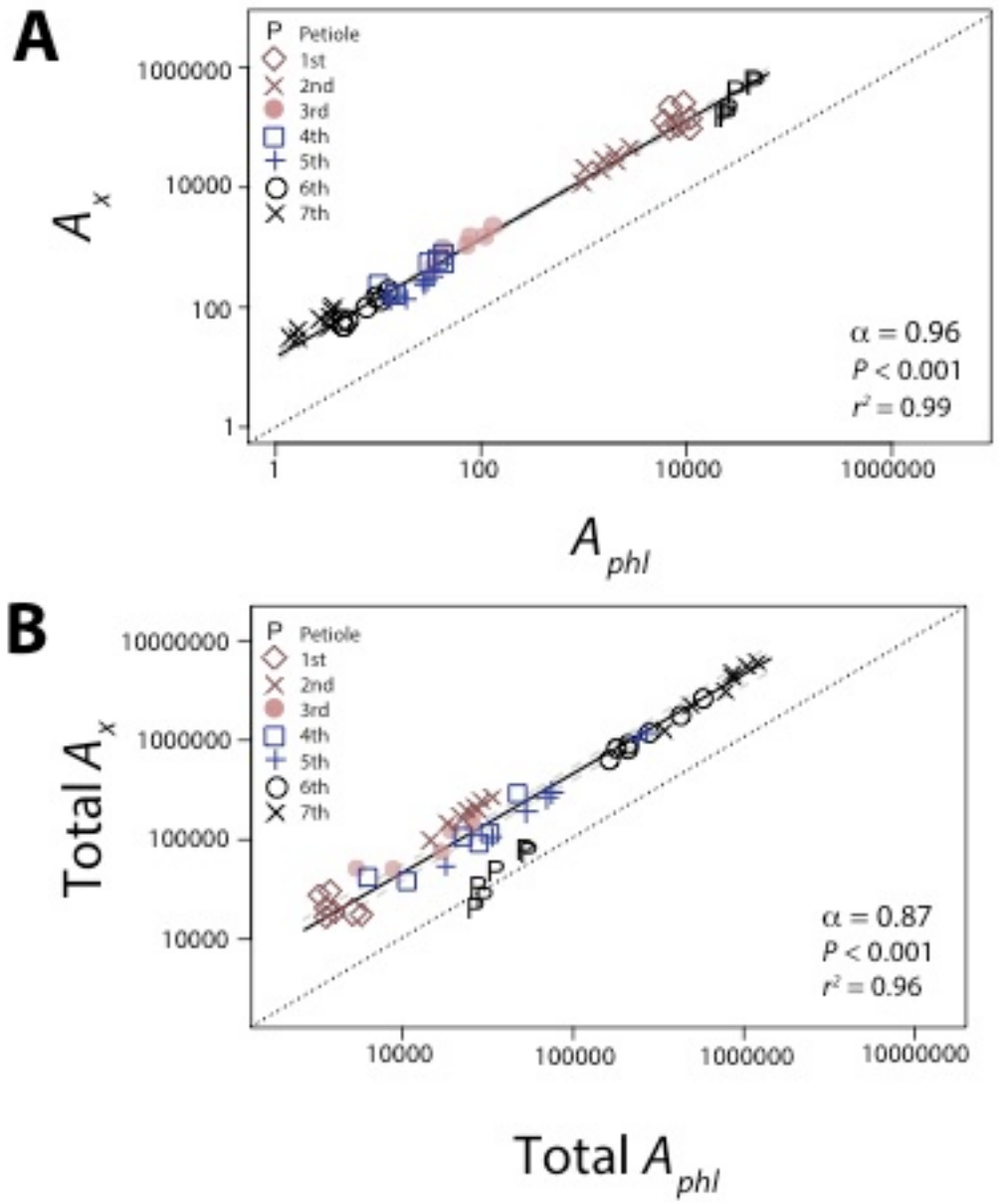

Figure 3.8. Allometry of phloem and xylem conductive areas across seven vein orders and petiole of leaves of *Populus x canescens*. A. Phloem vs. xylem conductive areas. B. Total conductive areas. Dashed line represents 1:1 relationship. Regression and 95% confidence interval represented with solid line.

Although the data revealed a spectrum in the diameters and lengths of conducting cells across all vein orders (Figure 3.6), anatomical differences

between the 1st and 3rd vein orders and the 5th and 7th vein orders were apparent. Inspection of transverse sections through the 1st to 3rd vein orders revealed a complete to nearly complete ring of lignified fibers enclosing the entire vascular bundle such that STMs have limited to no direct symplastic contact with the surrounding mesophyll, including the palisade layer (Figure 3.9). In contrast, transverse sections through the 5th to 7th vein orders showed that the vascular bundles have a significantly greater contact with palisade cells owing to a reduction in the peripheral distribution of fibers. In addition, there is a decreasing amount of parenchyma between the conducting cells and photosynthetic mesophyll in the 5th to 7th vein orders. The 4th vein order appears to be intermediate between the two classes of vein orders in its symplastic contact with photosynthate source cells. Specifically, the amount of fibers enclosing the vascular bundle is notably reduced in the 4th vein order. Yet, one to two layers of parenchyma occur between the bundle sheath and the conducting tissues. This observation is consistent the overall trend of decreasing STM diameters, lengths, and volumes from the 1st to the 7th vein order (see Figures 3.5 – 3.7).

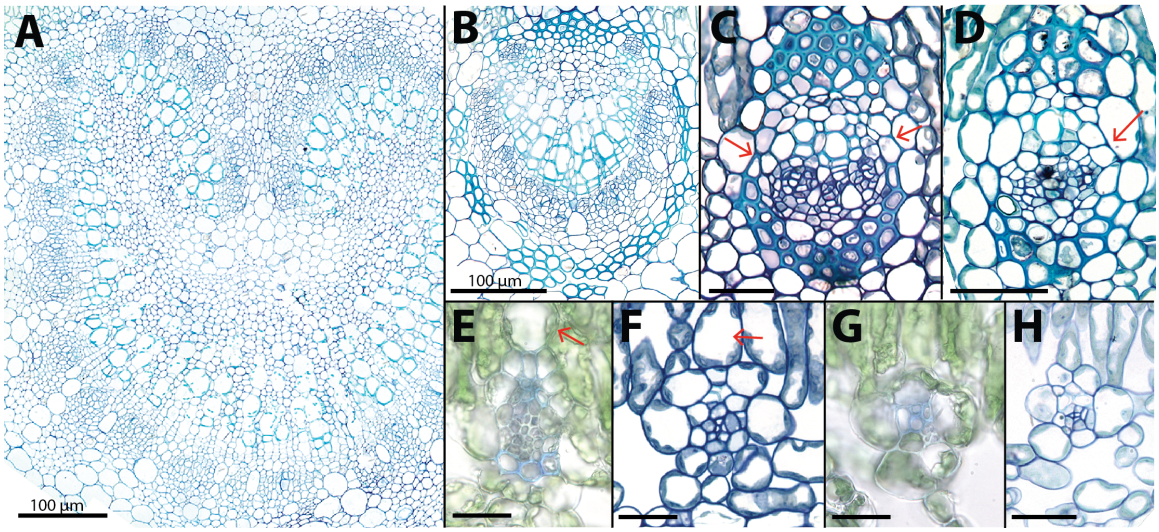

Figure 3.9. Representative cross-sections of the seven vein orders in leaves of *Populus x canescens*. Major veins include orders 1st to 3rd, and minor veins include orders 4th to 7th. Sections were stained with 0.1% toluidine blue. **(A)** 1st order vein. **(B)** 2nd order vein. **(C)** 3rd order veins. Arrows indicate the (nearly) continuous ring of fibers enclosing the vascular bundle. Scale bar = 30 μm. **(D)** 4th order vein. Arrow highlights reduced band of fibers and additional layer of parenchyma between the bundle sheath and conductive tissues. Scale bar = 30 μm. **(E)** 5th order vein. Arrow indicates bundle sheath extension to upper epidermis that differentiates 5th from 6th vein orders. Scale bar = 20 μm. **(F)** 6th order vein. Arrow indicates lack of bundle sheath extension (*cf.* 5th order vein). Scale bar = 20 μm. (G) 7th order vein. Scale bar = 20 μm. (H) 7th order vein. Scale bar = 20 μm.

Predicted vs. Observed Conductive Areas According to the Murray and da Vinci Models

We compared predicted STM and VM diameters obtained from Equations 1 – 2 against those observed (i.e., A_{plu} and A_x) for each vein order, using sequentially smaller vein orders as the 'parent branch' diameter (i.e., d_0 in Equations 1 – 2). We rejected the Murray or the DaVinci model if the slopes obtained for observed vs. predicted STM or VM diameters statistically significantly deviated from a numerical value of 1.0, where a slope of 1.0

indicates a perfect agreement between predicted and observed diameters across all vein orders, or over a range of vein orders. When the data from all leaves were pooled, da Vinci's model (Equation 3.1) provided the best statistical fit between predicted and observed diameters across vein orders 3rd – 7th, i.e., the slope of the predicted vs. observed diameters did not statistically significantly differ from 1.0 (Figure 3.10A). With one exception, DaVinci's model was also successful in predicting conductive diameters across the vein orders of individual leaves. In contrast, using the pooled data or the data from individual leaves, Murray's model did not provide a good predictor of observed conduit diameters, since the slopes of predicted vs. observed diameters significantly differed from 1.0 (Figure 3.10B).

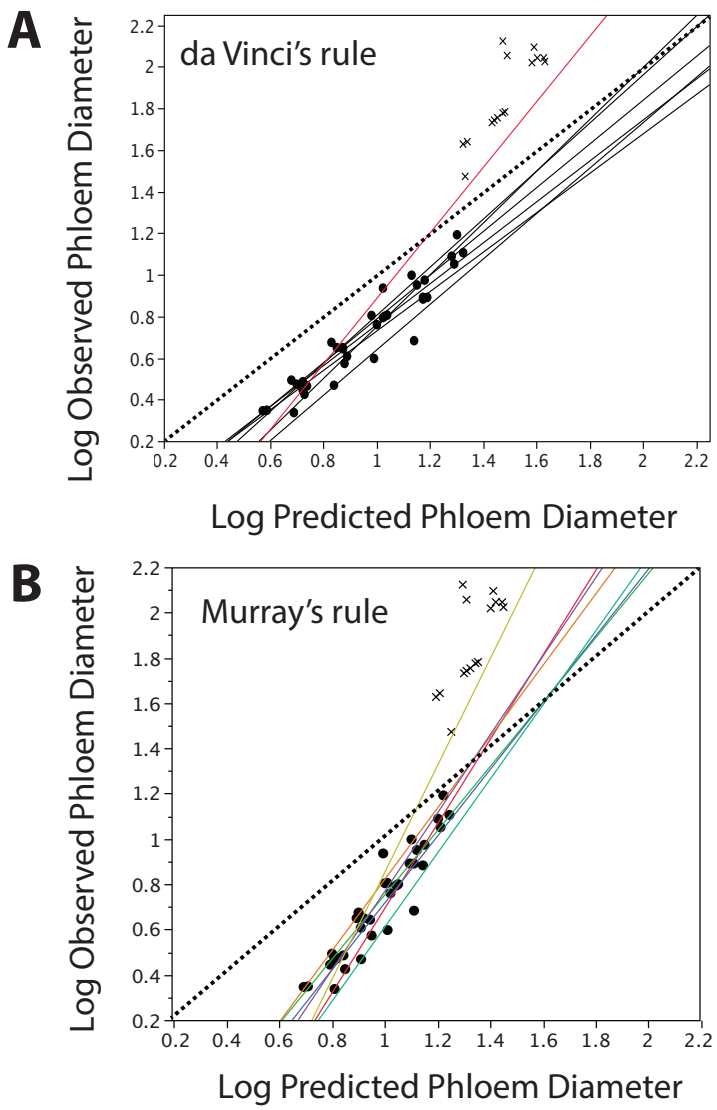

Figure 3.10. Measured and predicted phloem conductive diameters, estimated following (A) DaVinci's rule and (B) Murray's law. Each regression line represents a case in which expected values were estimated using a given vein order as 'parent branch'. Colored lines represent regressions with slopes significantly different than 1, meaning that observed values differ greatly from expectation. A single regression line differs from expectation when considering DaVinci's model, and this is when including primary and secondary veins in the regression. Even though all other vein hierarchies conform to an area-preservnig model, primary and secondary vein conductive areas exceed expectation for DaVinci's model. All regressions slopes from Murray's expectation are significantly different than 1.

Equations 3.1 – 3.2 describing Murray's and da Vinci's models assume that corresponding derivative branches have comparable diameters. Equations 3.3 – 3.4 include the dimensionless parameter g, which describes the relation between corresponding branches of the same branch order that differ in diameter. Referring to Equations 3–4 (and Figure 3.2B), any deviation in the equality of branch diameters within the same vein order (i.e., $g \neq 1.0$) will result in an anisometric relationship between observed and predicted diameters for both the Murray and da Vinci models that will be immediately evident in the regression curve slope for observed vs. predicted diameters, which will deviate from one (Figure 3.3). We found no evidence that the diameters of comparable branches in each of the different vein orders significantly differed from one another. The fact that the slope for observed vs. predicted diameter using the da Vinci model did not differ significantly from unity indicates that $g \approx 1.0$ such that Equation 3.1 holds true across successive vein orders of the hierarchical network in poplar leaves.

Note, however, that da Vinci's model consistently predicted larger conduit diameters than those observed, with the exception of the conduit diameters observed in petioles. When including the data from the petiole and from 1st and 2nd vein orders, da Vinci's model under estimated conduit diameters. This was interpreted to indicate that da Vinci's model is only an approximate model for a reticulated hydraulic network (see Discussion).

Discussion

The data reported here indicate that (1) phloem and xylem conductive areas within single veins, across the different vein orders increase toward the petiole, (2) the sum of phloem (and xylem) conductive areas across each vein order decreases toward the petiole, (3) the volume of sieve tube members and vessel members increase toward the petiole, (4) an isometric (one-to-one) scaling relationship between phloem and xylem conductive areas holds across all vein orders, and (5) phloem and xylem conductive areas scale in a manner that is consistent with a branching network predicted by da Vinci's hydraulic model. In addition, differences in the diameters and lengths of sieve tube members and vessel members, which can serve as proxies for flow resistance, provide circumstantial evidence for a division of function between minor veins (4^{th} – 7^{th} orders) and major veins (1^{st} – 3^{rd} orders). This speculation is consistent with additional differences between the anatomy of major and minor veins (see Figure 3.9). Based on the morphometrics and anatomy reported here, the phloem in minor veins appears to function primarily as a network for the collection of photosynthates, whereas phloem in the major veins appears to function as a rapid efflux network for photosynthates. These observations are discussed in the following sections, starting with a summary of the previous literature and concluding with a discussion of the two contending hydraulic models (Murray's rule and da Vinci's rule) for branching transport systems.

Prior observations

Structural and hydraulic correlations similar to those reported here have been observed for annually produced phloem and xylem within stems of *Abies*

and *Picea* (Gricar et al., 2006; Jyske and Holtta, 2016). The 1:10 phloem to xylem ratio across vein orders found for *P. x canescens* (Figure 3.8) matches the annual growth ratio reported for other species of *Populus* (Evert & Kozlowski, 1967), and falls within the 1:4 to 1:10 ratio reported for vascular tissue production in other deciduous temperate trees (Artschwager, 1950; Waisel *et al.*, 1966). The similarity among phloem to xylem ratios in leaf veins and stems might reflect similar behavior in procambium activity within the entire plant body. However, in contrast to annually produced vascular tissue where differentiation of both transport tissues is coordinated by the bifacial vascular cambium, xylem differentiation lags behind that of phloem in major veins during early leaf development (Esau, 1965), a phenomenology that is not expected *a priori* to yield an isometric scaling relationship between phloem and xylem conductive areas across all vein orders. The isometric scaling relationship between the transport areas of both tissues in leaves highlights a form-function coordination that is likely to reflect metabolic signaling involving auxin and sucrose (Novitskaya & Kushnir, 2006) that regulates the numbers and sizes of sieve tube members and vessel members.

A hydraulic coupling between phloem and xylem is essential for the long distance transport in plants. This coupling has been observed in the daily variations in phloem cell diameters within trees that are related to changes in the radial conductance between the xylem and phloem (Sevanto *et al.*, 2011). A tight coupling between phloem and xylem along the long distance transport pathway enables higher sugar flux rates (Hölttä *et al.*, 2006) as well as faster information transmission (Thompson & Holbrook, 2004; Thompson, 2006). In source leaves, the link between phloem and water is essential since the xylem must meet the

transpirational demands required to sustain photosynthesis, and because water influx into the phloem ultimately enables the turgor pressure gradient required for sugar transport. This coupling is observed in the functional maturation of xylem in minor veins of *Populus x canescens*, which spatially and temporally matches sink to source transition of the leaf blade (Carvalho *et al.*, 2016) and is consistent with sucrose participation in the development and maturation of transport tissues. The maturation of xylem in minor veins correlates with an enhancement of the transpiration stream and the onset of sugar export for the leaf, two processes that rely on water conductance.

In a study by Muller et al. (2014), maximum photosynthetic rates were shown to correlate with the cross-sectional areas of minor vein tracheids and sieve tube members (multiplied by venation density) in four symplastic loading species. Such correlations further link phloem and xylem transport areas and indicate that the phloem conductive areas for sugar export match leaf photosynthetic rates (Muller *et al.*, 2014), at least in symplastic loading species such as poplar. Photosynthetic rates of apoplastic loading species considered in the same study did not correlate to phloem conductive areas, although they did correlate with tracheid number and total cross-sectional area. Further studies addressing structural and hydraulic coupling between phloem and xylem in apoplastic loading and polymer trapping species are needed.

A phloem-xylem coupled hydraulic model

The interrelationship between phloem and xylem hydraulics within *Populus x canescens* leaves is diagrammed in Figure 3.11, which illustrates the linkage between sugar and water movement in a leaf. In symplastically loading

species such as *P. x canescens* (Zhang *et al.*, 2014), fixed sugars diffuse from the mesophyll into minor veins following a sugar concentration gradient (Rennie & Turgeon, 2009) fostered by an enhanced conductance related to plasmodesmatal frequency (Russin & Evert, 1985). As solutes move into sieve tubes, water flow follows solute movement and augments the turgor pressure of sieve tube members to maintain water potential equilibrium across the entire leaf (Figure 3.10A). Following Münch's pressure flow hypothesis, the turgor pressure difference between source and sinks triggers the bulk flow required to move nutrients to non-photosynthesizing tissues such as roots and developing leaves. Because loading mainly occurs in minor veins, these effectively act as the source sites in source-sink pressure gradients (Figure 3.11B).

Three observations reported here are noteworthy in the context of Münch's pressure flow hypothesis. First, the total conductive area of 7th order veins is about 50 times larger than that of the petiole, making the vascular system act as a funnel for sugar transport (Figure 3.10C). Second, the length and volume of individual sieve tube members disproportionately increases from the higher order veins toward the petiole (Figure 3.6), effectively reducing flow resistance along individual conduits in major veins. Third, although the volume of individual sieve tube members increases toward the petiole, the sum of sieve tube cross sectional area decreases toward the petiole. In addition, differences in the symplastic contact areas of sieve tubes members and surrounding photosynthetic tissues are evident between the two classes of vein orders (see Figure 3.9). The decreasing amount of parenchyma observed between the photosynthetic mesophyll and the sieve tube members in minor veins implies a greater symplasmic continuity and sugar loading function for minor veins.

Collectively, the minor veins function as a "drainage system" that gathers photosynthates, whereas the major veins drain the system owing to a gradient of decreasing sieve tube member solute potential toward the petiole. In addition, the overall size of the funnel-like construction of the phloem in the 1st to 3rd order veins is predicted to speed hydraulic transport. This functional distinction between major and minor veins is consistent with the timing of leaf vascular maturation, as minor veins only become functional during the leaf sink-to-source transition (Turgeon, 2006).

In hydrodynamic systems bounded by impermeable and uncompressible walls, such a constriction in total conductive area towards the petiole, is anticipated to cause an increase in flow velocity following the Venturi Effect. From a purely hydraulic perspective and under steady state conditions, sieve tube hydrostatic pressure would drop in correlation to the increase in phloem sap flow. However, because sieve tube members are living cells with semipermeable membranes and elastic cell walls, a decrease in turgor pressure would further draw water into cells to maintain water potential equilibrium. The addition of extra water into the phloem could effectively contribute to phloem sap bulk flow and the 'flushing' of photosynthates out of the leaf. This hypothesis further links phloem translocation to leaf water status and is consistent with modeling attempts indicating that xylem water potential affect phloem translocation rates (Hölttä *et al.*, 2009).

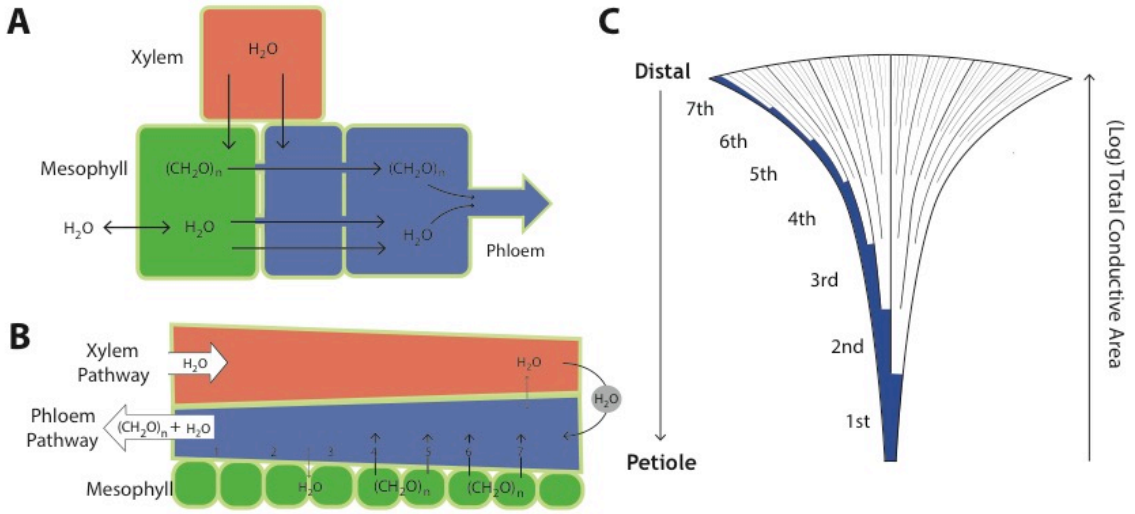

Figure 3.11. Phloem and xylem hydraulic coupling model for source leaves of *Populus x canescens*. A. Cross-section representation of phloem and xylem hydraulic coupling. Fixed sugars move symplastically from mesophyll into the phloem. Water flows along the transpiration stream into the leaf apoplast and back into phloem. B. Proximal-distal representation of phloem-xylem hydraulic coupling in source leaves. Sugar loading into the phloem occurs between vein orders 4th-7th, fueling phloem sap flow from higher order veins to major veins. Hydraulic connectivity between xylem and phloem along the apoplast throughout the vascular pathway. C. Funnel model representing the vascular transport system of a leaf. Width of each section is log-scaled to correspond to observed average areas.

Contending hydraulic transport models

Two contending models have been used to understand water flow in dichotomously branched systems: Murray's model and da Vinci's model (Murray, 1926; Richter, 1980; McCulloh *et al.*, 2003). Murray's model predicts that the diameters of successively higher order branches will scale as the third power, whereas da Vinci's rule predicts that the diameters of successively higher order branches will scale as the second power (see Equations 3.1–3.4). Our analyses of

sieve tube member diameters and vessel member diameters across the different vein orders are consistent with the predictions of da Vinci's rule and inconsistent with the predictions of Murray's law, both for the data gathered from individual leaves and for the data pooled from all sampled leaves (see Figure 3.10).

However, the consistency between observed and predicted vein diameters must be approached with skepticism because, like Murray's model, the da Vinci model model only holds true for dichotomously branched networks, and thus both fail to physically conform to reticulated phloem and xylem hydraulic networks. In a previous attempt to determine the scaling geometry of branching leaf veins, Price et al. (2012) compared vascular diameters at their junction, and reported that for angiosperm leaves, minor veins conformed to Murray's Law, whereas major veins followed an area-preserving scaling (Da Vinci) pattern. Xylem conduit dimensions have also been reported to comply with Murray's expectation in sunflower leaves (Canny, 1993). Our sampling strategy and analyses aimed to compare vascular hierarchy instead of individual veins, therefore condensing the leaf network into discrete categories. Consequently, although our data comply with the da Vinci model, it is likely that this is an example of where a model "gives the right answer for the wrong reasons", which may instruct future attempts to validate either model based on the scaling exponents that emerge from their mathematical imperatives. Importantly, the data presented here provide the numerical values for all of the parameters required to quantitatively describe phloem loading and photosynthate export in a spatially explicit mathematical model as conceptualized in Münch's pressure flow hypothesis.

Acknowledgements

This work made use of the Cornell Center for Materials Research (CCMR) Shared Facilities supported through the NSF MRSEC program (DMR-1120296). Imaging data was acquired through the Cornell University Biotechnology Resource Center, with NYSTEM (CO29155) and NIH (S10OD018516) funding for the shared Zeiss LSM880 confocal/multiphoton microscope. MRC thanks Nick Van Eck, Maria Gandolfo, John L. Grazul (CCMR); Rebecca Williams, Joanna de la Cruz, and Teresa Porri (Cornell Biotechnology Center).

Author contribution

All authors contributed to the development of this work. MRC, KJN, RT, TO designed the research; MRC, KJN performed the research and analyzed data; MRC, KJN, RT, TO interpreted results and wrote the manuscript.

CHAPTER IV

HYDRAULIC ARCHITECTURE OF *Ginkgo* LEAVES

Mónica R. Carvalho, Robert Turgeon, Thomas Owens, Karl J. Niklas[2]
Plant Biology Section, School of Integrative Plant Science, Cornell University, Ithaca, NY 14853, USA.

Short title: Ginkgo hydraulic architecture

Acknowledgements

The authors thank John L. Grazul (CCMR), Edward Cobb, Nicolas Glynos, and Maria Gandolfo for their help at various stages of sample collection and preparation. MRC thanks the Schlumberger Faculty for the Future Foundation. This work made use of the Cornell Center for Materials Research (CCMR) Shared Facilities supported through the NSF MRSEC program (DMR-1120296).

Abstract

- *Premise of the study:* The hydraulics of xylem has been widely studied in numerous species and organs. However, comparatively little is known about how phloem and xylem are hydraulically coupled, and about many of the basic structural properties of phloem (such as sieve element numbers and areas) that have direct effects on sap translocation.

- *Methods:* Using a combination of light, epifluorescent, and electron microscopy, we describe the leaf hydraulic architecture of *Ginkgo biloba*, examine the scaling relationships between phloem and xylem, and quantify changes in phloem and xylem conductive areas in five fully mature leaves.
- *Key results:* The conductive areas and lengths of sieve cells and tracheids increase basipetally along the leaf toward the petiole. This trend holds true for individual veins, for individual sieve cells and tracheids, and for the sum of conductive areas at any distance from the petiole. In addition, the conductive areas of phloem and xylem are isometrically coupled across the leaf vasculature, and follow a scaling that is consistent with predictions of da Vinci's model for branching systems.
- *Conclusions:* The scaling of *Ginkgo* leaf hydraulics complies with that observed in leaves of other gymnosperms and angiosperms, and is consistent with theoretical models based on phloem transport that minimize flow energy dissipation.

Key words: da Vinci's model, Gymnosperm, Leaf anatomy, Phloem, Sieve cell, Tracheid, Xylem

The phloem and xylem constitute the long-distance hydraulic transport system in vascular plants that mediates water and nutrient allocation and the long-distance signaling necessary for survival and growth. Increasing evidence

indicates that the phloem and xylem are functionally coupled in ways that ensure the transport of water and photosynthates (Savage *et al.*, 2016). Daily variations in phloem cell diameters within trees reflect changes in the radial hydraulic conductance between the xylem and phloem (Sevanto *et al.*, 2011), and indicate the effective movement of water between both tissues along the transport pathway. This exchange allows xylem to provide phloem with the water required for maintaining sugar translocation rates (Hölttä *et al.*, 2006; Windt *et al.*, 2006), and sufficient water to move from the phloem into the xylem following a water potential gradient such as that produced under drought conditions (Zweifel *et al.*, 2000; Sevanto *et al.*, 2005). Phloem has also been suggested to be functionally involved in mechanisms for xylem embolism repair (Salleo *et al.*, 2009; Nardini *et al.*, 2011; Brodersen & McElrone, 2013).

The structural linkages between phloem and xylem are also seen in the scaling relationships between the functional conductive transverse areas of both transport tissues in stems and leaves (Mencuccini *et al.*, 2011; Jyske & Hölttä, 2015; Carvalho *et al.*, 2017). However, the hydraulic, mechanical, and physiological implications of these scaling relationships remain unknown or at best poorly understood. This gap in our knowledge is largely due to a paucity of data quantifying the dimensional architecture of the phloem. Although the structure-function relationships of tracheary cell-types have been widely studied (e.g., Roth et al., 1995; Zwieniecki et al., 2002, 2007; Sack et al., 2004), the structure-function relationships of sieve cells and sieve tube members are still rarely reported (see however (Petit & Crivellaro, 2014; Woodruff, 2014; Jyske & Hölttä, 2015; Carvalho *et al.*, 2017). This general lack of data is explained in large part by the delicacy of phloem conducting cell types. Sieve elements are thin

walled, operate under positive pressure, and are deeply buried under layers of tissue. Collectively, these features make sieve elements highly susceptible to mechanical damage that, in turn, makes measurements of phloem translocation inherently difficult to visualize and quantify in living plants. It is also important to note that the basic descriptions of phloem structure and hydraulics have traditionally focused on single stem or leaf vascular bundles rather than across all levels of vascular branching at the organ and plant levels (see however, (Woodruff, 2014; Knoblauch *et al.*, 2016; Carvalho *et al.*, 2017).

Leaf vasculature ensures an effective distribution/collection system for water and sugars throughout the leaf lamina. In terms of the water transport pathway, leaves can account for ~ 30% of the resistance to water movement through plants, and leaf xylem can account for a large portion of this resistance (as reviewed in: Sack and Holbrook, 2006; Sack and Scoffoni, 2013). In terms of the phloem, sugar loading in leaves provides the osmotically-mediated pressure differential between sources and sinks required for long-distance transport (Münch, 1930; Turgeon & Ayre, 2005; Comtet *et al.*, 2017).

Herein, we quantify and describe the hydraulic architecture of *Ginkgo biloba* L. leaves at all levels of vein branching. This species is the only living species of what was a much more diverse and ecologically successful clade (Zhou, 2009), and was selected for study because of its distinctive fan-shaped leaves possessing an open-dichotomous venation that, with the rare exception of a few other seed plants such as *Kingdonia uniflora* and *Circaeaster agrestis* (Foster, 1959, 1963, 1966; Foster & Arnott, 1960; Foster *et al.*, 1971), are unlike the vast majority of the leaves of extant seed plants (Critchfield, 1970). The open-dichotomous venation of the leaves of *Ginkgo* is also conducive to testing the

predictions of two competing models for branching architecture, those of da Vinci's model (Richter, 1980) and Murray's model (Murray, 1926). Phloem transport in *Ginkgo* leaves (and perhaps in all other gymnosperm tree species) is likely to comply with Münch's Pressure Hypothesis (Jensen *et al.*, 2012a). In addition, it is likely that *Ginkgo* is a symplasmic, passive loader based on measurements of its phloem osmolarity and the lack of sugar uptake in leaf disc experiments (Blechschmidt-Schneider *et al.*, 1997; Liesche & Schulz, 2013). Consequently, the vascular architecture of *Ginkgo* leaves provides many opportunities to explore and compare the hydraulic architecture of an ancient seed plant lineage with that of evolutionarily more recent and derived seed plants.

Materials and Methods

Leaf morphology and anatomy were quantified using mature leaves from the short shoots of a large, well-established, ovulate *Ginkgo biloba* L. tree growing in an open field on the Cornell University campus (N42˚26'40.47", W76˚29'22.24"). It is important to note in this context that *Ginkgo* is heterophyllous. The leaves produced on short shoots are typically undivided or slightly divided, whereas the leaves produced by long shoots are typically deeply divided into two or rarely more lobes. Hydraulic parameters also differ between both types of leaves. Specifically, leaves produced by long shoots have consistently higher leaf water and stomatal conductance than leaves produced by short shoots (Leigh *et al.*, 2011). There is also evidence that the leaves produced by short or long shoots differ in their surface area and dry mass if removed from ovulate versus pollen-bearing trees (Christianson & Niklas, 2011; Niklas &

Christianson, 2011). Therefore, care was taken to sample leaves in a manner that likely reduced as much as possible any intrinsic variance in leaf architecture.

Sampling and microscopic analysis— Five fully expanded leaves were collected from short-shoot branches and fixed in a 50% methanol –10% acetic acid solution. Whole leaves were photographed under transmitted light using a Canon T2i camera with a 60mm macro lens and a Yonguo Speedlite YN685 external flash, following the protocols of (McNair, 2015). Images of the leaves were digitized using NEFI (Dirnberger *et al.*, 2015) to quantify the venation pattern, and all vein segments were ranked following the Strahler branching system (Strahler, 1957). In this system, the most distal, terminal veins on each leaf are assigned a rank of 1. Increasing ranks are assigned only to veins formed by the junction of two equally ranked veins, i.e., two veins of rank 1 converge into a vein of rank 2 (Figure 4.1).

Between 20 and 25 vascular strands from the petiole and representatives of all vein ranks were selected and sectioned transversely from each of the sample leaves. Veins within each leaf were selected from the leaf margin and from four arcs swept from the base of the leaf lamina (Figure 4.1). The vein fragments were dehydrated in a 10-30-50-75-100% ethanol series and embedded in Spur's resin (Electron Microscopy Sciences). Transverse, 1.75 mm thin sections were made using a Leica UTC Ultramicrotome (Leica Microsystems) and were stained with 1% toluidine blue in a 1% sodium borate solution. The thin sections were observed under bright-field microscopy at 800-1200X magnifications. For the largest veins, multiple overlapping images were taken and were subsequently merged into whole-vein images.

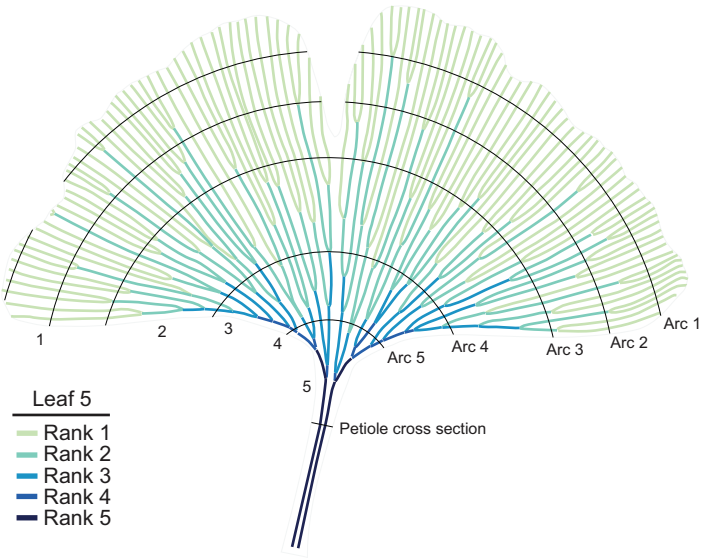

Figure 4.1. Strahler numbering system for vein orders and the positions of arcs used to sample veins shown on a representative *Ginkgo* leaf (leaf 5). Numbering to the left refers to coloring scheme showing increasing vein rank towards the leaf base. Note that the highest number of veins typically occur at the leaf margin as it converges onto the petiole. Numbering at the left indicates the five different arcs defined along the leaf for sampling the total conductive areas as they relate to lamina surface area between an arc and the leaf margin.

Sieve cell and tracheid diameter and length were measured from macerations of individual veins. Representative veins were excised from each of five arcs swept across two of the five leaf samples. These fragments and were digested in a 1% HCl–50% ethanol solution for 24 h, rinsed, and incubated in 5% ammonium peroxide for 24 h. Epidermal and mesophyll tissues were manually removed, and the remaining vascular strands were macerated directly on microscope slides. The macerated tissues were stained with 1% toluidine blue in aqueous solution, followed by 0.05% aniline blue in 100 mM potassium phosphate buffer for 15 minutes. The prepared samples were analyzed by

fluorescence and bright field microscopy, using an Olympus BX60 microscope equipped with a 100W high-pressure mercury burner and reflected fluorescence light source (Olympus BH2-RFL-T3) coupled to an Olympus UC90 camera.

Five additional vein fragments from a freshly collected leaf were prepared for sieve element visualization under TEM. The fragments were cut and immediately fixed in in 2% gluteraldehyde-cacodylate solution for 12 hours at 4˚C, stained with 1% osmium tetroxide for 1 hour, and dehydrated in a 10-30-50-75-100% ethanol series before embedding in Spur's resin. Transverse 100 nm thin sections were made using a Leica UTC Ultramicrotome (Leica Microsystems) and examined under a FEI T12 Spirit transmission electron microscope equipped with a LaB6 120 kV filament. Images were acquired using a coupled SIS Megaview CCD camera.

Length and Area Measurements— Leaf area and vascular conductive area measurements were made using ImageJ (Rasband, 2016). The conductive areas of metaxylem (A_x) and metaphloem (a_{phl}) were measured from images of vein cross-sections. The areas covered by tracheids or sieve cells were manually selected using Adobe Photoshop CC 2016 (Adobe Systems, Washington, USA). Both cell-types were identified based on position, cell wall thickness, and staining affinities. Metaxylem tracheids were distinguished from protoxylem by their size and cell wall thickness, and functional sieve cells were identified using TEM sections as a reference (Figure 4.2). Cell walls from tracheid or sieve element selections were digitally removed using ImageJ in order to only quantify the conductive areas of each tissue type. The numbers of sieve cells in each vein were recorded, and average sieve cell area was estimated based on ten cell diameter measurements on each vein cross-section. Because sieve cells of *Ginkgo* are

rectangular in cross-section, sieve cell area was measured by multiplying the diameters along the short and the long axis of the cell.

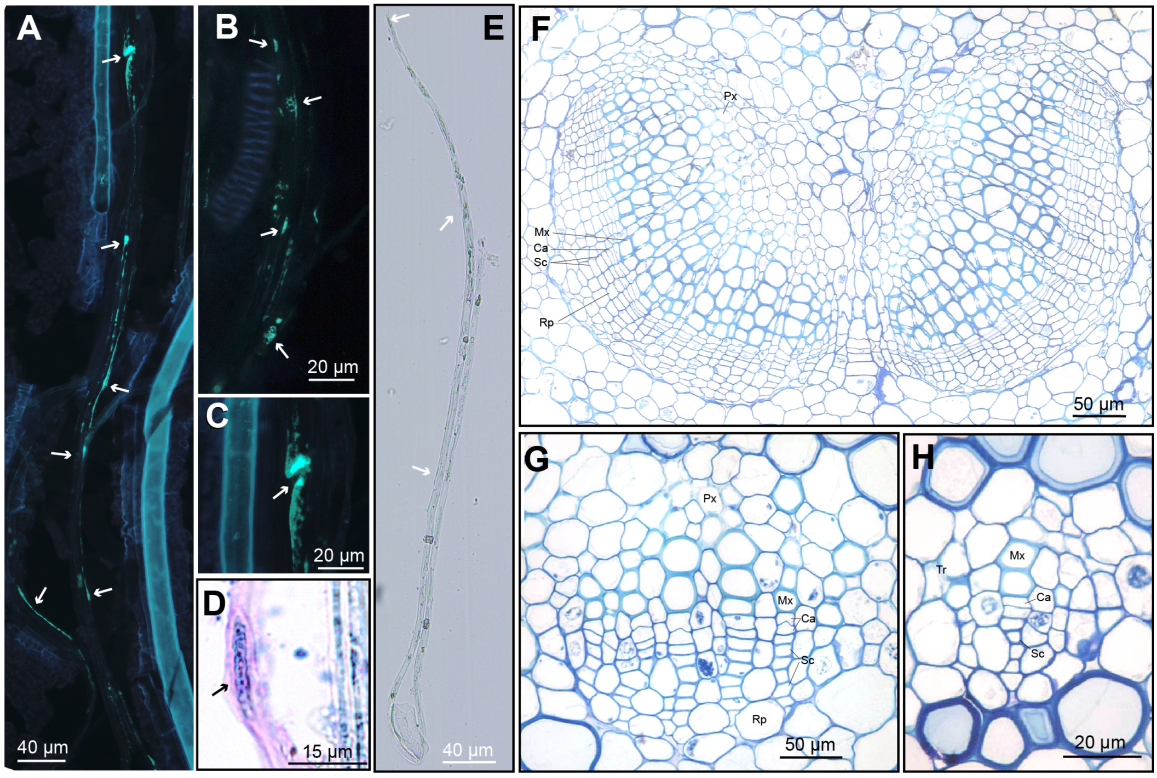

Figure 4.2. Vascular anatomy of *Ginkgo* leaves. (A) Representative sieve cells from vein maceration stained with aniline blue 0.05% and seen under epifluorescence. Arrows indicate lateral and end-wall sieve areas. (B) Detail of lateral sieve areas (arrows) stained with aniline blue 0.05%. (C) Detail of callose deposition at sieve cell end-wall (arrow). (D) Sieve areas (arrow) at the end of a sieve cell end-wall stained with toluidine blue 1%. (E) Isolated sieve cell obtained from maceration of an individual vein (rank 3). Arrows indicate lateral sieve areas. (F) Cross section of a petiole (see Figure 4.1). (G) Cross section of representative vein (rank 3). (H). Cross section of representative vein (rank 1). Note that sieve cells are typically rectangular in cross section and arranged in discrete files. Px, protoxylem; Mx, metaxylem; Ca, procambium cells; Sc, sieve cell; Tr, transfusion cell; Rp, ray parenchyma.

Sieve cell and tracheid length and diameter were measured from macerated tissues. Five to ten cells were analyzed for each of the vein ranks.

Sieve cell diameter and area measurements were compared for consistency across sample preparation techniques. Tracheid area (a_t) was estimated using cell diameter (d_t) and assuming a circular cross-section.

Total phloem conductive area was quantified for each of the arcs swept across the sample leaves (Figure 4.1). For this purpose, a multivariate linear model was created to estimate the phloem conductive area of any individual vein, using vein rank and distance from the leaf base as independent variables. Different regression models were used for each of the five leaves, and were built using measured phloem conductive areas (a_{phl}; Table 1). The total phloem conductive area along any given arc was then estimated as the sum of the conductive areas of all the individual veins intersected by an arc, and was compared with the corresponding cumulative leaf area. For each arc, the cumulative leaf area was defined as the area bounded by an arc and the leaf margin, as an approximation of the "maximum photosynthetic catchment area" collected by the vasculature at the arc. These areas were selected from leaf photographs using Adobe Photoshop, and were quantified using ImageJ.

Table 4.1. Coefficients for multiple linear regressions of phloem conductive areas on vein rank and distance from the leaf base. Regressions are leaf-specific and were subsequently used to estimate total conductive areas at any given distance from the leaf base. *a,* vein rank coefficient; *b*, distance from leaf base coefficient; *c*, interaction coefficient; *d*, *y*-intercept.

Leaf	*a*	s.e.	*b*	s.e.	*c*	s.e	*d*	s.e.
1	5.7 x 10^{-1}	7.9 x 10^{-2}	-3.2 x 10^{-5}	7.1 x 10^{-6}	1.6 x 10^{-6}	2.3 x 10^{-6}	4.3 x 10^{0}	4.1 x 10^{-1}
2	4.7 x 10^{-1}	1.7 x 10^{-1}	-4.3 x 10^{-5}	1.5 x 10^{-5}	-5.1 x 10^{-6}	4.4 x 10^{-6}	5.3 x 10^{0}	7.6 x 10^{-1}
3	3.6 x 10^{-1}	1.5 x 10^{-1}	-5.4 x 10^{-5}	1.5 x 10^{-5}	4.8 x 10^{-6}	4.3 x 10^{-6}	5.3 x 10^{0}	8.4 x 10^{-1}
4	3.9 x 10^{-1}	1.6 x 10^{-1}	-6.3 x 10^{-5}	1.7 x 10^{-5}	-2.3 x 10^{-6}	4.6 x 10^{-6}	5.6 x 10^{0}	7.6 x 10^{-1}
5	7.7 x 10^{-1}	1.6 x 10^{-1}	-7.4 x 10^{-5}	2.7 x 10^{-5}	-7.4 x 10^{-5}	2.7 x 10^{-5}	3.4 x 10^{0}	7.4 x 10^{-1}

Scaling of transport areas — Scaling relationships between transport areas of successively branching veins were assessed by comparing measured conductive areas of xylem and phloem to those expected under two different scaling models previously applied to biological and hydraulic branching systems (i.e., da Vinci's model and Murray's model) each of which predicts the relation between the cross-sectional areas of a bifurcation system (LaBarbera, 1990; Canny, 1993; McCulloh *et al.*, 2003; Eloy, 2011; Price *et al.*, 2013; Minamino & Tateno, 2014). In brief, da Vinci's model predicts the conservation of conducting area across successive branching levels, i.e., the cross-sectional area of any branching order n is equal to the sum of the areas of the next higher order of branching (n+1) (Figure 4.3), such that

$$d_n^2 = d_{n+1}^2 + d_{n+1}^2 \qquad \text{Equation 4.1}$$

Alternatively, Murray's model proposes that the optimal configuration for a hydraulic system is that in which energy dissipation is minimized and the hydraulic volume is conserved across all levels of branching, such that:

$$d_n^3 = d_{n+1}^3 + d_{n+1}^3 \qquad \text{Equation 4.2}$$

Equations 1 and 2 were used to test which of the two models better predicted the scaling relationships in the leaf vasculature of *Ginkgo*. It is important to note that the Strahler numbering system used to assign vein rank is inverted in relation to the "branching levels" used in da Vinci's and Murray's model formulations. Inspection of Figure 4.1 shows that the basalmost branching level (d_n) corresponds to veins of rank 6 and branching level *n+1* consequently corresponds to veins of decreasing rank (toward the leaf margin).

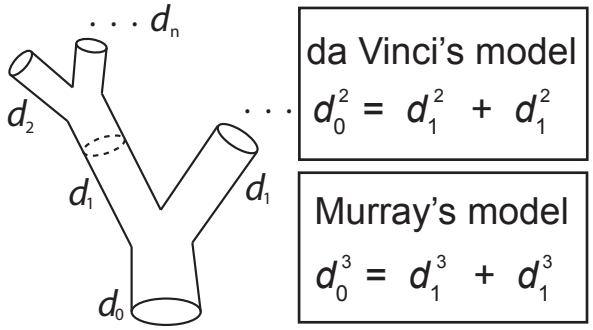

Figure 4.3. Illustration of an open dichotomous branching system depicting da Vinci's and Murray's models (left) and derivation of scaling relationships between parent branch order diameters (d_0) and higher branch orders (d_n) predicted by da Vinci's rule (top right) and Murray's rule (bottom right) (see Equations 4.1 and 4.2)

The conductive areas of each vein rank *n*+1 were used to estimate predicted diameter (*d*) values of the subjacent branching level *n*. Observed *d* values from vein rank 1 were used to predict *d* for vein rank 2, those of vein rank

2 were used to predict *d* for vein rank 3, and so forth, following da Vinci's and Murray's models. Observed *d* values were estimated from A_{phl} and A_x assuming the transport areas to behave as individual conduits. Equations 1 and 2 further assume that corresponding derivative branches have comparable diameters. This assumption is consistent with the Strahler numbering system used to designate vein rank, in that it states that branching levels only change at the junction of two vein segments of equal level. Given that xylem and phloem transport areas were seen to taper along the leaf, expected and observed values for *d* were only compared within each of the arcs established on the sample leaves. Ordinary least squares regression protocols were used to determine if the observed diameters of veins were equivalent to those predicted by da Vinci's model and by Murray's model. Either model was rejected if the slopes of regression curves for predicted vs observed conduit diameter statistically significantly differed from 1.0.

Results

The leaf hydraulic architecture of *Ginkgo* was analyzed from the perspective of (1) how the conductive areas of individual sieve cells and tracheids change along individual veins, and (2) how the sum of the conductive areas phloem and xylem in all the veins changes along the length of the leaf, from the margin to the petiole. Both approaches complement each other in that the former quantifies the transport for sugar and water transport along individual veins, whereas the latter quantifies sugar and water transport at the whole leaf level.

Conductive areas as a function of vein rank and position along the leaf— The vascular architecture of *Ginkgo* leaves is distinctively open-dichotomous. Leaf veins successively bifurcate and decrease in width toward the leaf margin without reconnection. Following the Strahler numbering system, all the vein segments at the leaf margin were assigned a Strahler number (vein rank) of 1, and increasing numbers were assigned to vein segments formed by the junction of two veins of equal rank. Five or six vein ranks were observed on any one leaf. Anatomically, the petioles of all leaves contained two separate vascular strands of the highest Strahler number (vein rank 5 or 6), each of which supplied one of the two leaf lobes. The conductive areas of both phloem (A_{phl}) and xylem (A_x) in individual veins increased with increasing vein rank (Figures 4.4A, C). However, significant variation in A_{phl} and A_x among veins of the same rank was observed for each leaf. Given that the length of any given vein rank varied (see Figure 4.1) and that each vein rank tapered in gauge as a function of vein length, the variation in A_{phl} and a_x for any vein rank was related to where along a vein conductive area was measured.

For each of the leaves examined in this study, A_{phl} and A_x were positively correlated with the distance from the leaf base (Figures 4.4B, D). Conductive areas of individual veins increased notably from the leaf margin to the base. Mean A_{phl} values ranged from 15.05 μm^2 (SD ± 9.88; $n = 33$) in veins near the leaf margin, to 2743.70 μm^2 (SD ± 458.48; $n = 5$) at the leaf base. Similarly, mean A_x values varied from 79.56 μm^2 (SD ± 49.38; $n = 33$) at the leaf margin to 15,612.83 μm^2 (SD ± 5939.88; $n = 5$) at the leaf base.

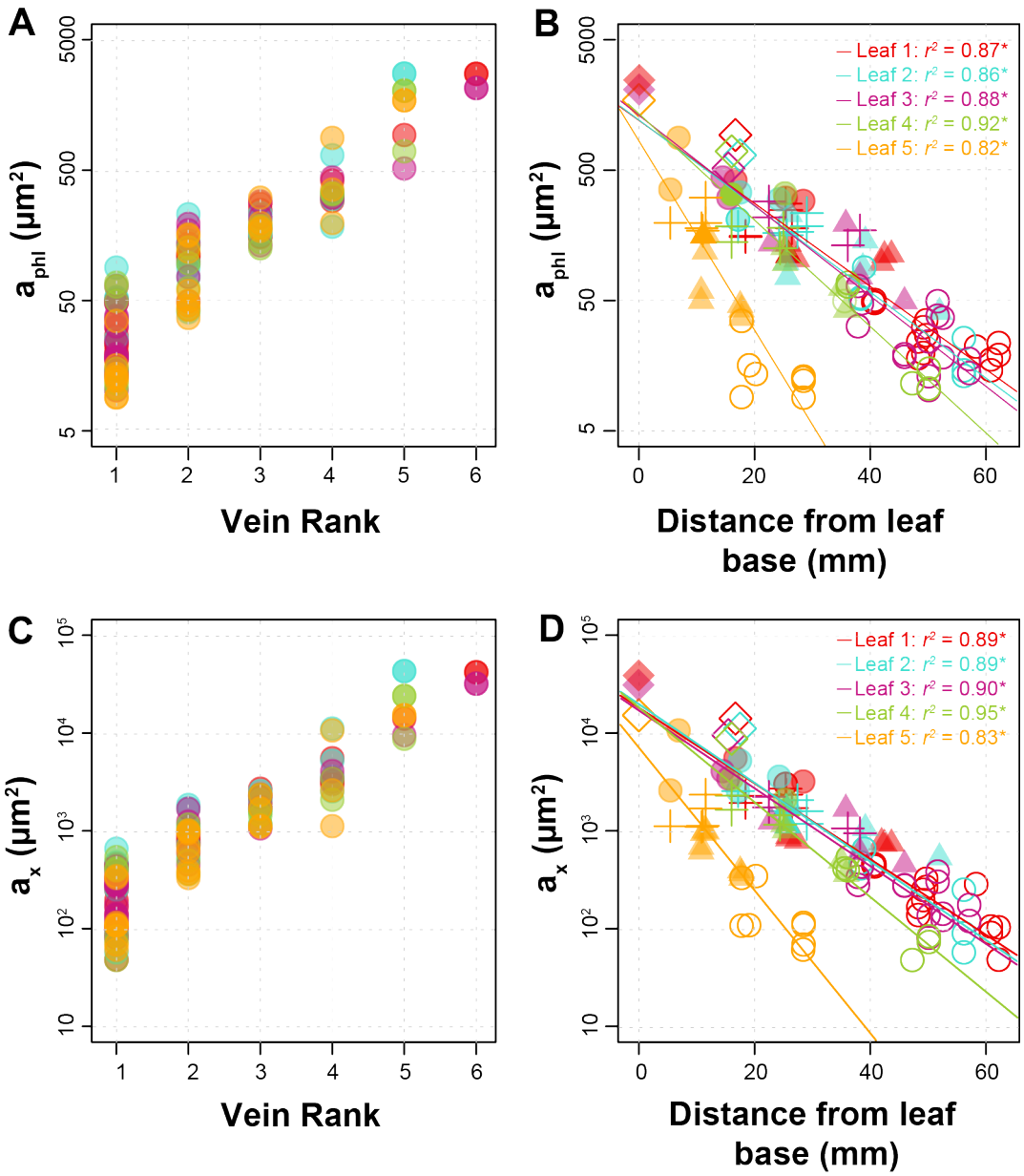

Figure 4.4 Conductive areas of phloem (A_{phl}) and xylem (A_x) of individual veins, measured in five leaves of *Ginkgo biloba*. For convenience, the data from each of the five leaves are color coded (see inserts in B and D). (A) Phloem conductive area (A_{phl}) across six vein ranks. Vein rank increases toward the leaf base, and was designated based on the Strahler branching system (see Materials and Methods and Figure 4.1). (B) Log-linear plot depicting phloem conductive area (A_{phl}) as a function of distance from the leaf base (e.g., distance 0 is at the leaf vase). Solid lines represent log-linear regression slopes for each leaf. (C) Xylem conductive area (A_x) across six vein ranks. (D) Log-linear plot depicting xylem conductive area (A_x) as a function of distance from the leaf base.

Solid lines represent regression slopes for each leaf. Leaf color-coding is consistent across all plots. Symbol coding represents vein rank: open circles = 1, solid triangles = 2, crosses = 3, solid circles = 4, open diamonds = 5, solid diamonds = 6. *$P < 0.001$.

Sieve cell and tracheid numbers and dimensions — The numbers and size of sieve cells and tracheids in a given vein increased with increasing vein rank. The diameters and lengths of individual sieve cells consistently increased with vein rank (Figure 4.5A). Sieve cell length ranged from 500 μm near the leaf margin to up to 822 μm in veins of rank 6. Cell diameters ranged from 3.6 μm to 11.4 μm, and positively correlated with cell lengths ($r^2 = 0.76$, $P < 0.001$; Figure 4.5A). The lumen area of sieve cells, measured from vein cross-sections, was consistent with sieve cell diameter and increased exponentially with increasing vein rank (Figure 4.5C). Consequently, sieve cell volume increased exponentially in veins from ranks 1 through 6 (Figure 4.5E).

Tracheid diameter and length were positively correlated with one another ($r^2 = 0.73$; $P < 0.001$) and, on average, increased with increasing vein rank (Figures 4.4B, D). However, a noticeable overlap in tracheid diameter and length was observed among veins of all ranks (Figure 4.5B). Lengths ranged from 698 μm in veins of rank 1, to >1600 μm in veins of rank 5. Thus, the longest tracheids were observed in veins rank 5 rather than vein rank 6. Tracheid diameter (and consequently tracheid cross-sectional area) consistently increased with increasing vein rank (Figure 4.5D). Tracheids ranged from 8μm in diameter in veins of rank 1 to 17μm in veins of rank 6.

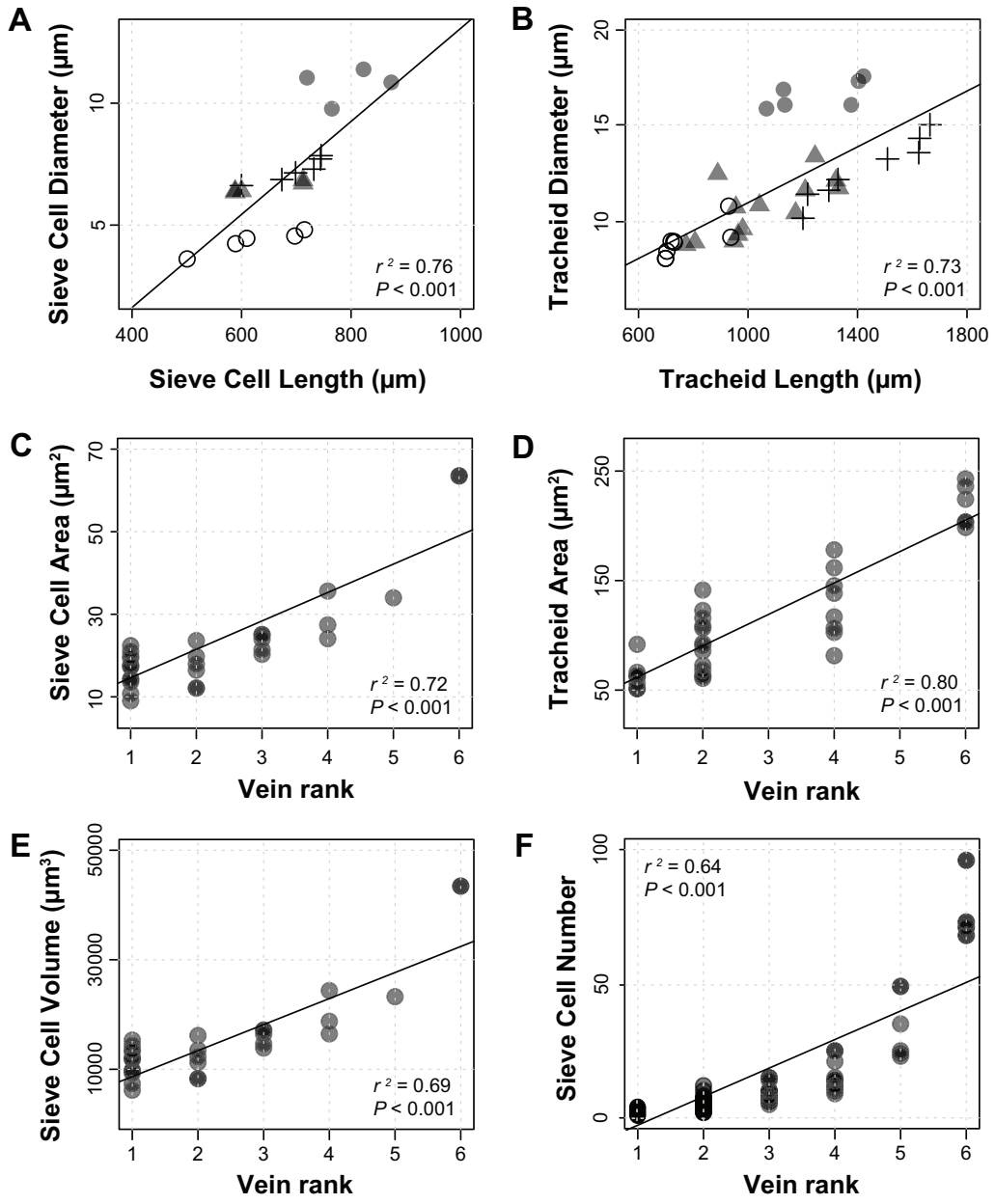

Figure 4.5. Sieve cell and tracheid dimensions measured from individual vein segments in leaves of *Ginkgo biloba*. (A) Scaling relationship of sieve cell diameter vs. cell length. Symbol coding represents vein rank. Open circles = 1, solid triangles = 3, crosses = 5, solid circles = 6. Solid line depicts regression slope. (B) Scaling relationship of tracheid diameter vs length. Symbol coding is consistent with A. (C) Sieve cell conductive area plotted as a function of 6 vein ranks (see Figure 4.1). (D) Tracheid conductive area plotted as a function of 6 vein ranks. (E) Sieve cell volume plotted as a function of 6 vein ranks. (F) Number of sieve cells in individual vein segments plotted as a function of 6 vein ranks.

The numbers of sieve cells and tracheids in individual veins increased both across veins of increasing rank, and within individual vein segments toward the leaf base. Near the leaf margin, veins of rank 1 had a single tracheid surrounded by transfusion tracheids, parenchyma, and the bundle sheath (Figure 4.3), whereas the number of tracheids reached ~ 120 on each of the two vascular strands that entered the petiole (not shown). Veins of rank 1 had between one sieve cell in the distalmost portions of the leaf to up to 4 sieve cells in the basal portions of the longest rank 1 vein segments. The number of sieve elements in veins of the highest rank reached ~50 (Figure 4.5F).

Isometric scaling of phloem and xylem — An isometric, positive relationship (a = 1.10, r^2 = 0.96, $P < 0.001$) was observed between the conductive areas of phloem (A_{phl}) and xylem (A_x) across veins (Figure 4.6). This correlation was significant when comparing within individual veins and for average values across vein ranks. On average, A_{phl} and A_x differed by a factor of five, indicating that the conductive area for xylem was consistently five times larger than that of phloem throughout the vasculature of *Ginkgo* leaves.

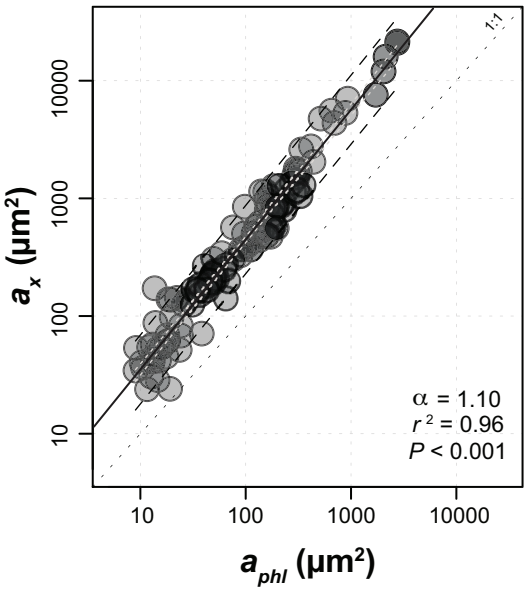

Figure 4.6. Bivariate log-log plot of the isometric relationship (a = 1.10) between phloem conductive area (A_{phl}) and xylem conductive area (A_x) in each of five *Ginkgo biloba* leaves. Solid line denotes the log-log linear scaling relationship; dashed black and white lines are the 95% prediction and 95% confidence intervals, respectively; dashed diagonal line denotes the one-to-one (1:1) relationship (note that A_x exceeds A_{phl} by one order of magnitude).

Phloem transport area increases basally along the leaf — Because individual veins of any specific vein rank differed in length on the same leaf and among the five sample leaves, phloem conducting area was normalized by dividing the phloem area measured at any distance x from the leaf base by the phloem conducting area measured at the base of the leaf. Likewise, vein length was normalized by dividing the distance x measured from the leaf base by the total vein length. Along individual veins, the normalized phloem conductive area increased exponentially with normalized leaf length (Figure 4.7A), conforming to a relationship of the form $y \sim e^{\lambda x}$, where l is the slope of the log-linear regression curve. Among the five sample leaves, l – values varied between 4.4 and 5.0. The pooled data from all 5 leaves yielded a l – value of 4.6 ($r^2 = 0.85$; $P < 0.001$).

Total phloem conductive area was calculated as the sum of a_{phl} of all individual veins at any given distance along the leaf (see Figure 4.1). The conductive areas of individual veins was calculated from regressions of measured a_{phl} for each of the vein ranks versus vein length measured from the base of the leaf (see Materials and Methods) summarized in Table 1. Within each leaf, the total phloem conductive area increased towards the leaf base (Figure 4.7B). When normalized total transport area increased with normalized vein length following a scaling relationship of the form $y \sim x^{\alpha}$ with $a = 0.42$ ($r^2 = 0.81$; $P < 0.001$) for all five sample leaves (Figure 4.7C). Individual per leaf estimates of a varied between $a = 0.44$ and 0.57.

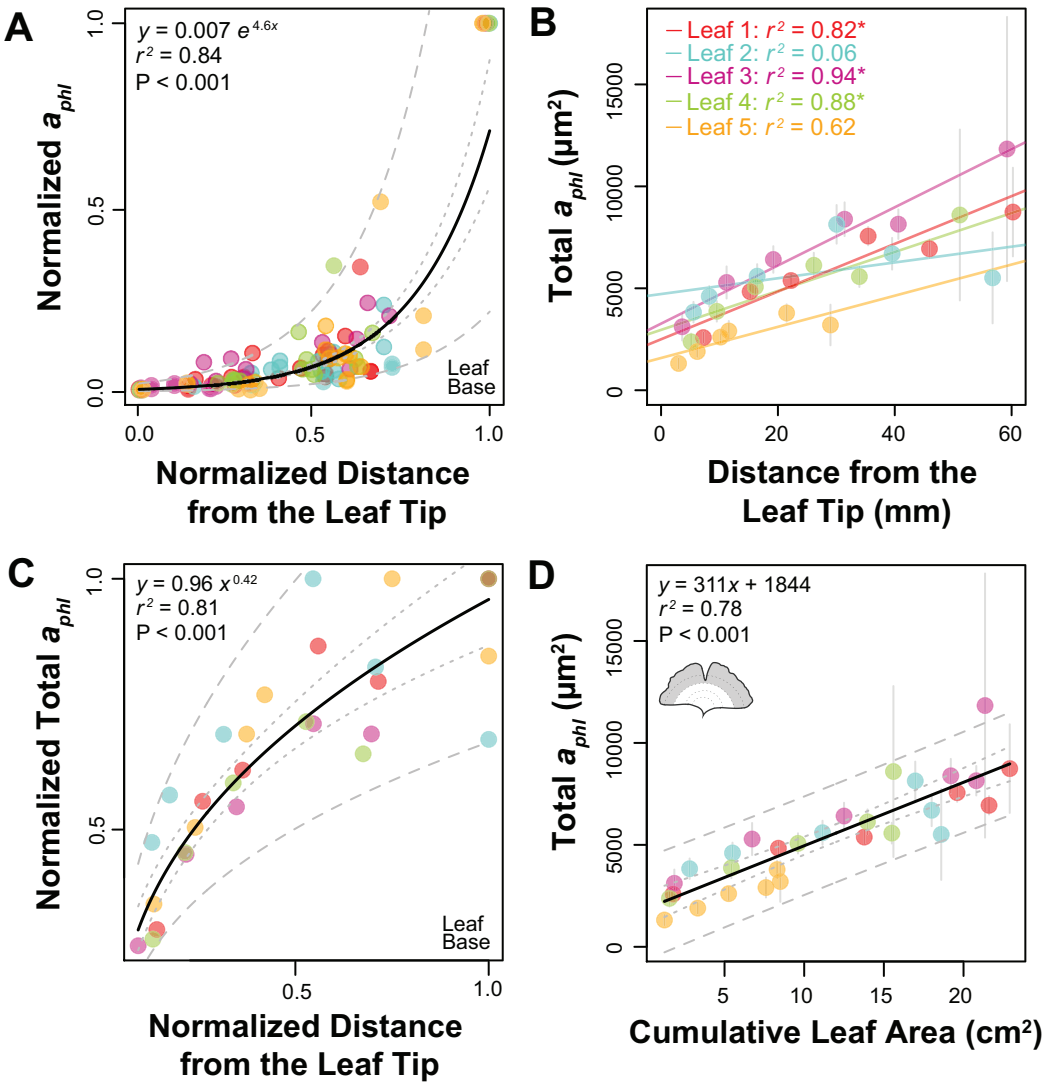

Figure 4.7 Phloem conductive area (a_{ph}), normalized conductive area, and total conductive area plotted as functions of leaf length and normalized leaf length. Dashed and dotted lines represent 95% prediction and 95% confidence intervals, respectively. Solid lines denote regression curves. Color coding (see insert in B) depicts the data from five different leaves. (A) Normalized phloem conductive area in individual veins vs. normalized leaf length. Normalized distance values converging onto 0.0 are convergent on the leaf tip; values approaching 1.0 are convergent on the leaf base. (B) Changes in total phloem conductive area (total a_{ph}) plotted as a function of leaf length. * represents $P < 0.01$ (C) Scaling relationship of normalized total phloem conductive area vs. normalized leaf length. (D) Scaling relationship between total phloem conductive area measured across different arcs (see Figure 4.1) and cumulative leaf area

measured distal to each arc. Cumulative leaf area increases toward the leaf base (see cartoon in upper left corner).

Cumulative leaf area (a measurement representing the photosynthetic leaf area that supplies the phloem at any given leaf length) was defined as the leaf area between the margin and each of the designated arches used for estimating total phloem conductive area. Both cumulative leaf area and total phloem transport area increased towards the leaf base and were linearly correlated to each other (Figure 4.7D). The regression slopes for total phloem conductive area versus cumulative leaf area of the five leaves varied between $m = 255$ and $m = 337$ (Figure 4.7D). The leaf-specific regression slopes were numerically insensitive to leaf size.

Scaling of transport areas across vein branching levels — We compared predicted phloem and xylem conduit diameters obtained from Equations 4.1–4.2 against those observed across all six vein ranks. Murray or Da Vinci's models were rejected if the slopes obtained for observed vs predicted diameters deviated from a numerical value of 1.0, where a slope of 1.0 indicates a perfect agreement between predicted and observed diameters across pairs of branching levels (vein ranks). The observed conductive diameters for phloem complied with the predictions of da Vinci's model compared to Murray's model (Figure 4.8). Because the conductive areas of the phloem and the xylem are tightly scaled to one another, comparable results were obtained for the xylem (not shown). Using da Vinci's model, the slope of predicted diameters versus observed diameters was 1.02. Using Murray's model, the slope of predicted diameters versus

observed diameters was 1.53. Thus, Murray's model was rejected as a viable mechanistic explanation for the hydraulic architecture of *Ginkgo* leaves.

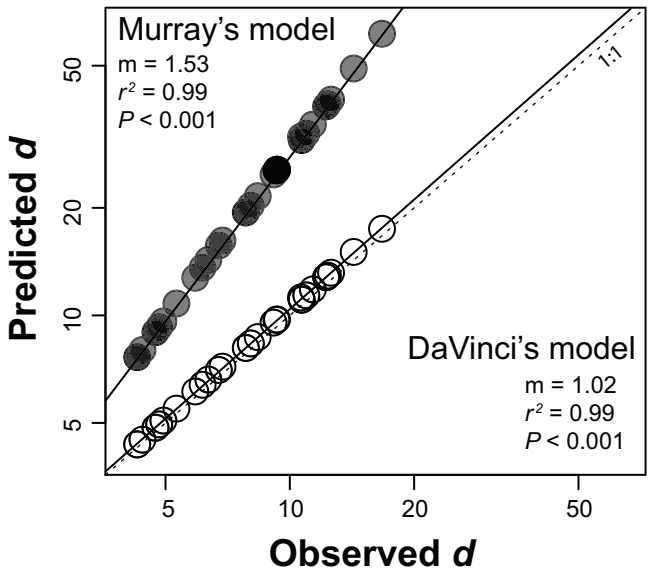

Figure 4.8 Bivariate plot of observed sieve cell conductive diameter (*d*) across all five *Ginkgo* leaves plotted against predicted cell diameter using da Vinci's model and Murray's model (Equations 4.1, 4.2). Solid lines are linear regression curves for non-transformed data (*m* = slope). Dashed line depicts a one-to-one scaling relationship (1:1). Both models obtain a linear relationship between predicted and observed cell diameters. However, the da Vinci model predicts a linear relationship with *m* = 1.02 and a *y*-intercept indistinguishable from zero.

Discussion

The data reported here show that (1) the phloem and xylem conductive areas in individual veins increase exponentially toward the leaf base, (2) sieve cell and tracheid size (length and diameter) likewise increase along the vascular

transport pathway toward the leaf base, (3) the sum of phloem (and xylem) conductive area across all veins increases basipetally and (4) conforms with a power law relationship with leaf length, (5) phloem transport area scales isometrically to that of xylem across the entire leaf, and (6) the scaling of phloem and xylem conductive areas across all vascular bifurcation levels is consistent with the area-preserving prediction of da Vinci's model. These observations are discussed in relation to comparable prior observations of vascular hydraulic structure, and their implications for phloem transport.

Leaf phloem and xylem are coupled systems — The scaling relationships between phloem and xylem conductive areas reported here for *Ginkgo* leaves have been also reported for the stems of *Abies* and *Picea* (Gričar *et al.*, 2006; Jyske & Hölttä, 2015) and for the vascular veins in poplar leaves (Carvalho *et al.*, 2017). Although phloem and xylem are structurally and developmentally coupled, an isometric scaling relationship between the transport areas of the two vascular tissues is neither a developmental nor biomechanical necessary expectation. Xylem differentiation lags behind that of phloem during primary growth and leaf development (Gunckel & Wetmore, 1946; Esau, 1965) such that neither the number nor the dimensions of tracheary and sieve elements need correspond in an isometric way, meaning that the conductive areas of xylem and phloem are not *a priori* expected to scale isometrically. Likewise, xylem water and phloem sap have very different viscosities and likely manifest different flow rates with respect to their corresponding transport areas as predicted by the Hagen-Poiseuille equation.

A hydraulic connection between phloem and xylem is necessary for long distance transport processes in plants. The continuous flux of water from the

xylem into the phloem is required for sustaining bulk flow and, under certain circumstances such as drought, the phloem can act as a reservoir of water for the xylem (Sevanto *et al.*, 2005; Sevanto, 2014a). This hydraulic connection arises because the phloem is not isolated from surrounding tissues and tends to maintain hydraulic equilibrium with the apoplast and the xylem (Thompson & Holbrook, 2003; Pfautsch *et al.*, 2015a,b). Water flow is therefore a function of water potential gradients and hydraulic conductance between the two tissues. Theoretical approaches indicate that xylem water potential can affect phloem transport rates (Sala *et al.*, 2010; Woodruff, 2014; Woodruff & Ryan, 2014), with less negative water potentials enabling higher phloem flux rates (Hölttä *et al.*, 2006, 2009). For example, in source leaves, the functional link between phloem and water is essential because the xylem must meet the transpirational demands required to sustain photosynthesis (Nikinmaa *et al.*, 2013) and because water influx into the phloem ultimately enables the turgor pressure gradient required for sugar transport. It is therefore likely that the structural correlation observed in *Ginkgo* (and previously in poplar; see Carvalho et al., 2017) reflects a balance between water supply and carbon transport needs (Savage et al., 2016) in sugar-exporting leaves.

Leaf topology and phloem hydraulic structure — Vascular topology (the spatial configuration of veins in a leaf) and conduit geometry affect the hydraulic structure of a leaf. Xylem hydraulics has been widely and intensively studied (e.g. (Sack *et al.*, 2004, 2015; Sack & Frole, 2006; Blackman *et al.*, 2010; Brodribb *et al.*, 2010; McKown *et al.*, 2010; Domec *et al.*, 2015). In contrast, phloem hydraulics has been previously described only for leaves with two distinct vascular topologies: a single veined system exemplified by *Picea* and *Pinus* and a

hierarchical reticulate vascular system such as those found in *Populus* leaves. The vasculature of *Ginkgo* leaves represents a third topological type characterized by an open dichotomous system in which the conductive areas of individual transport conduits and the total conductive area of all transport conduits increase towards the leaf base much like that reported for single vein leaves (Figure 4.9A–B). This geometry differs significantly from that of leaves typically produced by eudicots (Carvalho et al., 2017), wherein the total conductive area of all transport conduits increases toward the leaf margin (Figure 4.9C). Thus, despite the fan-shaped leaf lamina with an open dichotomous venation pattern, the phloem hydraulic architecture of *Gingko* is comparable to that of the single veined leaves of most conifers (Ronellenfitsch *et al*., 2015b), which manifest the simplest vascular topology among extant seed plants.

In this respect, the stereotypical leaves of eudicots are hydraulically more efficient than those of conifers and *Ginkgo* because a hierarchical reticulate transport system allows for a larger numbers of smaller veins and permits differences in vein functionality. The phloem in the minor and major veins of eudicot leaves have distinct photosynthate loading-transport functions, i.e., the minor veins function as photosynthate "collectors", whereas the higher order veins serve primarily as efflux transporters. Two observations indicate that this functional distinction between the vein classes appears not to be the case for *Ginkgo*. First, as seen in pine needles (Liesche *et al*., 2011), mesophyll cells are arranged in rows and are separated by intercellular spaces throughout the leaf lamina in a manner that likely restricts the axial pathway for fixed sugar transport out of the mesophyll. And second, anatomical differences that constrain the symplastic connectivity between sieve cells and surrounding

photosynthetic tissues are not evident across the different vein ranks of *Ginkgo*. We contend that these two observations are sufficient to conclude that the phloem hydraulic architecture of *Ginkgo*'s open dichotomous vascular system and the reticulate vasculature of leaves such as those of poplar are structurally and functionally very different.

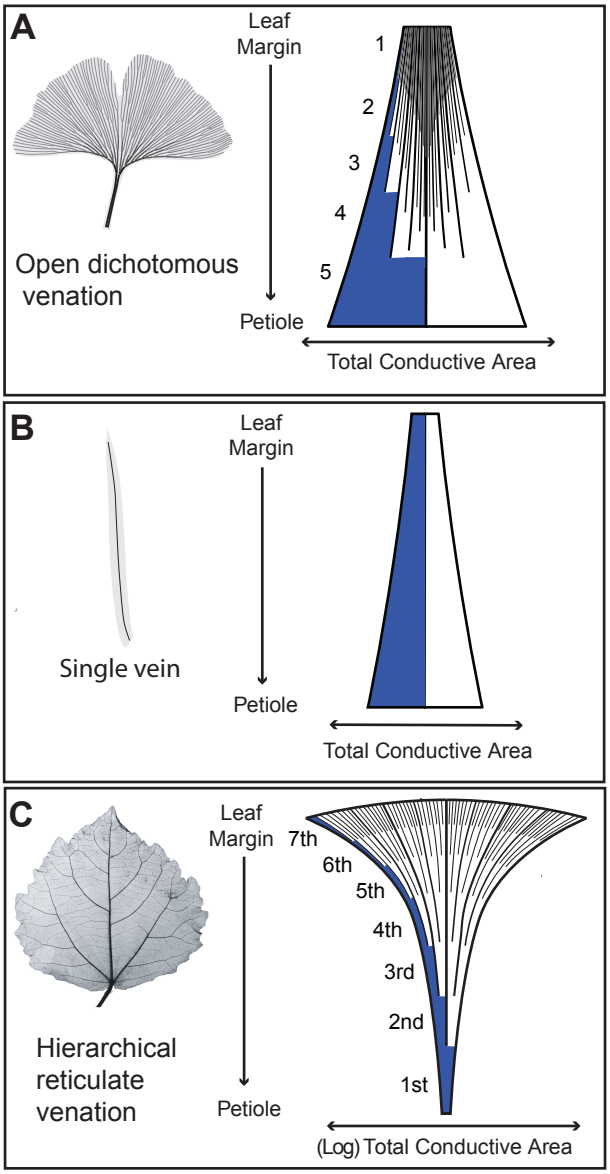

Figure 4.9. Hydraulic models for three different vascular topologies (open dichotomous, single vein, and hierarchical reticulate venation patterns). Areas colored in blue (shown to the right of each model) depict the increase in the conductive area of a single transport conduit (e.g., a single sieve tube or a single vessel). The width of the entire diagram represents the width of the total conductive area as initially separate transport conduits merge together. Note that, in each of the three models, the area of a single transport conduit increases toward the base of the leaf (as predicted by Münch's Pressure Flow Hypothesis), whereas the total conductive area increases toward the leaf margin only in the hierarchical reticulate venation model. (A) Open dichotomous venation model for leaves such as those produced by *Ginkgo*. In this model, total conductive area increases toward the leaf base (the widths of sections 1 to 5 are proportional to the total phloem conductive areas measured for actual *Ginkgo* leaves). (B) Single vein model representing the vascular architecture of leaves such as those produced by *Picea* or *Pinus* (width of total transport area is inferred from data reported by Ronellenfitsch et al., 2015). (C). Hierarchical reticulate venation model of the transport system of leaves such as those of poplar (the widths of vein orders 1 to 7 are proportional to the data reported by Carvalho et al., 2017).

Münch's Pressure Flow Hypothesis and the Hägen-Poiseuille Equation — The scaling of phloem transport area a_{phl} with respect to the distance x from the leaf margin (see Figure 4.7C) is consistent to that of *Picea* and *Pinus* and conforms to theoretical mathematical models that minimize the dissipation of transport energy. Specifically, the scaling observed in *Ginkgo* leaves follows the power law $A_{phl}(x) \sim x^{1/2}$ formulated by Ronellenfitsch et al. (2015) that emerges from the wedding of Münch's Pressure Flow Hypothesis and the Hägen-Poiseuille equation for laminar flow. According to the application of Hägen-Poiseille equations to phloem flow, the conductance of a conduit formed by sieve cells connected end-to-end scales with the fourth power of the conduit's radius, and sieve cell end-walls are the major resistance points flow (Thompson, 2006;

Knoblauch & Oparka, 2012; Sevanto, 2014a). Phloem conductance is expected therefore to increase towards the leaf base when phloem transport area in individual veins increases basipetally. This trend is matched empirically by the changes in the length and volume of individual sieve cells reported here. Given that cell end-walls are the greatest resistance points for transport, longer sieve cell lengths effectively reduce flow resistance for a given vein length. Similarly, end wall resistance is coupled to the resistance of the sieve cell lumen, both of which decrease with increasing cell diameter (Jensen *et al.*, 2012b). This sieve cell geometry contrasts with that previously reported for pine needles (Ronellenfitsch et al., 2015) and is inconsistent with phloem flux models that assume sieve element radii are constant throughout a phloem conduit (Thompson & Holbrook, 2003; Jensen *et al.*, 2012b). Although the available evidence indicates that hydraulic conductivity does not impose a significant (if any) constraint on phloem flux (Froelich *et al.*, 2011; Lucas *et al.*, 2013), the extent to which increasing sieve cell dimensions affect estimates of phloem translocation must be examined carefully.

Contending branching models — Two scaling relationships have been used to describe the hydraulic architecture of dichotomously branched systems: Murray's model and da Vinci's model (Murray, 1926; Richter, 1980; McCulloh et al., 2003). Murray's model predicts that the diameters of successively higher order branches will scale as the third power, whereas da Vinci's model predicts that the diameters of successively higher order branches will scale as the second power (see Equation 1–2). Our analyses of phloem and xylem conductive diameters across veins of increasing rank are consistent with the predictions of da Vinci's model and inconsistent with the predictions of Murray's model.

Murray's model has been previously found to describe the branching of stem and compound leaf rachides vasculatures (McCulloh *et al.*, 2003) as well as the branching in the lower rank leaf veins of various taxa (Canny, 1993; Price *et al.*, 2013). In this context, it is important to note that our study it did not evaluate scaling relationships at every vein branching point, but only considered the relationship between veins of increasing rank. One of the major issues with applying either da Vinci's or Murray's model to leaf vascular systems is that neither is based on physiological principals that govern leaf hydraulics. The leaf vasculature of *Ginkgo* is an open system in which veins continuously loose xylem water to transpiration whereas the phloem gains some water during sugar loading. This single fact invalidates Murray's model, which stipulates a steady-state system with constant flux rates along the entire transport pathway. Similarly, da Vinci's model is actually best seen as a structural model that predicts scaling relationships in self-supporting branching systems experiencing mechanical stress (Eloy, 2011; Minamino & Tateno, 2014). In the case of *Ginkgo* leaves, the area-preserving relationship predicted by da Vinci's model is expected for the conductive areas just above and below vein junctions. This model does not and cannot explain the functional significance (if any) of the significant tapering of phloem and xylem conductive areas along the lengths of individual veins, which clearly contradicts any area-preserving model across all levels of vascular branching in *Ginkgo*. These and other observations indicate that geometric models, such as those of da Vinci or Murray, are biologically simplistic. Although current hydraulic models for xylem water transport appear adequate, much future work is required to develop and refine corresponding mathematical models to deal with the complexity of phloem transport.

Concluding Remarks

We have described and quantified the hydraulic architecture of *Ginkgo biloba* leaves and shown that (1) the conductive areas of sieve cells and tracheids scale isometrically across all leaf vein ranks and the petiole, (2) the conductive areas of individual veins and the total conductive areas of all veins at any distance from the leaf base increase basipetally, and (3) the lengths and conductive areas of sieve cells and tracheids also increase toward the leaf base. When have also shown that, despite the open dichotomous venation of *Ginkgo* and the large number of veins at the leaf margin, the phloem hydraulic structure is consistent with that of single veined conifers in that the total conductive area of phloem increases toward the leaf base. This hydraulic architecture is distinct from that observed in hierarchical reticulate veined leaves, in which the reticulation allows for a much larger number (and consequently a much larger total conductive area) of smaller, collector veins. Further, we have shown that the scaling of phloem conductive area is consistent with mathematical predictions of Münch's Pressure Flow Hypothesis and with da Vinci's area-preserving model, although the latter fails to explain the tapering in conductive areas observed in the leaf vascular system of *Ginkgo*. Future work will be devoted to providing a numerical model for phloem loading using the data reported here and elsewhere.

CONCLUDING REMARKS

Leaf hydraulic structure and phloem transport

In leaves, the hydraulic structure of phloem is formed by the set of phloem transport conduits formed by files of sieve elements connected end-to-end that provide low-resistance pathways effectively connecting the mesophyll with the rest of the plant body. As a whole, this collection of conduits provides the structural framework required for the collection and export of fixed sugars. Consequently, the hydraulic structure of a leaf is not only determined by the spatial configuration of veins (vascular topology), but by the continuity, geometry and the lateral interconnectity of the transport conduits. Whereas vascular topology determines the specific pathway(s) for sap movement, the variations of conduit geometry along this pathway affect transport parameters such as flow velocity, resistance, and pressure-osmotic potentials. The extent to which these transport parameters vary in response to changes in conduit geometry remains to be experimentally explored. However, the hydraulic architectures described in chapters 3 and 4 provide a physical baseline that reconciles classic views of phloem transport dynamics along individual conduits with phloem transport at the organ level. The following sections conceptually explore some of the form-function relations between leaf hydraulic structure and phloem dynamics that must be considered when describing phloem transport.

Phloem loading and transport occur at the sieve element-level

The loading of sugars into the phloem provides the osmotically-mediated pressure differential between the sources and sinks required for long-distance transport (Münch, 1930; Turgeon & Ayre, 2005; Comtet *et al.*, 2016). This mechanistic process has been traditionally described following the Hägen-Poiseuille formulations for pipe flow

$$Q = K_T\ (P_{leaf} - P_{root})$$

where the volume flow rate (Q [$m^3\ s^{-1}$]), is determined by the pressure differential in the phloem between sources ('leaf') and sinks ('root'; P [Pa]), and a coefficient of proportionality determined by phloem conductance (K_T [$m^3\ Pa^{-1}\ s^{-1}$]). The Van't Hoff relation is a good aproximation for the osmotic potential of dilute solutions such as those observed in the leaf phloem (Nobel, 2011). This equation is typically expressed in terms of sugar concentration (c [$mmol\ l^{-1}$]):

$$Q = K_T \times RT(c_{leaf} - c_{root})$$

The loading of sugars into sieve elements can be mediated by passive or active loading mechanisms. Passive loading mechanisms require that sugars follow a concentration gradient from the mesophyll into the phloem via the symplast through plasmodesmata. In contrast, active loading mechanisms require the expenditure of ATP either in synthesizing sucrose-based oligosaccharides in intermediary cells and therefore "trapping" fixed sugar molecules, or in moving sucrose from the apoplast and into companion cells via sugar transporters (Rennie & Turgeon, 2009; Slewinski *et al.*, 2013). Active-loading mechanisms have only been described in some species of angiosperms, and the scant data available for gymnosperms indicate they are likely to load sugars passively (Liesche &

Schulz, 2013). Loading mechanisms in ferns, horsetails, and lycopods remain untested.

Sugar loading into the phloem is a process that occurs at the level of sieve elements. Whether leaves use active or passive loading mechanisms, the connectivity between sieve elements and surrounding cell-types can ultimately constrain the rate at which sugars are loaded into the phloem. This is particularly true for symplasmic, passive-loading species such as poplar and *Ginkgo*, where the number of plasmodesmata and contact areas between the sieve elements and companion or strasburger cells determine the sugar flux into the phloem transport conduits (Liesche & Schulz, 2012; Zhang *et al.*, 2014; Liesche, 2017). Because sieve elements are living and their membranes are semipermeable, their surface area mediates both the loading of fixed sugars and the concurrent influx of water required for water potential equilibrium across all leaf tissues.

Effects of sieve element size in transport dynamics — The size (length and width) of sieve elements along the sugar export pathway In most angiosperm leaves, sugars are loaded into the minor veins (orders 4^{th} – 7^{th}), whereas major veins are mainly involved in efflux transport (not loading) of photosynthates (see Chapter 3). In contrast, all vein ranks in *Ginkgo* appear to be capable of phloem loading due to symplastic continuity (see Chapter 4). Once loaded into the sieve elements, the transport of sugars is restricted to the phloem conduits. The conductive areas and lengths of the individual sieve elements that form these conduits increases along the sugar export pathway, as observed in leaves of both poplar and *Ginkgo*. Longer sieve elements decrease the resistance to phloem transport because they effectively reduce the number of end walls per conduit

length. In accordance to the physics described in the Hägen-Poiseuille formulations, the conductance of the phloem conduit is proportional to the 4th power of its radius (Nobel, 2009),

$$K_T = -\frac{\pi r^4}{8\eta}$$

where η is phloem viscocity. Wider sieve elements therefore increase conductance (or reduce resistance) within the lumen of each sieve element.

One of the problems associated with describing phloem transport exclusively using Hagen-Poiseuille equations is that these assume conduits to be closed systems in which volumetric flow is conserved, and therefore no water or solute exchange is considered. Experimental evidence indicates that significant water exchange between phloem conduits and surrounding tissues occurs throughout the entire long-distance transport pathway (Weatherley, 1973; Young *et al.*, 1973), and numerous approaches aiming to relax some of the assumptions in the Hagen Poiseuille equations have been proposed (Thompson & Holbrook, 2003; Jensen *et al.*, 2011, 2016; Sevanto, 2014).

Sieve element shape, described as the scaling relationship between cell diameter and length, determines the extent to which cell surface area and conductive areas change along the phloem pathway. In *Ginkgo*, the diameter of sieve cells scales with sieve cell length to the fourth power (Figure 5.1A). Consequently, the ratio of surface area to conductive area in sieve elements decrease as cells become larger (wider and longer) along the phloem export pathway (Figures 5.1B–C). Given that sieve element surface area mediates sugar loading and water exchange, it is likely that decreasing surface area to conductive area ratios can have significant effects on flow dynamics. Small sieve

cells have low axial conductive capacities given their small diameters and conductive areas, but have a proportionally much larger contact area that favors the radial flux of sugars and water into the sieve elements. Small sieve cells are found in veins of rank 1 and in the periphery of veins of increasing rank. Accordingly, the larger sieve elements found in veins of higher rank have a much higher conductance to axial flow than to radial flow, given their proportionally reduced surface areas. In contrast, lengths and widths of poplar sieve tube members scale almost isometrically (Figure 5.1A), such that the ratio of surface area to conductive area is nearly constant across sieve tubes of increasing size (Figure 5.1B–C).

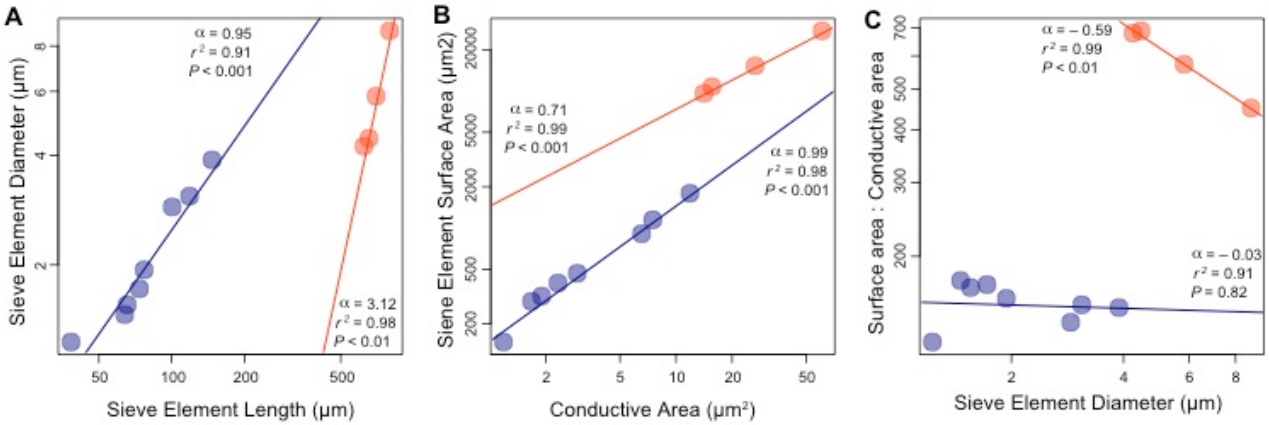

Figure 5.1. Allometry of sieve elements of poplar and *Ginkgo.* Blue depicts poplar, orange depicts *Ginkgo*. Each point represents the mean values for each vein order or vein rank. A. Sieve element shape represented by the scaling between sieve element diameter and length. B. Scaling of sieve element conductive area and surface area across veins of different order and rank. C. Relationship between surface area to conductive area ratio and sieve element diameter.

It is noteworthy that in the leaves of *Ginkgo*, the longest and most abundant veins are those of the two lowest ranks and are also those containing

the smallest sieve cells. Even though there is no apparent functional differentiation across veins of *Ginkgo*, sieve cell geometry indicates that as veins increase in rank, phloem conduits become more suited for axial transport and proportionally less suited for radial sugar collection. In addition, the anatomical organization of sieve cells further reduces the effective sieve element contact area in larger veins. Sieve cells are organized in a tightly packed grid-like manner (see Figure 5.2). In larger veins, strands of radial parenchyma separate groups of sieve cells into distinct "grids" of ranks and files, but as the number of sieve cells increases, some sieve cells may become completely surrounded by other sieve cells and are therefore effectively shielded from mesophyll cells. In this sense, the effective contact area between the phloem conduits and the surrounding transfussion tissue becomes restricted to the most peripheral sieve cell walls. It is worth noting, that sieve elements are typically arranged in sets with one or two files of cells bounded by ray parenchyma.

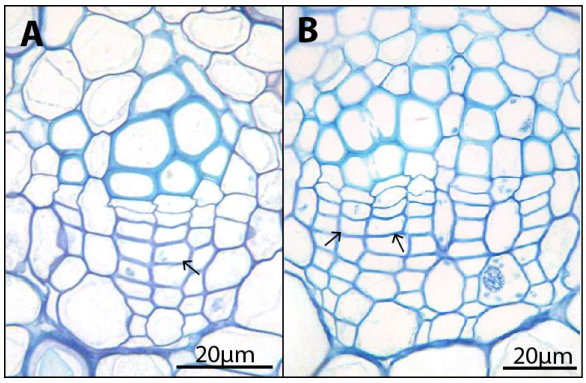

Figure 5. 2. Representative vein cross-sections showing the grid-like anatomical organization of sieve cells in leaves of *Ginkgo*. Arrows indicate sieve cells completely surrounded by other sieve cells and therefore lacking direct contact with transfusion cells. A. Vein of rank 2. B. Vein of rank 3.

Interconnections between sieve elements — The physical and functional interconnections between adjacent sieve elements ultimately determine the extent to which phloem transport is restricted to individual phloem conduits or can be simplified as such. In the leaves of both *Ginkgo* and poplar, the numbers of sieve elements in vein cross-sectional areas increase along the phloem export pathway, indicating that the number of phloem conduits in individual veins also increases as veins increase in rank (in the case of *Ginkgo*) or decrease in vein order (in the case of poplar). However, the number of phloem conduits in the petiole is less than the estimated total number of phloem conduits in the smallest collector veins (Figure 5.3), indicating that some phloem conduits must merge with each other along the phloem transport pathway. To the best of my knowledge, these sorts of detailed anatomical and structural data have not yet been produced from leaves.

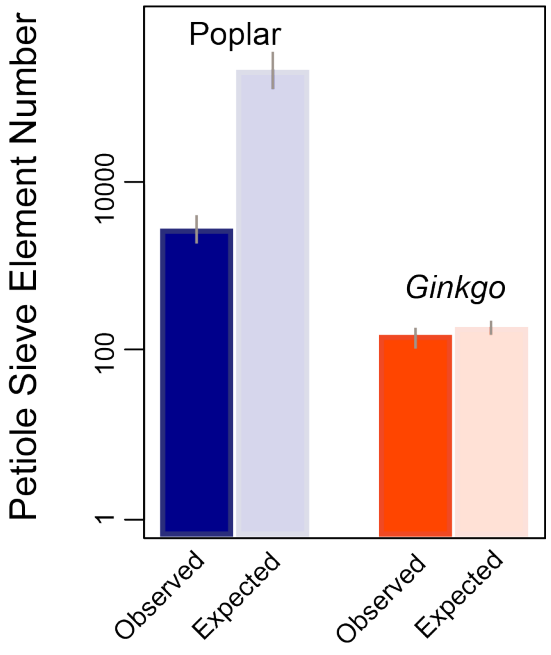

Figure 5.3. Observed and expected numbers of sieve elements in the petiole of poplar and *Ginkgo*. Expected values were estimated using the mean total numbers of 7th order veins in poplar leaves and the mean total number of veins of rank 1 in leaves of *Ginkgo*, and assuming that sieve element conduits do not merge along the vascular pathway.

Ontogenetic and anatomical differences between sieve tube members and sieve cells are particularly relevant in terms of phloem conduit interconnectivity. Lateral connections between sieve tube members (as seen in cross-section) along veins are typically minimal due to the presence of companion cells. However, sieve tubes have a complex 3D organization along individual veins and do not run as strictly parallel conduits. Sieve tube members from distinct sieve tubes may therefore connect laterally and form anastomosing structures within veins.

In contrast, sieve cells in *Ginkgo* are not developmentally coupled to companion cells and are instead organized in a tightly packed grid-like manner. Abundant sieve areas are found between adjacent sieve cells, however, the extent to which they allow cross-talk between laterally adjoining sieve cells remains untested. Functional interconnections between adjacent sieve elements allowing sufficient transport between phloem conduits would indicate that phloem transport in veins could be simplified and conceptualized to operate as one large phloem conduit, instead as the collection of numerous individual conduits.

Leaf topology and effective pathlengths

Formal topological descriptions of leaf vasculature are fairly recent (Katifori & Magnasco, 2012; Ronellenfitsch *et al.*, 2015a); however, some of the functional properties associated to vascular patterns have long been experimentally addressed (e.g. Wylie, 1938, 1939). Form-function relations between vascular topology and leaf hydraulics have focused on reticulate-veined leaves (such as those of poplar) and the redundancy in the water transport pathway. This redundancy, provides the leaf with resistance to mechanical or insect feeding damage that could severe the pathway for water distribution in

the leaf (Roth *et al.*, 1995; Roth-Nebelsick *et al.*, 2001), particularly at the lower levels of vascular hierarchy (i.e., major veins).

The vascular topology also provides functional implications for phloem loading and transport because it determines the numbers, lengths and interconnectivity of phloem conduits in the leaf lamina.

1. *Vein length* — Highly reticulate systems effectively divide the leaf lamina into small discrete functional areas and allow for the extensive packing of veins into small areas. Values of vein length per area (VLA) can reach up to 16 mm of minor vein length per mm^2 of leaf lamina in poplar, whereas *Ginkgo* leaves have values of up to 3.5 mm/mm^2. The density of veins per unit area has direct implications on sugar loading, given that it ultimately relates the sieve element surface contact area to the photosynthetic area of the leaf (Amiard *et al.*, 2005). Considering an average poplar sieve tube member with a 2 μm diameter, the surface contact area for a single sieve tube in minor veins can reach up to ~100,000 μm^2 in an area of 1 mm^2 (100,000 μm^2) of leaf lamina. As the numbers of sieve tubes increase in veins of increasing order, so does the ratio of sieve tube surface contact area to photosynthetic leaf lamina. Comparable estimations in *Ginkgo* and considering an average sieve cell measuring 2 and 5 μm along its short and long axis, respectively, predict that the surface area for a single phloem conduit can measure up to 56,000 μm^2 per 1 mm^2 of leaf lamina. Anatomical differences between *Ginkgo* and poplar also determine that the sieve element surface contact areas are not additive when the number of phloem conduits increases due to the lateral connections between adjacent sieve elements within veins (Figure 5.2).

2. *Vein number* — The differences in the shape of the hydraulic models proposed for poplar and *Ginkgo* (Figure 4.7) are to a great extent determined by their difference in vascular topology. Within individual veins, phloem conductive areas increase along the sugar export pathway in a similar way in leaves of poplar and *Ginkgo*, however, the total conductive areas in these leaves show opposite patterns. The extensive reticulation and packing of veins in poplar leaves dictates not only the length, but also the total number of veins in poplar leaves. For example, around 206,000 7th order veins were found in leaves of poplar, whereas the number of vascular strands in *Ginkgo* ranged between 150 and 160 . The number of minor veins established by vascular reticulation in poplar makes the total conductive areas of minor veins markedly higher than the total conductive areas of major veins. In contrast, the number veins of *Ginkgo* along the sugar export pathway are not as numerous as would be required to overcome the overall tapering observed along individual veins from the base of the leaf to its margin.

3. *Vascular hierarchy and vascular connections* — Highly reticulate or looped networks are also highly redundant, meaning that multiple pathways exist between two given points in the network. A representative leaf fragment containing vein orders 2nd – 7th was digitized into a node-edge graph using NEFI, and was analyzed using NetworkX (Hagberg *et al*., 2008). Over 5000 different pathways exist between a random 7th order vein and the closest 3rd order vein in leaves of poplar when vascular hierarchy is not taken into consideration. Vascular hierarchy allows for the functional distinction between minor and

major veins in a reticulate venation system, and also restricts the number of pathways that realistically connect two points in a biologically meaningful way. Assuming that phloem translocation can only proceed through veins of increasing order, the number of pathways connecting a 7th order vein with the major veins is reduced from >5000 to only 14 (Figure 5.4). Even though this approximation is on itself, a drastic simplification of a complex system, it provides a better idea of the biologically reasonable pathways that a sugar molecule could follow as it exists the leaf and shows that redundancy remains even when imposing restrictions to phloem translocation.

Theoretical approaches to transport in systems with high redundancy are better suited to cope with damage or load fluctuations (Katifori *et al.*, 2010). In terms of phloem dynamics of symplastic loading species, it is likely that at the level of minor veins, sugar loading and transport follow local gradients of pressure and concentration arising, for example, from uneven photosynthetic rates across the leaf lamina due to shading. Redundancy in the phloem transport network provides faster response time to transient changes on local pressure by allowing for changes in the direction of flow in interconnected networks. For example, flow along a 5th order vein connecting two 4th order veins can be preferentially redirected towards the vein with the lowest pressure.

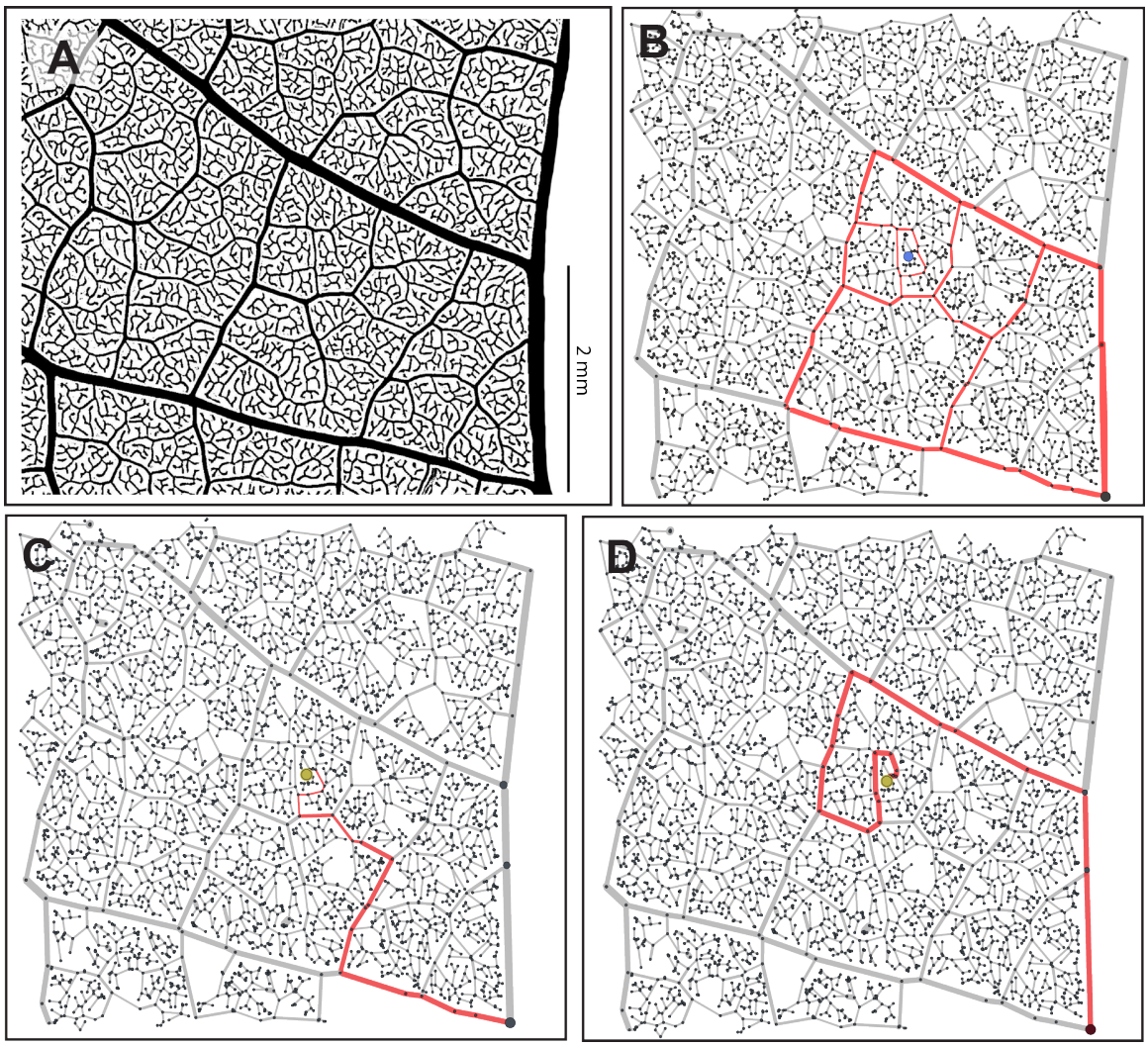

Figure 5.4. Network analysis of a representative leaf fragment of poplar indicating the redundancy in phloem transport pathways when phloem translocation is restricted to veins of decreasing order. A. Sample image. B. Fourteen pathways between a single 7th order vein and the major veins. C. Shortest pathway. D. Longest pathway.

It is important to note, however, that unless the radial movement of solutes across adjacent sieve tubes is significant, the redundancy of the vascular network will be restricted by the specific axial connections of sieve tubes. Once a sugar molecule is loaded into a given sieve tube member, its translocation will be

restricted to a single sieve tube (i.e., conduits) and its connection to other sieve tubes at vein branching points. In poplar, the numbers of sieve tubes increase from 7th order veins towards the major veins, but the total number of tubes in the leaf is not conserved across the different orders of branching. These two observations indicate that while some phloem conduits connect at vein branching points, others simply become adjacent conduits as vein order increases.

Summary

Given the complexity involved in phloem transport, current approaches in modeling transport dynamics are restricted to considering single conduits that oversimplify the sieve tube structure and does not fully describe phloem transport at the organ or plant level. The intricacy of leaf vasculature raises many questions regarding the form-function relations in phloem loading and transport dynamics. This thesis provides a structural framework for phloem transport, along with three key observations that should be considered in future modeling of leaf phloem transport:

1. Phloem conduit size (sieve element cross-sectional area) increases along the phloem pathway in a leaf, and the extent to which this affects phloem flow needs to be addressed.
2. Phloem conduits merge along the sugar loading/transport pathway, particularly in hierarchical reticulate leaves.
3. Vascular architecture determines how total conductive areas change along the phloem pathway.

BIBLIOGRAPHY

Amiard V, Mueh KE, Demmig-Adams B, Ebbert V, Turgeon R, Adams WW. **2005**. Anatomical and photosynthetic acclimation to the light environment in species with differing mechanisms of phloem loading. *Proceedings of the National Academy of Sciences of the United States of America* **102**: 12968–73.
Artschwager E. **1950**. The Time Factor in the Differentiation of Secondary Xylem and Phloem in Pecan. *American Journal of Botany* **37**: 15–24.
Babst B a, Ferrieri R a, Gray DW, Lerdau M, Schlyer DJ, Schueller M, Thorpe MR, Orians CM. **2005**. Jasmonic acid induces rapid changes in carbon transport and partitioning in Populus. *The New phytologist* **167**: 63–72.
Baker-Brosh K, Peet RK. **1997**. The ecological significance of lobed and toothed leaves in temperate forest trees. *Ecology* **78**: 1250–1255.
Blackman CJ, Brodribb TJ, Jordan GJ. **2010**. Leaf hydraulic vulnerability is related to conduit dimensions and drought resistance across a diverse range of woody angiosperms. *New Phytologist* **188**: 1113–1123.
Blechschmidt-Schneider S, Eschrich W, Jahnke S. **1997**. Phloem loading, translocation and unloading processes. In: Rennenberg H,, In: Eschrich W,, In: Ziegler H, eds. Trees: Contributions to Modern Tree Physiology. Leiden: Backhuys Publishers, 139–163.
Boodley J, Sheldrake, Jr. R. **1982**. Cornell Peat-Lite Mixes. *Cornell Cooperative Ext. Pub. Bul. 43.*: 1–8.
Boyce CK, Brodribb TJ, Feild TS, Zwieniecki M a. **2009**. Angiosperm leaf vein evolution was physiologically and environmentally transformative. *Proceedings. Biological sciences / The Royal Society* **276**: 1771–6.
Brodersen CR, McElrone AJ. **2013**. Maintenance of xylem Network Transport Capacity: A Review of Embolism Repair in Vascular Plants. *Frontiers in Plant Science* **4**: 108.
Brodribb TJ. **2009**. Xylem hydraulic physiology: The functional backbone of terrestrial plant productivity. *Plant Science* **177**: 245–251.
Brodribb TJ, Bienaimé D, Marmottant P. **2016**. Revealing catastrophic failure of leaf networks under stress. *Proceedings of the National Academy of Sciences* **113**: 201522569.
Brodribb TJ, Feild TS, Jordan GJ. **2007**. Leaf maximum photosynthetic rate and venation are linked by hydraulics. *Plant physiology* **144**: 1890–8.
Brodribb TJ, Feild TS, Sack L. **2010**. Viewing leaf structure and evolution from a hydraulic perspective. *Functional Plant Biology* **37**: 488.
Canny MJ. **1993**. The Transpiration Stream in the Leaf Apoplast: Water and Solutes. *Philosophical Transactions of the Royal Society B: Biological Sciences* **341**: 87–100.
Carvalho MR, Turgeon R, Owens T, Niklas KJ. **2017**. The scaling of the hydraulic architecture in poplar leaves. *New Phytologist*.
Carvalho MR, Woll A, Niklas KJ. **2016**. Spatiotemporal distribution of essential elements through *Populus* leaf ontogeny. *Journal of Experimental Botany* **67**: 2777–2786.
Christianson ML, Niklas KJ. **2011**. Patterns of diversity in leaves from canopies of Ginkgo biloba are revealed using Specific Leaf Area as a morphological

character. *American journal of botany* **98**: 1068–76.
Comtet J, Jensen KH, Turgeon R, Stroock AD, Hosoi AE. **2016**. Passive phloem loading and long-distance transport in a synthetic tree-on-a-chip. *ArXiv preprint*.
Comtet J, Jensen KH, Turgeon R, Stroock AD, Hosoi AE. **2017**. Passive phloem loading and long-distance transport in a synthetic tree-on-a-chip. *Nature Plants* **3**: 17032.
Conn S, Gilliham M. **2010**. Comparative physiology of elemental distributions in plants. *Annals of Botany* **105**: 1081–1102.
Conn SJ, Gilliham M, Athman A, Schreiber AW, Baumann U, Moller I, Cheng N-H, Stancombe M a, Hirschi KD, Webb A a R, *et al.* 2011. Cell-specific vacuolar calcium storage mediated by CAX1 regulates apoplastic calcium concentration, gas exchange, and plant productivity in Arabidopsis. *The Plant cell* **23**: 240–257.
Corson F, Henry H, Adda-Bedia M. **2010**. A model for hierarchical patterns under mechanical stresses. *Philosophical Magazine* **90**: 357–373.
Critchfield WB. **1970**. Shoot Growth and Heterophylly in Ginkgo Biloba. *Botanical Gazette* **131**: 150–162.
Deeken R, Sanders C, Ache P, Hedrich R. **2000**. Developmental and light-dependent regulation of a phloem- localised K + channel of Arabidopsis thaliana. **23**.
Dickmann DI. **1971**. Photosynthesis and resiration by developing leaves of cottonwood (Populus deltoides Bartr.). *Botanical Gazette* **132**: 253–259.
Dickmann D, Gordon JC. **1975**. Incorporation of 14C-Photosynthate into Protein during Leaf Development in Young Populus plants. *Plant Physiology* **56**: 23–27.
Dickson RE, Larson PR. **1981**. 14C fixation, metabolic labeling patterns, and translocation profiles during leaf development in Populus deltoides. *Planta* **152**: 461–470.
Dirnberger M, Kehl T, Neumann A. **2015**. NEFI: Network Extraction From Images. *Scientific Reports* **5**: 15669.
Domec J-C, Palmroth S, Oren R. **2015**. Effects of Pinus taeda leaf anatomy on vascular and extravascular leaf hydraulic conductance as influenced by N-fertilization and elevated CO2. *Journal of Plant Hydraulics* **3**: e001–e007.
Ellis B, Daly DD, Hickey LJ, Johnson KR, Mitchell JD, Wilf P, Wing SL. **2009**. *Manual of Leaf Architecture* (CU Press, Ed.). Ithaca, NY.
Eloy C. **2011**. Leonardo's rule, self-similarity, and wind-induced stresses in trees. *Physical Review Letters* **107**: 1–5.
Esau K. **1965**. *Plant Anatomy*. New York: John Wiley & Sons, Inc.
Evert RF, Kozlowski TT. **1967**. Effect of Isolation of Bark on Cambial Activity and Development of Xylem and Phloem in Trembling Aspen. *American Journal of Botany* **54**: 1045–1055.
Fellows RJ, Geiger DR. **1974**. Structural and Physiological Changes in Sugar Beet Leaves during Sink to Source Conversion. *Plant physiology* **54**: 877–885.
Foster AS. **1959**. The morphological and taxonomic significance of dichotomous venation in Kingdonia uniflora Balfour F. et W. W. Smith. *Notes from the Royal Botanic Garden* **23**: 1–12.
Foster AS. **1963**. The morphology and relationships of Circaeaster. *Journal of the Arnold Arboretum* **44**: 299–321.
Foster AS. **1966**. Morphology of Anastomoses in the Dichotomous Venation of Circaeaster. *American Journal of Botany* **53**: 588–599.

Foster AS, American S, Mar N. **1971**. Additional Studies on the Morphology of Blind-Endings in the Leaf of Circaeaster agrestis. *American Journal of Botany* **58**: 263–272.
Foster AS, Arnott HJ. **1960**. Morphology and Dichotomous Vasculature of the Leaf of Kingdonia uniflora. *American Journal of Botany* **47**: 684–698.
Fricke W, Hinde P, Leigh R, Tomos AD. **1995**. Vacuolar solutes in the upper epidermis of barley leaves. *Planta* **196**: 40–49.
Froelich DR, Mullendore DL, Jensen KH, Ross-Elliott TJ, Anstead JA, Thompson GA, Pélissier HC, Knoblauch M. **2011**. Phloem ultrastructure and pressure flow: Sieve-Element-Occlusion-Related agglomerations do not affect translocation. *The Plant cell* **23**: 4428–45.
Gilliham M, Dayod M, Hocking BJ, Xu B, Conn SJ, Kaiser BN, Leigh RA, Tyerman SD. **2011**. Calcium delivery and storage in plant leaves : exploring the link with water flow. *Journal of experimental botany* **62**: 2233–2250.
Gričar J, Zupančič M, Čufar K, Koch G, Schmitt U, Primož P. **2006**. Effect of local heating and cooling on cambial activity and cell differentiation in the stem of Norway spruce (Picea abies). *Annals of Botany* **97**: 943–951.
Gunckel JE, Wetmore RH. **1946**. Studies of Development in Long Shoots and Short Shoots of Ginkgo biloba L. II. Phyllotaxis and the Organization of the Primary Vascular System; Primary Phloem and Primary Xylem. *American Journal of Botany* **33**: 532–543.
Haberlandt G. **1914**. *Physiological Plant Anatomy*. London: Macmillan and Co., Limited.
Hargrave KR, Kolb KJ, Ewers FW, Davis SD. **1994**. Conduit Diameter and Drought-Induced Embolism in Salvia-Mellifera Greene (Labiatae). *New Phytologist* **126**: 695–705.
Hawkesford M, Horst W, Kichey T, Lambers H, Schjoerring J, Møller IS, White P. **2011**. *Functions of Macronutrients*.
Hirschi KD. **2004**. The Calcium Conundrum . Both Versatile Nutrient and Specific Signal 1. *Plant Physiology* **136**: 2438–2442.
Hölttä T, Mencuccini M, Nikinmaa E. **2009**. Linking phloem function to structure: analysis with a coupled xylem-phloem transport model. *Journal of theoretical biology* **259**: 325–37.
Hölttä T, Vesala T, Sevanto S, Perämäki M, Nikinmaa E. **2006**. Modeling xylem and phloem water flows in trees according to cohesion theory and Münch hypothesis. *Trees - Structure and Function* **20**: 67–78.
Hopkinson JM. **1964**. Studies on the expansion of the leaf surface IV. The carbon and phosphorous economy of a leaf. *Journal of Experimental Botany* **15**: 125–137.
Imlau A. **1999**. Cell-to-Cell and Long-Distance Trafficking of the Green Fluorescent Protein in the Phloem and Symplastic Unloading of the Protein into Sink Tissues. *the Plant Cell Online* **11**: 309–322.
Isebrands JG, Larson PR. **1973**. Anatomical changes during leaf ontogeny in Populus deltoides. *American Journal of Botany* **60**: 199–208.
Jensen KH, Bruus H, Holbrook NM, Liesche J, Schulz A, Zwieniecki MA. **2016**. Sap flow and sugar transport in plants. *Reviews of Modern Physics* **88**: 1–63.
Jensen KH, Lee J, Bohr T, Bruus H, Holbrook NM, Zwieniecki MA. **2011**. Optimality of the Münch mechanism for translocation of sugars in plants. *Journal of the Royal Society, Interface / the Royal Society* **8**: 1155–65.

Jensen KH, Liesche J, Bohr T, Schulz A. **2012a**. Universality of phloem transport in seed plants. *Plant, Cell and Environment* **35**: 1065–1076.
Jensen KH, Mullendore DL, Holbrook NM, Bohr T, Knoblauch M, Bruus H. **2012b**. Modeling the Hydrodynamics of Phloem Sieve Plates. *Frontiers in Plant Science* **3**: 1–11.
Jensen KH, Savage J a, Holbrook NM. **2013**. Optimal concentration for sugar transport in plants. *Journal of the Royal Society, Interface / the Royal Society* **10**: 20130055.
Jyske T, Hölttä T. **2015**. Comparison of phloem and xylem hydraulic architecture in Picea abies stems. *New Phytologist* **205**: 102–115.
Karley AJ, Leigh R a., Sanders D. **2000**. Where do all the ions go? The cellular basis of differential ion accumulation in leaf cells. *Trends in Plant Science* **5**: 465–470.
Karley AJ, White PJ. **2009**. Moving cationic minerals to edible tissues: potassium, magnesium, calcium. *Current Opinion in Plant Biology* **12**: 291–298.
Katifori E, Magnasco MO. **2012**. Quantifying loopy network architectures. *PloS one* **7**: e37994.
Katifori E, Szöllosi GJ, Magnasco MO. **2010**. Damage and fluctuations induce loops in optimal transport networks. *Physical Review Letters* **104**: 1–4.
Kerton M, Newbury HJ, Hand D, Pritchard J. **2009**. Accumulation of calcium in the centre of leaves of coriander (Coriandrum sativum L.) is due to an uncoupling of water and ion transport. *Journal of Experimental Botany* **60**: 227–235.
Knoblauch M, van Bel AJE. **1998**. Sieve Tubes in Action. *The Plant Cell* **10**: 35.
Knoblauch M, Knoblauch J, Mullendore DL, Savage JA, Babst BA, Beecher SD, Dodgen AC, Jensen KH, Holbrook NM. **2016**. Testing the Münch hypothesis of long distance phloem transport in plants. *eLife* **5**: e15341.
Knoblauch M, Oparka K. **2012**. The structure of the phloem - Still more questions than answers. *Plant Journal* **70**: 147–156.
Knoblauch M, Peters WS. **2016**. Think outside the sieve element! *Plant, Cell and Environment* **39**: 707–708.
Kockenberger W, Pope JM, Xia Y, Jeffrey KR, Komor E, Callaghan PT. **1997**. A non-invasive measurement of phloem and xylem water flow in castor bean seedlings by nuclear magnetic resonance microimaging. *Planta* **201**: 53–63.
Komor E. **2000**. Source physiology and assimilate transport: the interaction of sucrose metabolism, starch storage and phloem export in source leaves and the effects on sugar status in phloem Ewald. *Australian Journal of Plant Physiology* **27**: 497–505.
Koren Š, Arčon I, Kump P, Nečemer M, Vogel-Mikuš K. **2013**. Influence of CdCl2 and CdSO4 supplementation on Cd distribution and ligand environment in leaves of the Cd hyperaccumulator Noccaea (Thlaspi) praecox. *Plant and Soil* **370**: 125–148.
LaBarbera M. **1990**. Principles of design of fluid transport systems in zoology. *Science* **249**: 992–1000.
Lalonde S, Tegeder M, Throne-Holst M, Frommer WB, Patrick JW. **2003**. Phloem loading and unloading of sugars and amino acids. *Plant, Cell and Environment* **26**: 37–56.
Larson PR, Isebrands JG. **1971**. The plastochron index as applied to developmental studies of cottonwood. *Canadian Journal of Forest Research* **1**: 1–11.
Larson PR, Isebrands JG, Dickson RE. **1972**. Fixation Patterns of 14C within

Developing Leaves of Eastern Cottonwood. *Planta* **107**: 301–314.
Leigh A, Zwieniecki MA, Rockwell FE, Boyce CK, Nicotra AB, Holbrook NM. **2011**. Structural and hydraulic correlates of heterophylly in Ginkgo biloba. *New Phytologist* **189**: 459–470.
Lens F, Sperry JS, Christman MA, Choat B, Rabaey D, Jansen S. **2011**. Testing hypotheses that link wood anatomy to cavitation resistance and hydraulic conductivity in the genus Acer. *New Phytologist* **190**: 709–723.
Liesche J. **2017**. Sucrose transporters and plasmodesmal regulation in passive phloem loading. : 1–25.
Liesche J, Martens HJ, Schulz A. **2011**. Symplasmic transport and phloem loading in gymnosperm leaves. *Protoplasma* **248**: 181–190.
Liesche J, Schulz A. **2012**. In vivo quantification of cell coupling in plants with different phloem-loading strategies. *Plant physiology* **159**: 355–65.
Liesche J, Schulz A. **2013**. Symplasmic Transport in Phloem Loading and Unloading. In: Sokolowska K,, In: Sowinsky P, eds. Symplasmic Transport in Vascular Plants. New York: Springer, 133–163.
Lucas WJ, Groover A, Lichtenberger R, Furuta K, Yadav SR, Helariutta Y, He XQ, Fukuda H, Kang J, Brady SM, *et al.* 2013. The Plant Vascular System: Evolution, Development and Functions. *Journal of Integrative Plant Biology* **55**: 294–388.
McAinsh M, Pittman J. **2008**. Shaping the calcium signature. *New Phytologist* **181**: 275–294.
McCulloh KA, Sperry JS, Adler FR. **2003**. Water transport in plants obeys Murray ' s law. **421**: 939–942.
McKown AD, Cochard H, Sack L. **2010**. Decoding leaf hydraulics with a spatially explicit model: principles of venation architecture and implications for its evolution. *The American naturalist* **175**: 447–60.
McNair D. **2015**. Imaging venation of broadleaf plants using DSLR cameras, trasmitted light, and digital filters. *Phytoneuron* **39**: 1–12.
Meiri a, Silk WK, Läuchli a. **1992**. Growth and Deposition of Inorganic Nutrient Elements in Developing Leaves of Zea mays L. *Plant physiology* **99**: 972–978.
Mencuccini M, Hölttä T, Martínez-Vilalta J. **2011**. Comparative criteria for models of the vascular transport systems of tall trees. In: Meinzer FC,, In: Lachenbruch B,, In: Dawson TE, eds. Size- and age-related changes in tree structure and function. Dordrecht, Netherlands: Springer, 309–339.
Milthorpe FL, Moorby J. **1969**. Vascular Transport and its Significance in Plant Growth. *Annual Review of Plant Physiology* **20**: 117–138.
Minamino R, Tateno M. **2014**. Tree branching: Leonardo da Vinci's Rule versus biomechanical models. *PLoS ONE* **9**: e93535.
Moore KL, Chen Y, van de Meene AML, Hughes L, Liu W, Geraki T, Mosselmans F, Mcgrath SP, Grovenor C, Zhao FJ. **2014**. Combined NanoSIMS and synchrotron X-ray fluorescence reveal distinct cellular and subcellular distribution patterns of trace elements in rice tissues. *New Phytologist* **201**: 104–115.
Mullendore DL, Windt CW, Van As H, Knoblauch M. **2010**. Sieve tube geometry in relation to phloem flow. *The Plant cell* **22**: 579–93.
Muller O, Cohu CM, Stewart JJ, Protheroe J a, Demmig-Adams B, Adams WW. **2014**. Association between photosynthesis and contrasting features of minor

veins in leaves of summer annuals loading phloem via symplastic versus apoplastic routes. *Physiologia plantarum* **152**: 174–83.
Münch E. **1930**. *Die stroffbewegungen in der pflanze*. Jena: G. Fischer.
Murray CD. **1926**. The physiological principle of minumum work. *Proceedings of the National Academy of Sciences* **14**: 207–214.
Nardini A, Lo Gullo MA, Salleo S. **2011**. Refilling embolized xylem conduits: Is it a matter of phloem unloading? *Plant Science* **180**: 604–611.
Nikinmaa E, Hölttä T, Hari P, Kolari P, Mäkelä A, Sevanto S, Vesala T. **2013**. Assimilate transport in phloem sets conditions for leaf gas exchange. *Plant, cell & environment* **36**: 655–69.
Niklas K. **1999**. A mechanical perspective on foliage leaf function. *New Phytologist* **143**: 19–31.
Niklas KJ, Christianson ML. **2011**. Differences in the scaling of area and mass of Ginkgo biloba (Ginkgoaceae) leaves and their relevance to the study of specific leaf area. *American Journal of Botany* **98**: 1381–1386.
Nobel P. **2011**. *Physicochemical and environmental plant physiology*. Oxford: Elsevier-Academic Press.
Novitskaya LL, Kushnir F V. 2006. The role of sucrose in regulation of trunk tissue development in Betula pendula roth. *Journal of Plant Growth Regulation* **25**: 18–29.
Oparka K, Turgeon R. **1999**. Sieve elements and companion cells-traffic control centers of the phloem. *The Plant cell* **11**: 739–750.
Pantin F, Simonneau T, Muller B. **2012**. Coming of leaf age: control of growth by hydraulics and metabolics during leaf ontogeny. *The New phytologist* **196**: 349–66.
Petit G, Crivellaro A. **2014**. Comparative axial widening of phloem and xylem conduits in small woody plants. *Trees - Structure and Function* **28**: 915–921.
Pfautsch S, Hölttä T, Mencuccini M. **2015a**. Hydraulic functioning of tree stems - Fusing ray anatomy, radial transfer and capacitance. *Tree Physiology* **35**: 706–722.
Pfautsch S, Renard J, Tjoelker MG, Salih A. **2015b**. Phloem as Capacitor: Radial Transfer of Water into Xylem of Tree Stems Occurs via Symplastic Transport in Ray Parenchyma. *Plant Physiology* **167**: 963–971.
Price C a, Knox S-JC, Brodribb TJ. **2013**. The influence of branch order on optimal leaf vein geometries: Murray's law and area preserving branching. *PloS one* **8**: e85420.
Price C a, Wing S, Weitz JS. **2012**. Scaling and structure of dicotyledonous leaf venation networks. *Ecology letters* **15**: 87–95.
Rasband W. **2016**. ImageJ, U. S. National Institutes of Health, Bethesda, Maryland, USA.
Regvar M, Eichert D, Kaulich B, Gianoncelli a., Pongrac P, Vogel-Mikus K, Kreft I. **2011**. New insights into globoids of protein storage vacuoles in wheat aleurone using synchrotron soft X-ray microscopy. *Journal of Experimental Botany* **62**: 3929–3939.
Rennie E a, Turgeon R. **2009**. A comprehensive picture of phloem loading strategies. *Proceedings of the National Academy of Sciences of the United States of America* **106**: 14162–7.
Richter IA. **1980**. *The notebooks of Leonardo da Vinci*. Oxford: Oxford University Press.
Ronellenfitsch H, Lasser J, Daly DC, Katifori E. **2015a**. Topological phenotypes of leaf vascular networks. : 1–12.

Ronellenfitsch H, Liesche J, Jensen KH, Holbrook NM, Schulz A, Katifori E. **2015b**. Scaling of phloem structure and optimality of photoassimilate transport in conifer needles. *Proc. R. Soc. B* **282**: 20141863.
Roth-Nebelsick A, Uhl D, Mosbrugger V, Kerp H. **2001**. Evolution and Function of Leaf Venation Architecture : A Review. *Annals of Botany* **87**: 553–566.
Roth A, Mosbrugger V, Belz G, Neugebauer H. **1995**. Hydrodynamic modelling study of angiosperm leaf venation types. *Botanica Acta* **108**: 121–126.
Royer DL, Wilf P. **2006**. Why do toothed leaves correlate with cold climates? Gas exchange at leaf margins provides new insights into a classic paleotemperature proxy. *International Journal of Plant Sciences* **167**: 11–18.
Russin WA, Evert RF. **1984**. Studies in the leaf of Populus deltoides (Salicaceae): morphology and anatomy. *American journal of botany* **71**: 1398–1415.
Russin WA, Evert RF. **1985**. Studies on the Leaf of Populus deltoides (Salicaceae): Ultrastructure, Plasmodesmatal Frequency, and Solute Concentrations. *American Journal of Botany* **72**: 1232–1247.
Sack L, Frole K. **2006**. Leaf structural diversity is related to hydraulic capacity in tropical rain forest trees. *Ecology* **87**: 483–491.
Sack L, Holbrook NM. **2006**. Leaf hydraulics. *Annual review of plant biology* **57**: 361–81.
Sack L, Scoffoni C. **2013**. Leaf venation: structure, function, development, evolution, ecology and applications in the past, present and future. *New Phytologist* **198**: 983–1000.
Sack L, Scoffoni C, Johnson DM, Buckley TN, Brodribb TJ. **2015**. The Anatomical Determinants of Leaf Hydraulic Function. In: Hacke UG, ed. Functional and Ecological Xylem Anatomy. Springer, 255–271.
Sack L, Scoffoni C, McKown AD, Frole K, Rawls M, Havran JC, Tran H, Tran T. **2012**. Developmentally based scaling of leaf venation architecture explains global ecological patterns. *Nature communications* **3**: 837.
Sack L, Streeter CM, Holbrook NM. **2004**. Hydraulic Analysis of Water Flow through Leaves of Sugar Maple and Red Oak. *Plant Physiology* **134**: 1824–1833.
Sala A, Piper F, Hoch G. **2010**. Physiological mechanisms of drought-induced tree mortality are far from being resolved. *New Phytologist* **186**: 274–281.
Salleo S, Trifilò P, Esposito S, Nardini A, Lo Gullo MA. **2009**. Starch-to-sugar conversion in wood parenchyma of field-growing Laurus nobilis plants: a component of the signal pathway for embolism repair? *Functional Plant Biology* **36**: 815–825.
Savage JA, Clearwater MJ, Haines DF, Klein T, Mencuccini M, Sevanto S, Turgeon R, Zhang C. **2016**. Allocation, stress tolerance and carbon transport in plants: How does phloem physiology affect plant ecology? *Plant, Cell and Environment* **39**: 709–725.
Savage J a, Zwieniecki M a, Holbrook NM. **2013**. Phloem transport velocity varies over time and among vascular bundles during early cucumber seedling development. *Plant physiology* **163**: 1409–18.
Sevanto S. **2014a**. Phloem transport and drought. *Journal of Experimental Botany* **65**: 1751–1759.
Sevanto S. **2014b**. Phloem transport and drought. *Journal of experimental botany*.
Sevanto S, Hölttä T, Holbrook NM. **2011**. Effects of the hydraulic coupling between xylem and phloem on diurnal phloem diameter variation. *Plant, Cell and*

Environment **34**: 690–703.
Sevanto S, Hölttä T, Markkanen T, Perämäki M, Nikinmaa E, Vesala T. **2005**. Relationships between diurnal xylem diameter variation and environmental factors in Scots pine. *Boreal Environment Research* **10**: 447–458.
Slewinski TL, Zhang C, Turgeon R. **2013**. Structural and functional heterogeneity in phloem loading and transport. *Frontiers in plant science* **4**: 244.
Sommerville KE, Sack L, Ball MC. **2012**. Hydraulic conductance of Acacia phyllodes (foliage) is driven by primary nerve (vein) conductance and density. *Plant, Cell and Environment* **35**: 158–168.
Sperry JS, Hacke UG, Wheeler JK. **2005**. Comparative analysis of end wall resistivity in xylem conduits. *Plant, Cell and Environment* **28**: 456–465.
Storey R, Leigh R a. **2004**. Processes modulating calcium distribution in citrus leaves. An investigation using x-ray microanalysis with strontium as a tracer. *Plant physiology* **136**: 3838–3848.
Strahler AN. **1957**. Quantitative Analysis of Watershed Geomophology. *American Geophysical Union Transaction* **38**: 913–920.
Szczerba MW, Britto DT, Kronzucker HJ. **2009**. K + transport in plants : Physiology and molecular biology. **166**.
Thompson M V. **2006**. Phloem: the long and the short of it. *Trends in plant science* **11**: 26–32.
Thompson M V, Holbrook NM. **2003**. Application of a Single-solute Non-steady-state Phloem Model to the Study of Long-distance Assimilate Transport. *Journal of Theoretical Biology* **220**: 419–455.
Thompson M V., Holbrook NM. **2004**. Scaling phloem transport: Information transmission. *Plant, Cell and Environment* **27**: 509–519.
Tian S, Lu L, Labavitch JM, Webb SM, Yang X, Brown PH, He Z. **2014**. Spatial imaging of Zn and other elements in Huanglongbing-affected grapefruit by synchrotron-based micro X-ray fluorescence investigation. *Journal of Experimental Botany* **65**: 953–964.
Truernit E, Bauby H, Dubreucq B, Grandjean O, Runions J, Barthélémy J, Palauqui J-C. **2008**. High-resolution whole-mount imaging of three-dimensional tissue organization and gene expression enables the study of Phloem development and structure in Arabidopsis. *The Plant cell* **20**: 1494–503.
Turgeon R. **1989**. The sink-source transition in leaves. *Annual Review of Plant Physiology* **40**: 119–138.
Turgeon R. **2006**. Phloem loading: How leaves gain their independence. *Bioscience* **56**: 15–24.
Turgeon R. **2010**. The puzzle of phloem pressure. *Plant physiology* **154**: 578–81.
Turgeon R, Ayre BG. **2005**. Pathways and Mechanisms of Phloem Loading. In: Holbrook NM,, In: Zwieniecki MA, eds. Vascular Transport in Plants. Burlington: Elsevier, 45–67.
Tyree MT, Zimmermann MH. **2002**. *Xylem structure and the ascent of sap*. Berlin: Springer.
Vogel-Mikuš K, Regvar M, Mesjasz-Przybyłowicz J, Przybyłowicz WJ, Simčič J, Pelicon P, Budnar M. **2008**. Spatial distribution of cadmium in leaves of metal hyperaccumulating Thlaspi praecox using micro-PIXE. *New Phytologist* **179**: 712–721.
Vogelmann TC, Dickson RE, Larson PR. **1985**. Comparative distribution and

metabolism of xylem-borne amino compounds and sucrose in shoots of Populus deltoides. *Plant Physiology* **77**: 418–428.
Wagner WHJ. **1979**. Reticulate Veins in the Systematics of Modern Ferns. *Taxon* **28**: 87–95.
Waisel Y, Noah I, Fahn A. **1966**. Cambial Activity in Eucalyptus camaldulensis Dehn . II . The Production of Phloem and Xylem Elements. *New Phytologist* **65**: 319–324.
Weatherley PE. **1973**. Short Communication Solution Flow in Tubular Semi-permeable Membranes. *Planta* **110**: 183–187.
Wheeler JK, Sperry JS, Hacke UG, Hoang N. **2005**. Inter-vessel pitting and cavitation in woody Rosaceae and other vessel led plants: A basis for a safety versus efficiency trade-off in xylem transport. *Plant, Cell and Environment* **28**: 800–812.
White PJ. **2011**. Long-distance Transport in the Xylem and Phloem. *Marschner's Mineral Nutrition of Higher Plants: Third Edition*: 49–70.
Wilson TP, Canny MJ, Mccully ME. **1991**. Leaf teeth , transpiration and the retrieval of apoplastic solutes in balsam poplar. *Physiologia Plantarum* **88**: 225–232.
Wilson TP, Canny MJ, McCully ME. **1988**. Proton pump activity in bundle sheath tissues of broad-leaves trees in relation to leaf age. *Physiologia Plantarum* **73**: 465–470.
Windt CW, Vergeldt FJ, De Jager PA, Van As H. **2006**. MRI of long-distance water transport: A comparison of the phloem and xylem flow characteristics and dynamics in poplar, castor bean, tomato and tobacco. *Plant, Cell and Environment* **29**: 1715–1729.
Woodruff DR. **2014**. Experimental analysis of the role of water and carbon in tree stem diameter variations. *Tree Physiology* **34**: 5–14.
Woodruff DR, Ryan M. **2014**. The impacts of water stress on phloem transport in Douglas-fir trees. *Tree Physiology* **34**: 5–14.
Wu B, Becker JS. **2012**. Imaging techniques for elements and element species in plant science. *Metallomics* **4**: 403.
Wylie RB. **1938**. Concerning the Conductive Capacity of the Minor Veins of Foliage Leaves. *American Journal of Botany* **25**: 567–572.
Wylie RB. **1939**. Relations Between Tissue Organization and Vein Distribution in Dicotyledon Leaves. *American Journal of Botany* **26**: 219–225.
Wylie RB. **1951**. Principles of foliar organization shown by sun-shade leaves from ten species of deciduous dicotyledonous trees. *American Journal of Botany* **38**: 355–361.
Yamaji N, Ma JF. **2014**. The node, a hub for mineral nutrient distribution in graminaceous plants. *Trends in Plant Science* **19**: 556–563.
Young JH, Evert RF, Eschrich W. **1973**. On the volume-flow mechanism of phloem transport. *Planta* **113**: 355–366.
Zhai Z, Gayomba SR, Jung H-I, Vimalakumari NK, Piñeros M, Craft E, Rutzke M a, Danku J, Lahner B, Punshon T, *et al.* 2014. OPT3 Is a Phloem-Specific Iron Transporter That Is Essential for Systemic Iron Signaling and Redistribution of Iron and Cadmium in Arabidopsis. *The Plant cell* **26**: 2249–2264.
Zhang C, Han L, Slewinski TL, Sun J, Zhang J, Wang Z-Y, Turgeon R. **2014**. Symplastic phloem loading in poplar. *Plant physiology* **166**: 306–13.
Zhao FJ, Moore KL, Lombi E, Zhu YG. **2014**. Imaging element distribution and speciation in plant cells. *Trends in Plant Science* **19**: 183–192.

Zhou ZY. **2009**. An overview of fossil Ginkgoales. *Palaeoworld* **18**: 1–22.
Zweifel R, Item H, Häsler R. **2000**. Stem radius changes and their relation to stored water in stems of young Norway spruce trees. *Trees - Structure and Function* **15**: 50–57.
Zwieniecki M a, Brodribb TJ, Holbrook NM. **2007**. Hydraulic design of leaves: insights from rehydration kinetics. *Plant, cell & environment* **30**: 910–21.
Zwieniecki M a., Melcher PJ, Boyce CK, Sack L, Holbrook NM. **2002**. Hydraulic architecture of leaf venation in Laurus nobilis L. *Plant, Cell and Environment* **25**: 1445–1450.